UNIVERSITÄT ZU LÜBECK

From the Institute of Virology and Cell Biology
of the University of Lübeck
Director: Prof. Dr. Norbert Tautz

"Reporter-based reverse genetics of murine norovirus reveals insertion-tolerant sites and a position in the capsid linked to antibody escape"

Dissertation
for Fulfillment of
Requirements
for the Doctoral Degree
of the University of Lübeck

from the Department of Natural Sciences

Submitted by

Miranda Sophie Lane
from Reading, United Kingdom of Great Britain and Northern Ireland

Lübeck 2026

First referee: Prof. Dr. rer. nat. Stefan Taube

Second referee: Prof. Dr. Lars Redecke

Date of oral examination: 25th March 2026

Approved for printing. Lübeck, 31st March 2026

“These Things will not bite you.
They want to have fun.”
Then, out of the box
Came Thing Two and Thing One!

Abstract

Noroviruses are members of the *Caliciviridae* family: positive-sense, single-stranded RNA encased within a 90-dimer protein capsid. Human norovirus (HNoV) is a major cause of gastrointestinal disease. Murine norovirus (MNV) is used as a surrogate in the study of HNoV due to it being the only norovirus currently reliably cultivatable in cell culture and possessing a reverse genetics system. Previous studies have used MNV to develop our understanding of norovirus capsid protein structure with regards to infection. Various ligands have been observed to bind the norovirus capsid including divalent cations, neutralising antibodies, bile acids, and a cellular receptor mCD300lf (MNV only). The effect of bile acids on MNV infection was previously investigated in this lab but recent research suggests dynamic conformational changes observed in the MNV capsid are due to environmental factors such as bile acid binding, pH change and divalent cation binding. This study set out to determine the effects of divalent cation binding with regards to infection.

Multiple reverse genetics techniques have been developed for MNV with an RNA-based technique in a recombinant cell line developed within the last few years. This technique allows for the indirect observation of protease production via a GFP reporter system. This work compared wild-type MNV-1.CW1 RNA transfections with transfected MNV-1.CW1 RNA with mutations introduced to a cDNA plasmid construct via site-directed mutagenesis. This system was used in the testing of the non-structural (NS) polyprotein, protease cleavage sites with the aim of identifying potential sites for the insertion of a short protein-coding sequence, and to generate recombinant mutant MNVs used in the study of divalent cations.

Transfection experiments of MNV-1.CW1 RNA with an HNoV protease cleavage site identified a potential site of NS1-2/NS3 as being suitable for a potential inserted protein, with the site receptive to a short peptide-coding sequence insertion. Five recombinant MNV-1.CW1s with mutations in the major capsid protein were generated. The generation of two divalent cation non-binding mutants (D410A and D440A) and the extensive testing of these in cell culture assays identified D440 as a crucial site of cation binding, preventing the neutralisation of the virus with a monoclonal antibody. Previous work identifying bile acid in preventing neutralisation from monoclonal antibodies was revaluated, this time controlling for divalent cations. Divalent cations were found to be essential in small concentrations – that alone could not prevent neutralisation – but assisted bile acid in neutralisation escape.

Zusammenfassung

Noroviren gehören zur Familie der *Caliciviridae*: positivsträngige, einzelsträngige RNA, umhüllt von einem 90-Dimer-Proteinkapsid. Das humane Norovirus (HNoV) ist eine der Hauptursachen für Magen-Darm-Erkrankungen. Das murine Norovirus (MNV) wird aufgrund seiner derzeit einzigen zuverlässigen Kultivierbarkeit in Zellkulturen und seines reversen genetischen Systems als Ersatz für die Untersuchung von HNoV verwendet. In früheren Studien wurde MNV verwendet, um unser Verständnis der Struktur des Norovirus-Kapsidproteins im Hinblick auf Infektionen zu vertiefen. Es wurde beobachtet, dass verschiedene Liganden an das Norovirus-Kapsid binden, darunter zweiwertige Kationen, neutralisierende Antikörper, Gallensäuren und ein zellulärer Rezeptor mCD300lf (nur MNV). Die Wirkung von Gallensäuren auf die MNV-Infektion wurde bereits zuvor in diesem Labor untersucht, aber neuere Forschungen deuten darauf hin, dass die im MNV-Kapsid beobachteten dynamischen Konformationsänderungen auf Umweltfaktoren wie Gallensäurebindung, pH-Änderung und zweiwertige Kationenbindung zurückzuführen sind. Diese Studie hatte zum Ziel, die Auswirkungen der zweiwertigen Kationenbindung in Bezug auf die Infektion zu bestimmen.

Für MNV wurden mehrere Techniken der reversen Genetik entwickelt, darunter eine RNA-basierte Technik in einer rekombinanten Zelllinie, die in den letzten Jahren entwickelt wurde. Diese Technik ermöglicht die indirekte Beobachtung der Proteaseproduktion über ein GFP-Reporter-System. In dieser Arbeit wurden Wildtyp-MNV-1.CW1-RNA-Transfektionen mit transfizierter MNV-1.CW1-RNA verglichen, in die durch ortsspezifische Mutagenese Mutationen in ein cDNA-Plasmidkonstrukt eingeführt worden waren. Dieses System wurde zum Testen des nicht-strukturellen (NS) Polyproteins und der Protease-Spaltstellen verwendet, um potenzielle Stellen für die Insertion einer kurzen proteinkodierenden Sequenz zu identifizieren und rekombinante mutierte MNVs zu erzeugen, die in der Untersuchung von zweiwertigen Kationen verwendet wurden.

Transfektionsexperimente mit MNV-1.CW1-RNA mit HNoV-Protease-Spaltstelle identifizierten eine potenzielle Stelle von NS1-2/NS3 als geeignet für ein potenziell eingefügtes Protein, wobei die Stelle für die Insertion einer kurzen Peptid-Codierungssequenz empfänglich war. Es wurden fünf rekombinante MNV-1.CW1 mit Mutationen im Hauptkapsidprotein erzeugt. Die Erzeugung von zwei Mutanten, die keine zweiwertigen Kationen binden (D410A und D440A), und deren umfangreiche Prüfung in Zellkultur-Assays identifizierten D440 als eine entscheidende Stelle für die Kationenbindung, die die Neutralisierung des Virus durch einen monoklonalen Antikörper verhindert. Frühere Arbeiten, in denen Gallensäure als Mittel zur Verhinderung der Neutralisierung durch monoklonale Antikörper identifiziert wurde, wurden neu bewertet, diesmal unter Berücksichtigung zweiwertiger Kationen. Es wurde festgestellt, dass zweiwertige Kationen in geringen Konzentrationen unerlässlich sind – allein konnten sie die Neutralisierung nicht verhindern –, aber sie unterstützten die Gallensäure bei der Neutralisationsumgehung.

Contents

Table of figures

Table of tables

Abbreviations

Abbreviation	Full terminology	Definition (if applicable)
293T	Human embryonic kidney	Cell line
Ab	Antibody	
BHK	Baby hamster kidney	Cell line
BSR-T7	T7 RNA polymerase-expressing baby hamster kidney	Cell line
CA	Cholic acid	
CAS	Chemical Abstracts Service	
CDCA	Deoxycholic acid	
CPE	Cytopathic effect	
DCA	Deoxycholic acid	
DMEM	Dulbecco's Modified Eagle Medium	Eukaryotic cell growth medium
DNA	Deoxyribose nucleic acid	
eIF	Eukaryotic initiation factor	
ER	Endoplasmic reticulum	
FLAG-tag	--	Peptide protein tag with the sequence: DYKDDDDK
F/S	Frame-shift	
GCA	Glycocholic acid	
GCDCA	Glycochenodeoxycholic acid	
HA-tag	Human influenza haemagglutinin tag	Peptide protein tag with the sequence: YPYDVPDYA
HAV	Hepatitis A virus	
huCD300lf	Human CD300lf	Human cell receptor protein
HNoV	Human norovirus	
IVT	*In vitro* transcription	
LCA	Lithocholic acid	
m^7G	$m^7G(5')ppp(5')G$	5' terminal 7-methylguanosine, capping structure at the 5'-end of viral RNA
MAb	Monoclonal antibody	
mCD300lf	Murine CD300lf	Murine cell receptor protein (MNV binding)
MNV	Murine norovirus	
NCBI	National Center for Biotechnology Information	
NIH	National Institutes of Health	
NMR	Nuclear magnetic resonance	
NS	Non-structural	
ORF	Open reading frame	
P-domain	Protruding domain	
RAW 264.7	Murine macrophage	Cell line
RdRp	RNA-dependant RNA polymerase	
RNA	Ribonucleic acid	
S-domain	Shell-domain	
TAE	Tris-acetate-EDTA	Buffer
TCA	Taurocholic acid	
TCDCA	Taurochenodeoxycholic acid	
T_m	Melting temperature	

UTR	Untranslated region	
VP1	Viral protein 1	Major capsid protein
VP2	Viral protein 2	Minor capsid protein
VPg	Viral protein genome-linked	
WT	Wild-type	

Introduction

Noroviruses

Noroviruses belong to the *Caliciviridae* family and are non-enveloped, positive-sense, single-stranded RNA viruses (Sutherland *et al.*, 2021). The viral genome is encased in an icosahedral capsid, composed of 180 copies of the major capsid protein (VP1) and twelve copies of the minor capsid protein (VP2) (Conley *et al.*, 2019). Members of the norovirus genus are currently categorised into ten genogroups of which genogroups GI, GII, GIV, GVII, GVIII and GIX are known to infect humans with human norovirus (HNoV) (Chhabra *et al.*, 2019). This is genogrouping based upon the sequence of VP1. Noroviruses can also be grouped by the sequence of a non-structural protein, an RNA-dependant RNA polymerase. These genogroups can be subdivided further into genotypes.

HNoV is the major cause of gastroenteritis worldwide causing approximately 20% of cases (Ahmed *et al.*, 2014) and has a seasonal tendency, being more prevalent in autumn and winter months (Amodio *et al.*, 2022). Although some recent research has indicated a possibility for the development of a norovirus vaccine (Atmar *et al.*, 2024), availability is limited to clinical trials.

Cultivation of HNoV can be achieved in both animal and cell models. Animal models such as gnotobiotic pigs (Cheetham *et al.*, 2006), zebrafish larvae (Van Dycke *et al.*, 2019) and neonatal mice (Roth *et al.*, 2020) can be used for cultivation. Replication of HNoV is possible in human B cells (Jones *et al.*, 2015) and in human intestinal enteroids (Ettayebi *et al.*, 2016). Cost, ease of technique and reproducibility make the zebrafish and human intestinal enteroids the current respective animal and cell models of choice.

However, the generation of a viral stock of any HNoV genotype is not, with current methods, reliable. A surrogate system of study is therefore frequently utilised in the form of a related norovirus, murine norovirus (MNV).

Clustered into its own genogroup (GV), MNV was first identified in 2003 (Karst *et al.*, 2003). It is currently the only norovirus that can be reliably cultivated by cell culture. Two cell lines, macrophages RAW 264 (Raschke *et al.*, 1978) and microglial BV-2 (Blasi *et al.*, 1990), are naturally susceptible to MNV infection. This is due to the presence of murine cellular receptor mCD300lf (Haga *et al.*, 2016; Orchard *et al.*, 2016) and is necessary for MNV infection. Thus far, no equivalent receptor has been found for HNoV and the human CD300lf (huCD300lf) counterpart is functionally dissimilar (Graziano *et al.*, 2020). Non-murine cell lines such as Huh7 (Nakabayashi *et al.*, 1982) have recently been genetically modified and can also support both MNV replication and reverse genetics techniques (Lingemann, 2020; Wobus *et al.*, 2023). Infection of mice with MNV is also possible.

Norovirus genome structure

The usability of MNV in cell culture, in particular the ability to generate viral stocks, has made it useful for the study of noroviruses in general. Genetically, both MNV and HNoV are similar, sharing open reading frame (ORF) structures and protein sequences in both structural and non-structural (NS) proteins (**Figure 1**). Caliciviruses all follow the same, basic genetic structure: an ORF containing the genes for NS proteins preceding the two ORFs coding for the capsid proteins (Clarke & Lambden, 2000). Specifically for both HNoV and MNV, ORF1 encodes the NS proteins, ORF2 encodes VP1, and ORF3 the minor capsid protein (VP2) with an ORF4 present for MNV only (Thorne & Goodfellow, 2014). There is a small overlap of ORF1 and ORF2. The NS proteins are cleaved from a polyprotein made by ORF1 (Sosnovtsev *et al.*, 2006). The structural proteins are made from a sub-genome with its own attached genome-linked viral protein.

Non-structural proteins and polyprotein processing

The function of NS1-2 has not yet been fully determined, however it is understood that it contributes to the cell tropism. A recent publication suggests its MNV role is important in glycolysis and glutaminolysis, the breakdown of monosaccharide glucose and amino acid glutamine respectively (Hafner *et al.*, 2024). A study into its function in HNoV indicates NS1-2 is involved in the recruitment of lipids and proteins to the endoplasmic reticulum (ER) and interaction with NS4 (Hung *et al.*, 2023). This is suggestive of NS1-2 playing a role in viral replication.

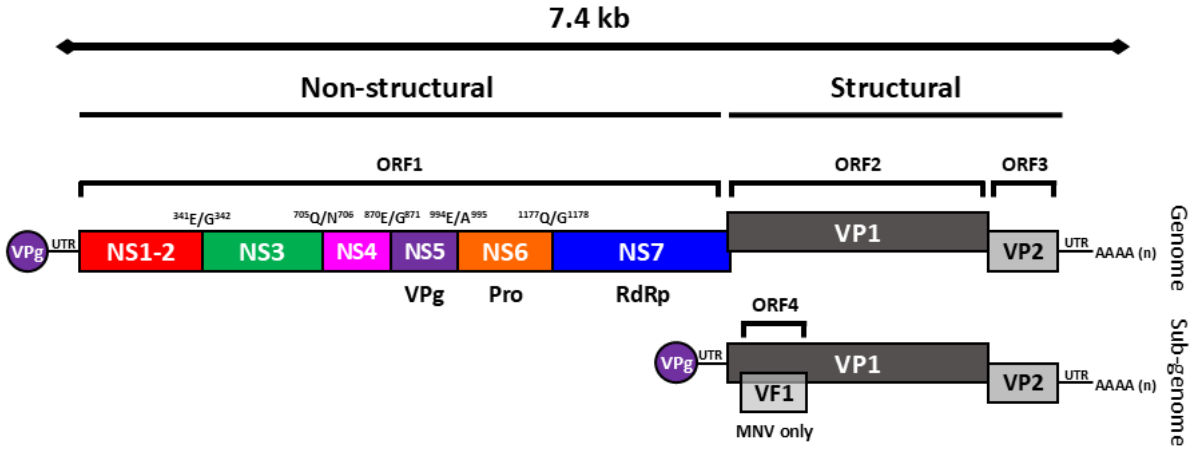

Figure 1: Genome structure of noroviruses

Open reading frames indicated (ORF4 for MNV only). Non-structural proteins with functions, if known, indicated. Protease cleavage sites (MNV-1) indicated. Structural proteins indicated. The untranslated regions (UTR) and polyamine tail are shown at the N-terminus and C-terminus respectively. Both the full genome and sub-genome are shown with the N-terminal VPg.

Cellular protein, caspase 3 cleaves the N-terminal protein NS1-2, rather than a viral protease. This occurs at the ^{118}DRPD^{121} and ^{128}DAMD^{131} sites generating a small protein of 13.6 kDa and a slightly larger protein of 23.7 or 24.7 kDa depending on the second cleavage (Sosnovtsev *et al.*, 2006). Interestingly both human and murine caspase 3 are capable of performing this cleavage with both sites ^{118}DRPD^{121} and ^{128}DAMD^{131} conserved as DXXD across human and multiple MNV strains (Sosnovtsev *et al.*, 2006).

Another NS protein function that proves elusive is NS3. At present, NS3 has been described as having RNA helicase and chaperoning activities in both HNoV (Li *et al.*, 2018) and MNV (Han *et al.*, 2018). Helicases and chaperones are generally utilised to promote correct RNA folding and stabilise the structure (Yang *et al.*, 2015) ensuring a functionally correct RNA. Importantly, a high degree of amino acid conservation was observed between HNoV and MNV helicase regions suggesting function remains conserved (Cotton *et al.*, 2017). More recent studies have suggested that NS3 may have another role in norovirus infection, namely the induction of cell death (Wang *et al.*, 2023; Yen *et al.*, 2021). The N-terminal domain (amino acids 1-158) is sufficient to induce cell death when expressed in multiple cell types, with no other function currently known (Wang *et al.*, 2023).

The final NS protein not yet fully described is NS4 and may be involved in multiple functions with other NS proteins. It is understood that NS4 disassembles the Golgi apparatus and inhibits protein secretion in both MNV and HNoV (Sharp *et al.*, 2010, 2012). More recent reports indicate NS4 is the main driver in single- and double-membrane vesicle accumulation in the Golgi apparatus and ER which may play a key role in replication (Doerflinger *et al.*, 2017). Although NS4 does not induce apoptosis alone, its cotransfection with NS3 can, suggesting NS4 acts as a proapoptotic factor to boost apoptosis by NS3 (Yen *et al.*, 2021). Self-assembly of HNoV NS4 has been described with a suggestion that this facilitates a clearly observed bridging of lipid membranes (Royet *et al.*, 2024).

Caliciviruses lack a 5' cap, that would normally initiate translation, but utilise a VPg (viral protein genome-linked) or NS5 that is covalently linked to the 5' end of the genome (Burroughs & Brown, 1978; Schaffer *et al.*, 1980). A VPg is necessary for infectious virus (Dunham *et al.*, 1998), although recovery of infectious virus by reverse genetics has been shown to be possible with the addition of a 5' terminal 7-methylguanosine (m^7G) cap analogue (in full, $m^7G(5')ppp(5')G$) when introduced simultaneously with *in vitro* transcription (IVT) (Sosnovtsev & Green, 1995) or indeed after IVT but before transfection (Wobus *et al.*, 2023). These latter two examples are demonstrative of calicivirus and norovirus reverse genetics techniques.

Noroviral protease (NS6) co- and post-translationally cleaves itself off the polyprotein and other NS proteins, with these sites specifically identified in MNV-1 as $^{341}E/G^{342}$, $^{705}Q/N^{706}$, $^{870}E/G^{871}$, $^{994}E/A^{995}$, and $^{1177}Q/G^{1178}$ (Sosnovtsev *et al.*, 2006), see **Figure 1**. These amino acids are relatively conserved across all noroviruses, however mostly within the same genogroup. There are differences between the HNoV protease cleavage sites (Belliot *et al.*, 2003) and the MNV protease sites (Sosnovtsev *et al.*, 2006), notably with repetition present in the HNoV sites. The identification of these sites noted "early" and "late" cleavage sites as being NS1-2/NS3 and NS3/NS4; and NS4/NS5, NS5/NS6 and NS6/NS7 respectively. In the past decade this has permitted for the more specific identification of the four amino acids preceding and the two proceeding the cleavage site (P4-P2') as being crucial for not only permitting cleavage but defining the cut as either "early" or "late" (Emmott *et al.*, 2015; May *et al.*, 2014).

Catalytic cleavage by the NS6 protease occurs at the active site, consisting of a triad of C139, H30 and E54 (Hussey *et al.*, 2011). Most prominent in this triad is C139 contained within a loop between two β-strands of six that make up a β-barrel, the larger domain of the two-domain protein. The other two residues of the active site lie in the smaller domain. For the purposes of generating a crystal structure, C139 has been mutated to an alanine, inactivating the site (Leen *et al.*, 2012).

The RNA-dependant RNA polymerase (RdRp) is the final NS protein in ORF1, NS7. At approximately 57 kDa in size (Hyde & Mackenzie, 2010), NS7 is associated with intracellular, single-membrane vesicles forming a replication complex that itself associates with the Golgi apparatus, ER and endosomes (Hyde *et al.*, 2009). All NS proteins have been shown to localise to dsRNA indicating that all are involved in genome replication (Hyde *et al.*, 2009).

Norovirus capsid structure

The noroviral capsid proteins are encoded in ORF2 and ORF3 making the VP1 and VP2 respectively. A sub-genomic RNA with a covalently linked VPg codes for these ORFs. After the translation and termination of VP1, reinitiation of translation for VP2 occurs due to a crucial RNA sequence or element upstream of the start site, dubbed the "termination upstream ribosomal binding site" or TURBS (Meyers, 2007). Two VP1 monomers form a dimer and 90 of these dimers assemble into the icosahedral capsid (Prasad *et al.*, 1999), generally reminiscent of a T3 symmetry. Each VP1 monomer is composed of two major domains, the shell (S)-domain and the protruding (P)-domain (Prasad *et al.*, 1999), of which the latter contains multiple binding sites for antibodies (Taube *et al.*, 2010), bile acids and metal ions (Nelson *et al.*, 2018). The P-domain can be further divided into the more conserved P1 subdomain and more variable P2 subdomain (Prasad *et al.*, 1999). This more variable P2 subdomain contains the binding site for the MNV cell receptor mCD300lf (Haga *et al.*, 2016; Nelson *et al.*, 2018; Orchard *et al.*, 2016).

Ligands to MNV VP1 and capsid flexibility

In MNV, the P-domain has been observed to both float above and contract onto the S-domain, with a notable degree of flexibility of several loop structures located distal from the capsid centre (Katpally *et al.*, 2010; Taube *et al.*, 2010). First described by Katpally *et al.* (2010) the two conformations that the P-domain appears to be presented in is either a closed conformation, where the A'B' and E'F' loops are close together with a raised C'D' loop, or open, where the A'B' and E'F' loops are splayed apart and the C'D' loop is down (**Figure 2**). These structures and their flexibility is crucial for MNV binding as they are not only the epitope for the aforementioned mCD300lf (Nelson *et al.*, 2018), but are also the sites for neutralising monoclonal antibodies (MAbs) (Kolawole *et al.*, 2017; Kolawole, Li, *et al.*, 2014; Kolawole, Xia, *et al.*, 2014). Mutations in the P-domain that permit the escape from neutralising MAb 2D3 have been shown to be permanently in a closed conformation, lacking the ability to be splayed open making them susceptible to neutralisation (M. B. Sherman *et al.*, 2025).

Flexibility in the capsid is not just restricted to the loop regions, but the entire P-domain. Bile acids, that are molecules found in the bile and therefore the intestine, have been noted to bind a pocket between the two P-domain dimers of MNV (Nelson *et al.*, 2018). Bile acids are formed from cholesterol in the liver (Hofmann, 1999) and are present in the bile of mammals. Bile acids that are synthesised in the hepatocyte, cholic acid (CA) and chenodeoxycholic acid (CDCA), are called "primary" bile acids (Hofmann, 1999) and become conjugated with either taurine or glycine (Chiang, 2013). Most bile acids are conjugated, with derivatives of CA being taurocholic acid (TCA) and glycocholic acid (GCA), and derivatives of CDCA being taurochenodeoxycholic acid (TCDCA) and glycochenodeoxycholic acid (GCDCA). Conjugation increases solubility and prevents Ca^{2+} precipitation (Chiang, 2013). Upon release and interaction within the intestine, primary bile acids are altered by bacterial enzymes (Hofmann, 1999). Some bile acids are deconjugated which are absorbed and returned to the liver, whereas others are further attacked by the bacterial enzymes removing a hydroxy group (Hofmann, 1999). The resultant deoxy bile acids, deoxycholic acid (DCA) and lithocholic acid (LCA), are termed "secondary" bile acids and are the products of CA and CDCA respectively (Hofmann, 1999). More than 90% of human biliary bile acids of made up of CA and CDCA conjugates and DCA (Hofmann, 1999), with a glycine to taurine conjugation ratio of approximately 3 to 1 (Chiang, 2013).

Specifically GCDCA has been demonstrated to bind the pocket and stabilise the P-domain permitting for a rotation of approximately 90° and contraction onto the S-domain (M. B. Sherman *et al.*, 2019). The addition of GCDCA and this conformational change permits more efficient binding of P2 to mCD300lf and prevents MAb binding (Williams *et al.*, 2021a) and neutralisation in a cell culture model (Creutznacher *et al.*, 2022). Crucially with regards to infection, it is likely that the observed stabilisation and forcing of the P-domains into a dimer (Creutznacher *et al.*, 2022) keeps the capsid in a rigid state that is more favourable to mCD300lf binding.

Bile acids are not the only factor in determining P-domain conformation. The pH of the environment surrounding VP1 can reversibly change the P-domain conformation (Song *et al.*, 2020; Williams *et al.*, 2021b). Acidic conditions, such as that of the upper duodenum, trigger the P-domain into the contracted and closed conformation, stabilising the viral capsid for efficient mCD300lf binding (Williams *et al.*, 2021b). Similar observations have been made with cations (M. Sherman *et al.*, 2024; Song *et al.*, 2020; Williams *et al.*, 2021b) suggesting GCDCA, low pH and cations work synergistically to improve MNV infection (ligands indicated in **Figure 2**).

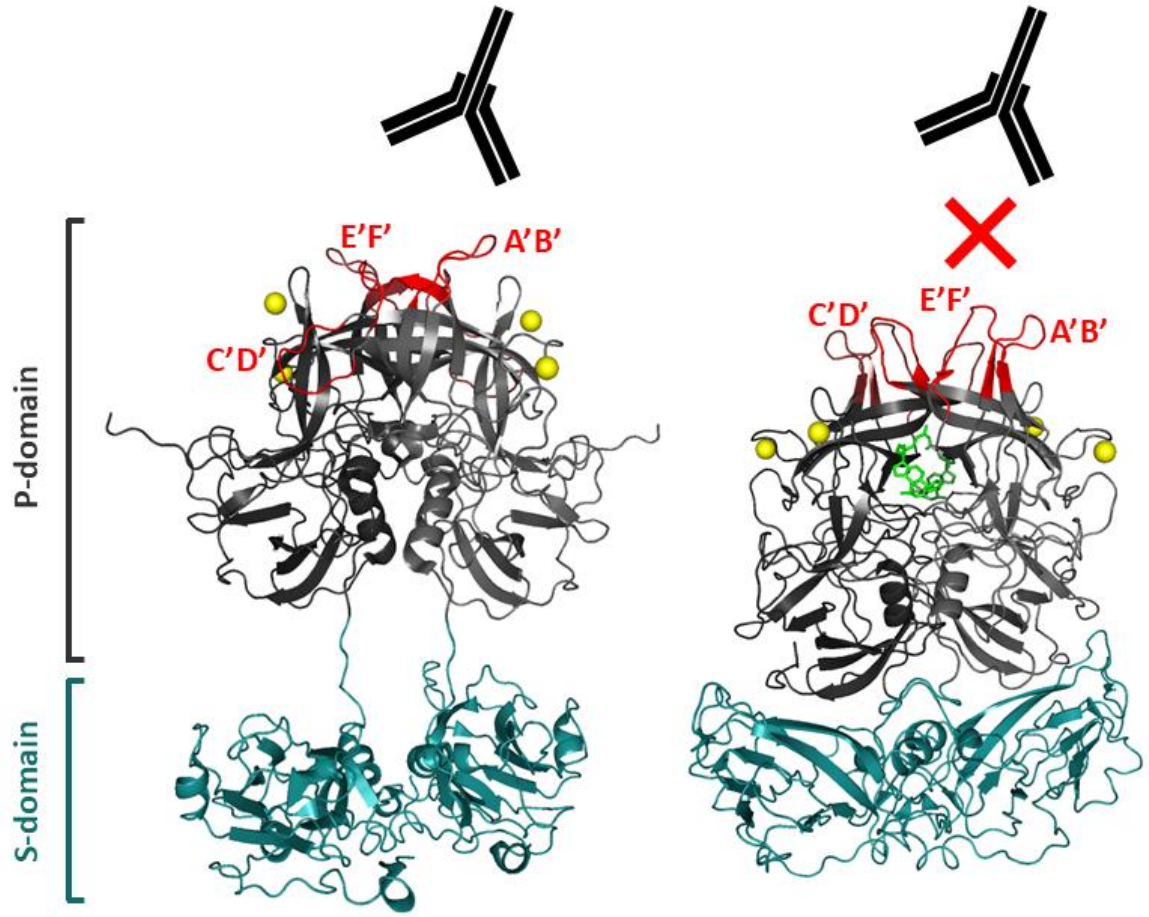

Figure 2: MNV VP1 dimer in the extended and contracted conformations onto the S-domain with ligands

The P-domain (grey) above the S-domain (turquoise) shown in the open, extended and antibody-binding conformation (left) and the closed, contracted and GCDCA-binding conformation (right). The A'B', C'D' and E'F' loops are indicated in red. Bound Mg^{2+} (yellow) and GCDCA (green) are indicated. Figure assembled in PyMOL from PDBs: 3LQ6 and 6CRJ (extended) and 6P4J (contracted).

Norovirus replication cycle

Sialic acids are used by MNV as attachment receptors to bind the cell (Taube *et al.*, 2009). The MNV VP1 binds to receptor mCD300lf (Orchard *et al.*, 2016) in order to enter the cell. Entry of MNV is pH independent (Perry *et al.*, 2009) and occurs via cholesterol and dynamin II dependent endocytosis (Perry & Wobus, 2010). The human equivalent huCD300lf does not initiate viral entry for HNoV (Graziano *et al.*, 2020) and may rely on another receptor or antigens such as human blood group antigens (HBGAs) that bind HNoV particles (Marionneau *et al.*, 2002).

Once entry has been gained, the viral genome is released into the cytoplasm (**Figure 3**). Caliciviruses being positive-sense, single-stranded RNA viruses dictate that the RNA is replication-ready and can act in the same manner as cellular mRNA. The initial round of translation takes place by the cellular machinery. Rather than the utilisation of an m^7G cap, caliciviruses have a VPg that binds eukaryotic initiation factors (eIFs) in the recruitment for a translation initiation complex. Specifically in the case of HNoV and MNV, eIF3 and eIF4E have been shown to bind VPg (Daughenbaugh *et al.*, 2003; Goodfellow *et al.*, 2005).

The translation of ORF1 to a polyprotein generates a functional viral protease (NS6) that cleaves the other NS proteins from the polyprotein. Once the cleaved RdRp (NS7) is accessible, replication of the viral genome commences.

The negative strand synthesis of the genome and sub-genome is conducted by priming and initiating synthesis of the positive-strand by VPg, from the 3'-end of the negative-strand RNA (Chaudhry *et al.*, 2006; Subba-Reddy *et al.*, 2011). This is by *de novo* initiation and the synthesis of a negative-strand genome copy (Rohayem *et al.*, 2006).

The VP1 and VP2 assemble into the capsid containing the viral genome. Most virions are released by cell lysis. Additionally MNV can also be released as vesicles (Santiana *et al.*, 2018). As recently described by Wang *et al.* (2023), the N-terminal region of NS3 disrupts the mitochondrial membrane by the promotion of membrane depolarisation. Assembled virions are released by apoptosis (Deerain *et al.*, 2024).

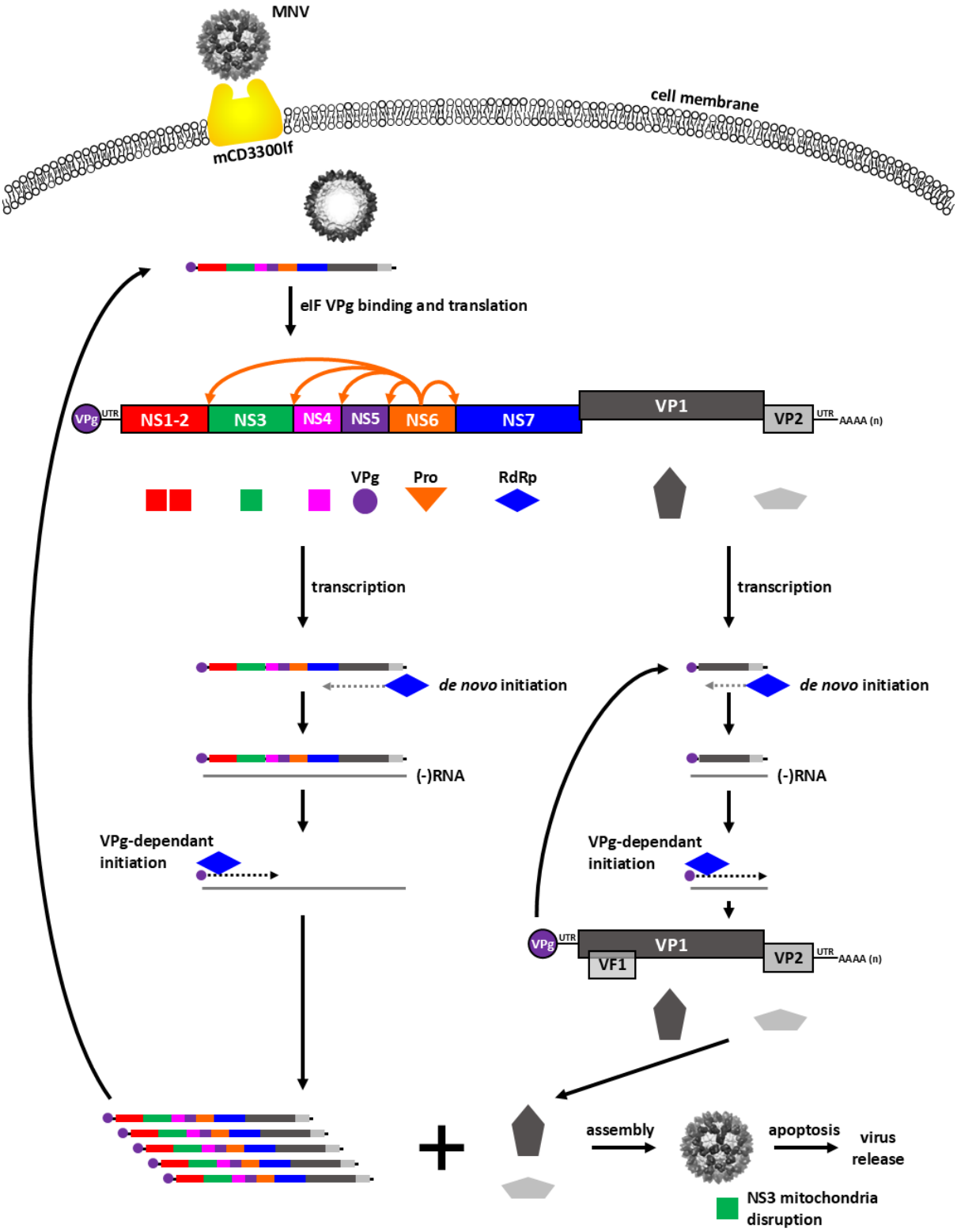

Figure 3: Murine norovirus replication cycle

The murine norovirus capsid binds the mCD300lf gaining entry to the cell. The VPg binds eIF initiating translation of the NS and structural proteins. With a translated RdRp present, transcription of first (-)RNA by *de novo* initiation and then (+)RNA by VPg-dependant initiation occurs. New VPg-linked genome can be utilised for further translation or packaged into the capsid proteins. The NS3 disrupts the mitochondrial membrane. Assembled virus is released by apoptosis.

Reverse genetics approach to MNV study

This study has made extensive use of reverse genetics for the generation of wild-type (WT) and mutant MNVs in the investigation of divalent cations. Throughout this body of work, the already established system has also been tested for its robustness and its flexibility in potentially generating an infectious virus with an inserted peptide-coding sequence. The technique used here is based upon decades of techniques developed for multiple viruses.

Reverse genetics can be defined as a method used to determine the function of a gene by its manipulation at a genetic level and analysing its phenotype. This is in contrast to the more traditional or "forward genetics" technique of phenotypic observation and subsequent sequencing to determine the gene function. A reverse genetics technique was first described by Taniguchi *et al.* (1978) in which a plasmid containing the genome of bacteriophage Qβ was introduced to its natural host, *Escherichia coli*, eliciting phage formation. A few years later, a similar approach was used to generate infectious poliovirus. A plasmid was constructed from three cDNA clones of the positive-strand RNA virus and transfected into mammalian cells (Racaniello & Baltimore, 1981).

This cloning and transfection technique was used for the study of hepatitis A virus (HAV), another non-enveloped, positive-sense, single-stranded RNA virus of the *Picornaviridae* family. Almost the entire 7.5 kb RNA genome was synthesised to cDNA and cloned into a plasmid (Ticehurst *et al.*, 1983). Cloning permitted for the determination of the genomic sequence of HAV (Cohen, Ticehurst, Purcell, *et al.*, 1987) and its comparison to an attenuated strain (Cohen, Rosenblum, *et al.*, 1987). Incidentally, this type of comparison between strains and why they may behave differently in cell culture is crucial when developing culturing techniques. It is also important to be aware of these differences in strains if one is chosen over the other for the basis of future investigations. A robust virus in cell culture can be very useful, but the reason for its fitness may impact its response in experimentation and should always be considered.

A reverse genetics technique was finally available for HAV by the middle of 1987 (Cohen, Ticehurst, Feinstone, *et al.*, 1987). The generation of infectious virus was only possible once the cDNA had been excised and cloned into an RNA transcription vector without cloning procedure artifact oligos. The transfection of this cDNA, and the transfection of IVT RNA transcripts yielded infectious virus. This same strain was used for the licensed HAV vaccine developed by the next decade (Innis, 1994). The success shown with HAV indicates the importance of a tool such as reverse genetics and subcloning techniques being available.

The techniques described by Cohen, Ticehurst, Feinstone, *et al.* (1987) are demonstrative that a non-enveloped, positive-sense, single-stranded RNA virus can be generated by both the transfection of the cDNA in an RNA transcription vector, and the transfection of IVT RNA. For MNV reverse genetics, both the transfection of a DNA construct and RNA can result in the production of virus. A reverse genetics technique was first described by Chaudhry *et al.* (2007) which required the infection of cells with poxvirus expressing T7 RNA polymerase and a subsequent transfection with a cDNA construct. The cell line, baby hamster kidney (BHK), is robust and permits for the transfection and replication of MNV, but not subsequent infection from generated virus. This can limit the yield of a transfection. This type of transfection also requires the prior infection of BHK with poxvirus in order to introduce T7 RNA polymerase as it is neither present in the cells, nor in the construct. Another reverse genetics technique was described at the same time and officially published within a few months of the former. Ward *et al.* (2007) described a DNA-based technique that required a transduction-based baculovirus delivery of viral cDNA under the control of a polymerase II promoter to human hepatoma cells. A second technique also described the transfection of the polymerase II promoter construct into human embryonic kidney (293T) cells. Yields were also limited due to the lack of reinfection from generated virus.

Further work was performed to address the possibility of an RNA transfection and eliminating the need for a prior poxvirus infection to introduce T7 RNA polymerase. The previous attempt of a synthetic RNA transfection failed to yield infectious virus due to inefficient capping in a co-transcription system

(Chaudhry *et al.*, 2007). Enzymatically capped RNA was transfected into robust cell lines, 293T and T7 RNA polymerase-expressing BHK (BSR-T7) cells resulting in an infectious yield (Yunus *et al.*, 2010). This method introduced a translation-ready genome transfection and eliminated the complication of a prior poxvirus infection, however the yield was still limited to a single round of replication. Neither cell line is susceptible to infection with MNV.

The permissive murine macrophage cell line RAW 264.7 was transfected by electroporation with enzymatically capped RNA resulting in virus that was infectious within the transfected cells for the first time (Yunus *et al.*, 2010). A translation-ready genome in a susceptible cell line is a necessary tool for the analysis or replication and growth kinetics, especially for the study of growth-defective MNVs. Although RAW 264.7 cells are a more delicate cell line, they have the advantage over the kidney cell lines in that they are naturally susceptible due to the mCD300lf receptor. The ability to recover genetically defined recombinant MNVs is vital to the study of both the structural and non-structural proteins.

This study has sought to utilise the reverse genetics techniques as described in Wobus *et al.* (2023) to generate both recombinant WT and recombinant MNV with mutations in functional epitopes for the assessment of noroviral entry and infection. Mutations were hereby inserted into the genome by site-directed mutagenesis using the technique described by Liu & Naismith (2008), see **Figure 4**. Expanding on previous thesis work (Lane, 2021) that utilised this technique to introduce the MNV-1 VP1 Ab escape mutations V378F and L386F, and recent publications exploring the function of GCDCA in relation to MNV infection (Creutznacher *et al.*, 2022; Williams *et al.*, 2021a), this study aims to expand our understanding of the role of other ligands, divalent cations, in MNV infection. Divalent cations were demonstrated to bind at noted amino acids (D410 and D440) on the MNV VP1 (Nelson *et al.*, 2018). This study explores these two binding sites through the generation of WT MNV-1.CW1 and two mutant recombinant MNVs. The effect of GCDCA on MNV infection was reassessed, controlling for divalent cation concentration.

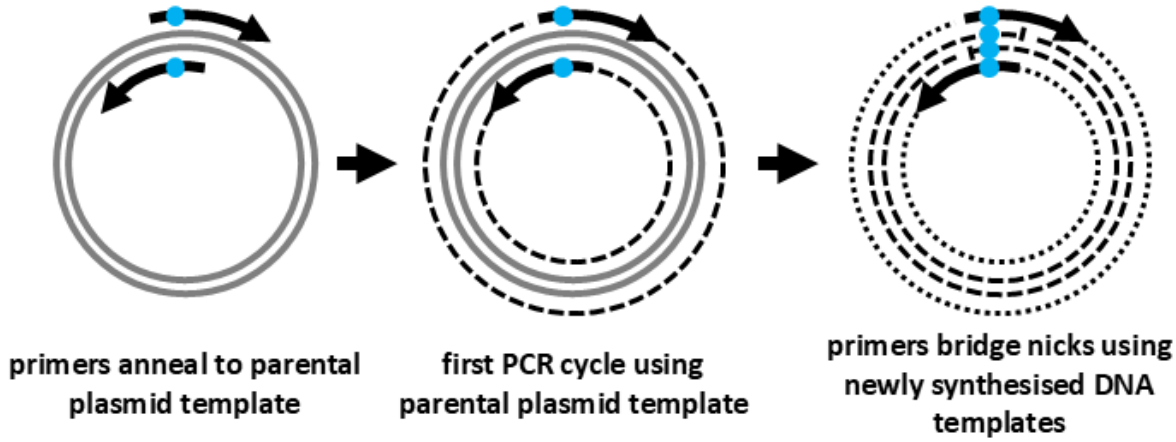

Figure 4: Site-directed mutagenesis technique utilising overlapping and non-overlapping primer/template regions

Based on the technique described by Liu & Naismith (2008), specially designed primers anneal to a parental plasmid template and can be used for the first PCR amplification cycle. For subsequent amplification rounds, the newly synthesised DNA with the introduced mutation can be used as template with the nicks in the DNA bridged by the primers. Parental plasmid template shown in grey. Newly synthesised DNA shown in black with the first cycle production in large dashes and the subsequent cycles shown in small dashes. Mutation location highlighted in blue.

This study has also intended to expand upon the knowledge of an RNA-based reverse genetics system and recombinant cell line previously developed (Lingemann, 2020). Although a reliable transfection protocol has been developed and described (Wobus *et al.*, 2023), an extensive transfection progression analysis must be described. The genetically modified cell line Huh7$^{mCD300lf\text{-}Sec61b}$ containing not only the receptor mCD300lf, but also a GFP-based reporter system (Lingemann, 2020), was assessed by

extensive microscopy. Transfection progression was monitored for WT, VP1 single amino acid mutants, and mutations in NS6 and NS7, with the aim of describing any perceivable visual differences and a quantification of results.

Previous work

While multiple versions of MNV reverse genetics systems had been established in the lab and elsewhere (Chaudhry *et al.*, 2007; Ward *et al.*, 2007; Yunus *et al.*, 2010), they lacked reproducibility and yield. The RNA-based reverse genetics system (**Figure 5**) had been the most reliable and yielding (Wobus *et al.*, 2023). The establishment of a transfectable cell line that was susceptible to MNV infection by stably expressing the recently identified entry receptor reproducibly allowed rescue of recombinant virus at titres comparable to the natural infection (Lingemann, 2020).

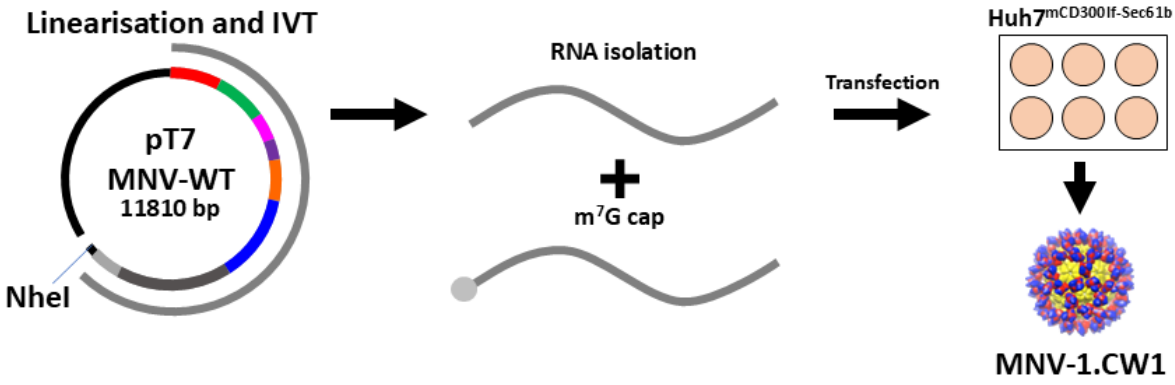

Figure 5: Reverse genetics technique in Huh7$^{mCD300lf\text{-}Sec61b}$

RNA-based reverse genetics technique for the generation of recombinant MNV-1.CW1. The pT7:MNV\3'RZ plasmid is linearised with NheI at the end of the poly-A tail. The linear DNA is used as a template for IVT. The RNA is isolated and capped with m^{7}G before transfection with Lipofectamine™ MessengerMAX™ into Huh7$^{mCD300lf\text{-}Sec61b}$ cells. After incubation for 48 hours, the cells are lysed by freezing at -80°C to release all remaining virus.

Aims

Aim 1: Expand and optimise an RNA-based MNV reverse genetics system with a reporter for infection

Aim 1.1: Cellular reporter – Implement an integrated cellular GFP reporter into an RNA-based MNV reverse genetics platform to monitor protease production from transfected m^{7}G-capped RNA

The recombinant cell line Huh7$^{mCD300lf\text{-}Sec61b}$ previously developed by Lingemann (2020) was used to generate recombinant virus (**Figure 5**), and later extended to include a reporter to monitor the production of protease in cells transfected with m^{7}G-capped MNV-1.CW1 RNA (**Figure 6**). This system was yet lacking robustness and a negative control for the protease reporter as there was no difference in nuclear shift between WT MNV-1 and recombinant virus with a dysfunctional RdRp containing a frame-shift (F/S). To introduce a functional negative control, a single amino acid change from a two-base substitution in the protease NS6, C139A, was introduced by site-directed mutagenesis on a plasmid containing a DNA copy of the MNV-1.CW1 genome. *In vitro* transcribed and capped WT and RNA

with mutations in the NS6 (protease) and NS7 (RdRp) regions were then analysed for the GFP-shift reporter.

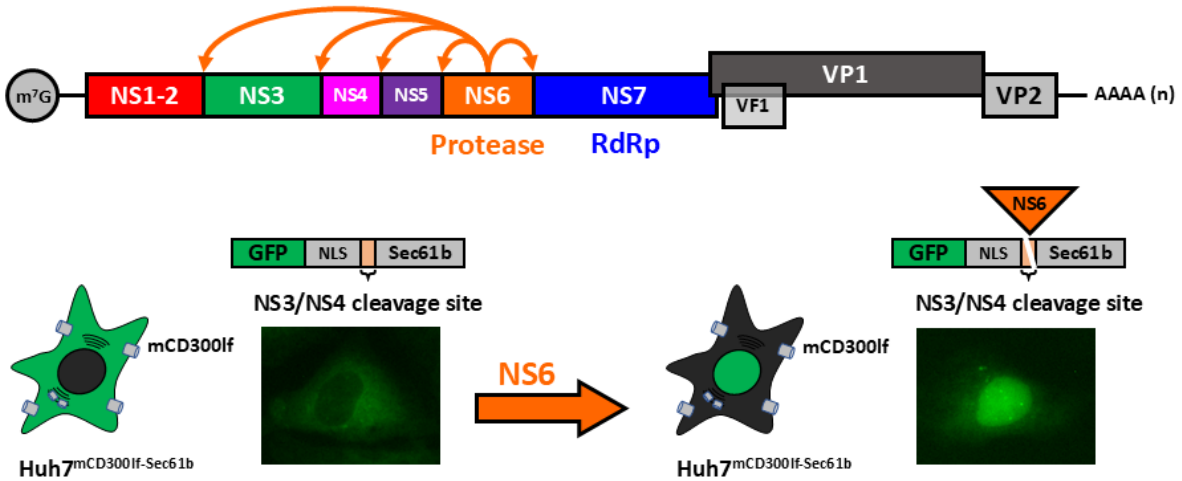

Figure 6: Reverse genetics nuclear GFP shift mechanism in Huh7$^{mCD300lf\text{-}Sec61b}$

The GFP nuclear shift mechanism present in Huh7$^{mCD300lf\text{-}Sec61b}$ cells. Capped and transfected RNA is translation ready, permitting the generation of protease. The MNV-1.CW1 protease can recognise the HNoV NS3/NS4 cleavage site present in the Huh7$^{mCD300lf\text{-}Sec61b}$ cells. This cleaves off the ER localisation signal, Sec61b, exposing the nuclear localisation signal. The nuclear localisation signal drags the GFP into the nucleus. This change can be observed using fluorescence microscopy.

Aim 1.2: Viral reporter – Find a tolerant insertion site within the MNV-1.CW1 genome that may permit the addition of a protein

To find a tolerant insertion site within the MNV-1.CW1 genome, a short genetic sequence coding for haemagglutinin (HA)-FLAG was inserted into the ORF1 between two NS proteins replicating a protease cleavage site that would act as a basis for future insertion of larger tagged proteins, reporters, or selective markers.

Aim 2: Analyse the role of ions and bile acid in MNV infection using reverse genetics

Aim 2.1: Investigate a potential synergistic effect of bile acid and divalent metal ions on antibody escape

Nuclear magnetic resonance (NMR) data revealed a synergistic role of divalent metal cations with bile acid in capsid plasticity (Maass *et al.*, 2024). Recombinant MNV-1 was used in functional neutralising MAb and polyclonal Ab assays to investigate the simultaneous presence of divalent cations and GCDCA in MNV infection.

Aim 2.2: Reverse genetics of bile acid and ion binding sites

Divalent cations and the bile acid GCDCA have been shown to bind the MNV capsid protein VP1 (Nelson *et al.*, 2018). Building upon previous work showing that bile acid GCDCA impacts MNV infection and antibody binding (Lane, 2021), the role of metal ions in infection was now investigated in more detail. Reverse genetics was used to generate recombinant MNV-1 with (and without) mutations in metal (D410A and D440A) and bile acid (Y250A) binding sites. Recombinant viruses were then investigated in functional assays with regards to infection and escape from neutralising antibodies.

Materials and Methods

Materials

Plastics

Consumable	Manufacturer	Catalogue Number
6-well plate	Greiner/CELLSTAR®	657160
24-well plate	TPP™	92024
96-well plate	TPP™	92096
Cell culture filter flask, 25 cm^2	TPP™	90026
Cell culture filter flask, 75 cm^2	TPP™	90076
Cell culture filter flask, 150 cm^2	TPP™	90151
Cell scraper	SARSTEDT	83.3952
Centrifuge tube, 15 ml	Greiner/CELLSTAR®	7608487
Centrifuge tube, 50 ml	Greiner/CELLSTAR®	6052080
Cryo tube, 1.5 ml	TPP™	89020
Microcentrifuge tube, 1.5 ml	SARSTEDT	72.690.001
Microcentrifuge tube, 2.0 ml	SARSTEDT	72.691
Micro pipette filter tips, 10 µl	SARSTEDT/Biosphere®	70.3010.255
Micro pipette filter tips, 100 µl	SARSTEDT/Biosphere®	70.3030.255
Micro pipette filter tips, 200 µl	SARSTEDT/Biosphere®	70.3031.255
Micro pipette filter tips, 1250 µl	SARSTEDT/Biosphere®	70.1186.210
PCR tube strip	Biozym	710975
Screw cap micro tube, 2 ml	SARSTEDT	72.694.005
Syringe filter with Luer-Lock, 0.2 µm	SARSTEDT	83.1826.102
Syringe with Luer-Lock	Braun Petzold/Omnifix®	4616200V
Vacuum filter, Filtermax™	TPP™	99505

Kits

Consumable	Manufacturer	Catalogue Number
Ambion™ MAXIscript™ T7 *In Vitro* Transcription Kit	Invitrogen™/Thermo Fisher Scientific	AM1314M
Direct-zol RNA Miniprep Plus	Zymo Research	R2073
Montage® Gel Extraction Kit	Merck/Millipore®/Sigma-Aldrich	LSKGEL050
NucleoBond® PC 100, midi-prep kit	MACHEREY-NAGEL	740573.100
NucleoSpin® Gel and PCR Clean-up kit	MACHEREY-NAGEL	740609.50
pGEM®-T Vector Systems	Promega	A3600
QIAquick® Gel Extraction Kit	QIAGEN	28706
ScriptCap™ m^7G Capping System	CELLSCRIPT™	C-SCCE0625

Chemicals

Consumable	Manufacturer	Catalogue Number
Agarose Standard	Carl Roth	3810.3 9012-36-6 (CAS)
Ammonium sulphate, $(NH_4)_2SO_4$, MW=132.14 g/mol	Carl Roth	3746.1 7783-20-2 (CAS)
Ampicillin sodium salt, $C_{16}H_{18}N_3NaO_4S$, MW=371.39 g/mol	Merck/Sigma-Aldrich	A9518 69-52-3 (CAS)
Bacto™-Tryptone	Becton Dickinson/Thermo Fisher Scientific	211705
Bacto™ Yeast Extract	Becton Dickinson/Thermo Fisher Scientific	212750
D(+)-Glucose, MW=180,16 g/mol	Carl Roth	X997.2 50-99-7 (CAS)
di-Sodium hydrogen phosphate, Na_2HPO_4, MW=141.96 g/mol	Carl Roth	P030.1 7558-79-4 (CAS)
Ethanol ≥99,8 %, p.a., C_2H_6O, MW=46.07 g/mol	Carl Roth	9065.4 64-17-5 (CAS)
Glycochenodeoxycholic acid (GCDCA), $C_{26}H_{42}NNaO_5$, MW=471.61 g/mol	Merck/Sigma-Aldrich	G0759 16564-43-5 (CAS)
Hydrochloric acid ≥32 %, p.a., HCl, MW=36.46 g/mol	Carl Roth	P074.4 7647-01-0 (CAS)
IPTG, MW=238.30 g/mol	Carl Roth	CN08.2 367-93-1 (CAS)
Isopropanol ≥99,8 %, p.a., C_3H_8O, MW=60.10 g/mol	Carl Roth	6752.4 67-63-0 (CAS)
LB Agar (Luria/Miller)	Carl Roth	X969.2
LB Broth (Luria/Miller)	Carl Roth	X968.2
Magnesium chloride, $MgCl_2$, MW=95.21 g/mol	Merck/Sigma-Aldrich	M8266 7786-30-3 (CAS)
Magnesium sulphate heptahydrate, $MgSO_4 \cdot 7H_2O$, MW=246.48 g/mol	Carl Roth	P027.1 10034-99-8 (CAS)
ortho-Phosphoric acid, H_3PO_4, MW=98.00 g/mol	Carl Roth	9079.1 7664-38-2 (CAS)
Potassium chloride, KCl, MW=74.56 g/mol	Carl Roth	6781.1 7447-40-7 (CAS)
Potassium dihydrogen phosphate, KH_2PO_4, MW=136.09 g/mol	Carl Roth	3904.1 7778-77-0 (CAS)
SDS Pellets, $C_{12}H_{25}NaO_4S$, MW=288.38 g/mol	Carl Roth	CN30.3 151-21-3 (CAS)
Sodium chloride, NaCl, MW=58.44 g/mol	Carl Roth	3957.2 7647-14-5 (CAS)
Sodium dihydrogen phosphate monohydrate, $NaH_2PO_4 \cdot H_2O$, MW=137.99	Carl Roth	K300.3 10049-21-5 (CAS)
Sodium hydrogen carbonate, $NaHCO_3$, MW=84.01 g/mol	Fluka	71628 144-55-8 (CAS)

Sodium hydroxide, NaOH, MW=40.0 g/mol	Carl Roth	P031.2 1310-73-2 (CAS)
Store-bought bleach: • Sodium hypochlorite, NaOCl, 4.5 g per 100 g • Soap	Domestos	--
X-β-Gal, MW=408.6 g/mol	Carl Roth	2315.3 7240-90-6 (CAS)

Medium

Eukaryotic cell culture medium and reagents

Consumable	**Manufacturer**	**Catalogue Number**
Avicel® RC-581	International Flavors & Fragrances (IFF)	9004-34-6 (CAS)
DMEM, high glucose	Gibco™/Thermo Fisher Scientific	41965062
Erythrosine B	Sigma-Aldrich	16423-68-0 (CAS)
Foetal Bovine Serum Advanced (FBS Advanced), Collected in South America	Capricorn Scientific	FBS-11A Lot: CP22-5445
L-glutamine (100×) • 29.2 g/l L-glutamine	c.c.pro	Z-10-M
MEM Non-essential Amino Acids Solution (100×) • 0.75 g/l Glycine • 0.89 g/l L-Alanine • 1.50 g/l L-Asparagine Monohydrate • 1.33 g/l L-Aspartic Acid • 1.47 g/l L-Glutamic Acid • 1.15 g/l L-Proline • 1.05 g/l L-Serine	Capricorn Scientific	NEAA-B
MEM, powder	Gibco™/Thermo Fisher Scientific	61100087
Opti-MEM™, Reduced Serum Medium	Gibco™/Thermo Fisher Scientific	31985070
Penicillin/Streptomycin Solution (100×) • 10^7 U/l Penicillin G Sodium • 10000 mg/l Streptomycin Sulphate • 9000 mg/l NaCl	Capricorn Scientific	PS-B
Sodium bicarbonate, 7.5% $NaHCO_3$	c.c.pro	Z-30-L
Trypsin – EDTA Solution 10× • 2000 mg/l EDTA 4Na monohydrate • 8500 mg/l Sodium chloride • 5000 mg/l Porcine trypsin (1:250)	Sigma-Aldrich	59418C 9002-07-7 (CAS)

Medium	Components
DMEM-5	DMEM, high glucose 5% (v/v) FBS Advanced 1% Non-essential Amino Acids 1% Penicillin/Streptomycin 1% L-glutamine
DMEM-10	DMEM, high glucose 10% FBS Advanced 1% Non-essential Amino Acids 1% Penicillin/Streptomycin 1% L-glutamine
2× MEM	Per 1000 ml: 19.06 g MEM powder 58 ml 7.5% $NaHCO_3$ pH adjustment to 7.4 (HCl or NaOH) ddH_2O up to 1000 ml Sterile-filtered with 0.2 µm membrane
2× MEM with supplements	2× MEM 20% FBS Advanced 2% Non-essential Amino Acids 2% Penicillin/Streptomycin 2% L-glutamine
MEM/Avicel	One part 2× MEM with supplements, not autoclaved One part 2.4% Avicel in ddH_2O, autoclaved

Bacteria cell culture

Medium	Components
LB-Agar, 0.1% Ampicillin	LB Agar (Luria/Miller), 40 g per 1 l 0.1% Ampicillin
LB-Agar, 0.1% Ampicillin, 100 mM IPTG, 40 mg/ml X-β-Gal	LB-Agar, 0.1% Ampicillin 100 mM IPTG, 40 mg/ml X-β-Gal spread on agar immediately prior to bacterial plating
Lysogeny Broth (LB), 0.1% Ampicillin	LB Broth (Luria/Miller), 25 g per 1 l 0.1% Ampicillin
Super Optimal Broth with Catabolite repression (SOC)	2% Bacto™-Tryptone 0.5% Bacto™ Yeast Extract 10 mM NaCl 2.5 mM KCl pH adjustment to 7.5 (1 M NaOH) 10 mM $MgCl_2$ 10 mM $MgSO_4 \cdot 7H_2O$ 20 mM D(+)-Glucose ddH_2O up to 100 ml Sterile-filtered with 0.2 µm membrane

Reagents and enzymes

Reagents – Commercial Products

Consumable	Manufacturer	Catalogue Number
GlycoBlue™ Coprecipitant	Invitrogen™/Thermo Fisher Scientific	AM9515
Lipofectamine™ MessengerMAX™ Transfection Reagent	Invitrogen™/Thermo Fisher Scientific	LMRNA003
MIDORI Green Xtra	NIPPON Genetics EUROPE	MG10

Reagent	Components
NaOH washing, RNase/DNase decontamination solution	15% Store-bought bleach (Domestos) 0.05% SDS Pellets 1.0% Sodium hydroxide 90.0 mM Sodium hydrogen carbonate Dissolved in deionised H_2O

Enzymes and nucleotides

Consumable	Manufacturer	Catalogue Number
dNTP Set (100 mM)	Invitrogen™/Thermo Fisher Scientific	10297018
GeneRuler 1 kb Plus DNA Ladder	Thermo Fisher Scientific	SM1331
Pfu-X Polymerase	Jena Bioscience	PCR-207L
T4 DNA Ligase	New England Biolabs	M0202L
Taq DNA Polymerase with ThermoPol® Buffer	New England Biolabs	M0267L

Buffers

Buffer	Components
1× Phosphate-Buffered Saline (PBS) pH 7.4	137 mM NaCl 4.3 mM Na_2HPO_4 2.7 mM KCl 1.5 mM KH_2PO_4 pH adjustment to 7.4 (HCl or NaOH) usually prepared from a 10× filtered stock solution
100 mM Sodium phosphate buffer pH 7.4	Per 50 ml: 50 mM Na_2HPO_4 (3.87 ml 1 M solution) 50 mM NaH_2PO_4 (1.13 ml 1 M solution) ddH_2O up to 45 ml pH adjustment to 7.4 (H_3PO_4 or NaOH) ddH_2O up to 50 ml Sterile-filtered with 0.2 µm membrane
1× Modified Tris-acetate-EDTA (TAE) Buffer pH 8.0	Diluted from 50× Modified TAE Buffer from Montage® Gel Extraction Kit, Merck/Millipore®/Sigma-Aldrich (LSKGEL050): 40 mM Tris-acetate 0.1 mM Na_2EDTA (pH 8.0), modified Added 0.001% MIDORI Green Xtra

Bacteria

Strain	Species	Usage
DH5α	*Escherichia coli K12 derived*	Cloning, blue/white selection
HB101	*Escherichia coli K12 derived*	Cloning

Eukaryotic cells

Name	Type	Origin
BV-2	C57BL/6 (murine) brain microglial cells	Christiane Wobus
Huh7$^{mCD300lf\text{-}Sec61b}$	Human hepatocyte-derived	Lab-derived (Lingemann, 2020).

Viruses

Name	Plasmid derived from	Average stock titre [$TCID_{50}$/ml]
WT	#245	1×10^7 to 1×10^8
VP1-D410A	#340	1.26×10^8
VP1-D440A	#341	1.08×10^6
VP1-Y250A *	#348	2.60×10^3
VP1-S504C	#395	7.32×10^7
VP1-D440R (attempted D440C)	#356	1.76×10^8
NS1-2/NS3 felq/GP *	#456	1.19×10^6 (transfection titre)
NS1-2/NS3(HA-FLAG[LQGP]) *	#422	1.76×10^7

* indicates the genomic sequence is unconfirmed

Proprietary equipment

Equipment	Manufacturer	Function
Amersham™ ImageQuant™ 800	Cytiva	Western blot imaging
Avanti JXN-30 with JA-14 rotor	Beckman Coulter	Centrifuge
Axio Observer. Z1, Light source HXP 120, Power supply 232	ZEISS	Fluorescence microscope
Axio Vert.A1	ZEISS	Light microscope
Eppendorf® Centrifuge 5804R	Eppendorf®	Centrifuge
Eppendorf® Microcentrifuge 5417R	Eppendorf®	Centrifuge
GelDoc FastGene Blue/Green LED Transilluminator	NIPPON Genetics EUROPE	Nucleic acid gel imaging
Infors HT Multitron	Infors HT	Incubator shaker
NanoDrop™ One^C	Thermo Fisher Scientific	Spectrophotometer
NuAire NU-5820 CO_2 Incubator	ibs tecnomara	CO_2 and humidity incubator

Enzymes from NEB

NEB Enzyme	Buffer	Product Code
BamHI-HF	rCutSmart	R3136S
DpnI	rCutSmart	R0176S
EcoNI	rCutSmart	R0521S
EcoRV-HF	rCutSmart	R3195L
FseI	rCutSmart	R0588S
HindIII-HF	rCutSmart	R3104S
NdeI	rCutSmart	R0111S
NheI-HF	rCutSmart	R3131S
NotI-HF	rCutSmart	R3189S
PmlI	rCutSmart	R0532S
SpeI-HF	rCutSmart	R3133L
XhoI	rCutSmart	R0146S
Quick CIP	rCutSmart	M0525S

Methods

Cloning strategies

Plasmid designs

Plasmids for MNV RNA-based reverse genetics (#245 and #246) and cloning (#324) were available. Additional plasmids were constructed for the purpose of mutagenesis on a smaller plasmid to then reintroduce the mutation back into the full plasmid using subcloning. Alternatively plasmids were synthesised by BioCat GmbH (#399) for the ease of direct cloning and site-directed mutagenesis.

Table 1: Table of plasmids

Plasmid #	Plasmid name	Length (bp)	Function
#27	pRevGen-MNV-1	10827	MNV DNA RevGen
#245	pT7:MNV\3'RZ	11810	MNV RNA RevGen
#246	pT7:MNV\3'RZ(NS7-F/S)	11806	MNV RevGen (+)con.
#322	pBluescriptSK(-)	2958	Cloning
#324	pT7:MNV-DEcoRV-PmlI	7626	Cloning
#338	pT7:MNV-DEcoRV-PmlI-D410A	7626	Cloning/mutagenesis
#339	pT7:MNV-DEcoRV-PmlI-D440A	7626	Cloning/mutagenesis
#340	pT7:MNV\3'RZ-D410A	11810	MNV RevGen (mut.)
#341	pT7:MNV\3'RZ-D440A	11810	MNV RevGen (mut.)
#344	pT7:MNV-DEcoRV-PmlI-Y250A	7626	Cloning/mutagenesis
#348	pT7:MNV\3'RZ-Y250A	11810	MNV RevGen (mut.)
#353	pT7:MNV-DEcoRV-PmlI-D440C	7626	Cloning/mutagenesis
#356	pT7:MNV\3'RZ-D440C	11810	MNV RevGen (mut.)
#367	pT7:MNV-DEcoRV-PmlI-S504C	7626	Cloning/mutagenesis
#376	pT7:MNV\3'RZ(NS6-C139A)	11810	MNV RevGen (-)con.
#377	pGEM-T-NS5/NS6	4154	Cloning
#378	pGEM-T-MNV1.CW1-NS6-C139A	4154	Cloning/mutagenesis
#395	pT7:MNV\3'RZ-S504C	11810	MNV RevGen (mut.)
#398	pBluescriptSK(-)fragment[GV-CW1-NS]	6595	Cloning
#399	pUC18-CW1[NS1-2/3-HA/FLAG-NotI/NdeI-FseI/EcoNI]	3259	Cloning/mutagenesis
#404	pBluescriptSK(-)fragment[GV-CW1-NS]-NS1-2/NS3(HA/FLAG)	6691	Cloning
#406	pT7:MNV\3'RZ-NS1-2/NS3(HA/FLAG)	11906	MNV RevGen (mut.)
#421	pBluescriptSK(-)fragment[GV-CW1-NS]-NS1-2/NS3(HA-FLAG[LQGP])	6691	Cloning/mutagenesis
#422	pT7:MNV\3'RZ-NS1-2/NS3(HA-FLAG[LQGP])	11906	MNV RevGen (mut.)
#447	pBluescriptSK(-)fragment[GV-CW1-NS]-NS1-2/NS3(felq/GP)	6595	Cloning/mutagenesis
#448	pBluescriptSK(-)fragment[GV-CW1-NS]-NS1-2/NS3(WQlq/GP)	6595	Cloning/mutagenesis
#449	pBluescriptSK(-)fragment[GV-CW1-NS]-NS3/NS4(FeLQ/gp)	6595	Cloning/mutagenesis
#450	pBluescriptSK(-)fragment[GV-CW1-NS]-NS3/NS4(FGLQ/gp)	6595	Cloning/mutagenesis
#451	pBluescriptSK(-)fragment[GV-CW1-NS]-NS4/NS5(felq/GK)	6595	Cloning/mutagenesis
#452	pBluescriptSK(-)fragment[GV-CW1-NS]-NS4/NS5(felq/Gp)	6595	Cloning/mutagenesis
#453	pBluescriptSK(-)fragment[GV-CW1-NS]-NS5/NS6(felq/gP)	6595	Cloning/mutagenesis

#454	pBluescriptSK(-)fragment[GV-CW1-NS]-NS6/NS7(fElQ/GP)	6595	Cloning/mutagenesis
#456	pT7:MNV\3'RZ-NS1-2/NS3(felq/GP)	11810	MNV RevGen (mut.)
#457	pT7:MNV\3'RZ-NS1-2/NS3(WQlq/GP)	11810	MNV RevGen (mut.)
#458	pT7:MNV\3'RZ-NS3/NS4(FeLQ/gp)	11810	MNV RevGen (mut.)
#459	pT7:MNV\3'RZ-NS3/NS4(FGLQ/gp)	11810	MNV RevGen (mut.)
#460	pT7:MNV\3'RZ-NS4/NS5(felq/GK)	11810	MNV RevGen (mut.)
#461	pT7:MNV\3'RZ-NS4/NS5(felq/Gp)	11810	MNV RevGen (mut.)
#462	pT7:MNV\3'RZ-NS5/NS6(felq/gP)	11810	MNV RevGen (mut.)
#463	pT7:MNV\3'RZ-NS6/NS7(fElQ/GP)	11810	MNV RevGen (mut.)

Primer designs

Primers used for mutagenesis of a full-length plasmid were designed based on the methods outlined by Liu & Naismith (2008). Mutagenesis primers were designed with an overlapping region and two non-overlapping regions with the introduced changes contained within the overlapping region. Crucially, the non-overlapping regions were 5-10°C higher in T_m than the overlapping region.

Table 2: Table of mutagenesis primers

Primer name	Sequence	T_m (°C)	T_m (overlap)	T_m (non-overlap)
MSL-338	GAATACAACGcTGGGCTACTGGTTCCCCTTGC	67.0	45.3	50.8
MSL-339	CCCAgCGTTGTATTCAGGGATGGTGTCCTGAAAAC	66.4		53.8
MSL-340	CAGATCGcCACCGCTGACGCCGCAGCAGAGGCG	75.6	54.9	63.0
MSL-341	CAGCGGTGgCGATCTGACGCATGTAGGTCCGGAACC	72.4		58.6
MSL-344	CCGGTCgcTGGTCTCTTGGTGGACCCATCCCTCCCCTCAAATCCC	75.4	59.2	64.7
MSL-345	CCAAGAGACCAgcGACCGGGGCAGGCCAACGTGCGTGCGTG	78.3		68.0
MSL-354	CAGATCtgCACCGCTGACGCCGCAGCAGAGGC	73.2	51.9	60.2
MSL-355	CAGCGGTGcaGATCTGACGCATGTAGGTCCGGAACCTC	71.5		60.4
MSL-408	GGCGACgcTGGCTGTCCCTATGTTTA TAAGAAGGGTAACACCTGGGTTG	71.7	55.0	62.1
MSL-409	CAGCCAgcGTCGCCCGGGATGGTCCCGAGGTCCTG	76.3		62.5
MSL-461	CCTTgGagCTGCCATTCCATATGCTTGTCGTCATCGTCTTTGTAGTCAGC	71.0	54.8	62.1
MSL-462	GGAATGGCAGctCcAAGGGCCCTTCGACCTTGCTCTTGACG	73.4		62.0
MSL-504	CCCTTgGagCTcgaATTCCCCGAAGATAGAGATCATCCAGTTGGTCACATC	70.7	54.5	61.5
MSL-505	GGAATtcgAGctCcAAGGGCCCTTCGACCTTGCTCTTGACGTG	72.6		61.6

MSL-506	CCCTTgGagCTGCCATTCCCCG AAGATAGAGATCATCCAGTTG GTCAC	71.6	54.8	61.5
MSL-507	GAATGGCAGctCcAAGGGCCCT TCGACCTTGCTCTTGACGTG	73.2		61.6
MSL-508	GACCggGccCTGGAGctCGAAAT CATCATGGCGCTCATGGACAA GAGCAACCGCTCTC	77.4	63.7	69.4
MSL-509	CGagCTCCAGggCccGGTCTATG ACTTTGATGCCGGCAAGATCA CCGCCTTCAAAGCCATG	77.5		70.1
MSL-510	GACCggGccCTGGAGGCCGAAA TCATCATGGCGCTCATGG	74.9	55.3	62.8
MSL-511	CTCCAGggCccGGTCTATGACT TTGATGCCGGCAAGATCACCG	73.5		62.8
MSL-512	CTTTCCCTgAagcTcGaACCACC CATCATCGTCATCCTCAAAGA TGTCAAAGGATCCAG	72.0	57.6	64.3
MSL-513	GTGGTtCgAgctTcAGGGAAAGA AGGGCAAGAACAAGAAGGGC CGGG	73.7		64.9
MSL-514	CTTCggTCCCTgAagcTcGaACCA CCCATCATCGTCATCCTCAAA GATGTCAAAGGATCCAG	73.5	59.4	66.2
MSL-515	GTtCgAgctTcAGGGAccGAAGG GCAAGAACAAGAAGGGCCGG GGGC	76.5		67.6
MSL-516	GGGcCCTgtAAcTcGAaCTTCTC GCCGTAGTCGACCTGGCGGTC	74.7	57.0	66.4
MSL-517	GAAGtTCgAgTTacAGGgCCCAG TCTCCATCTGGTCCCGTGTTGT GCAG	73.5		65.3
MSL-518	CCTGcAACTCgAaAGCCTCAAG TGTGGGTTCTCCGTGAGTGGC G	73.6	55.5	64.6
MSL-519	GAGGCTtTcGAGTTgCAGGGAC CCCCCATGCTTCCCCGC	75.3		64.1

Primers used for amplifying fragments from plasmids or used for sequencing analysis were designed to be between 15 and 30 nucleotides in length, with the exception of ST-280 as it binds to the MNV poly-A tail. Primers used for fragment amplification were designed with a similar T_m.

Table 3: Table of subcloning primers

Primer name	**Sequence**	**T_m (°C)**
ST-19	AGTCAGTGAGCGAGGAAGCGG	60.7
AS-85	CATGTTCTGGCGTACCTCGC	57.9
MST-112	TCTCTGGGGCTCTGACCTTGGC	62.0
ST-280	TTTTTTTTTTTTTTTTTTTTTTTTAAAATGCATCTAACTACC ACAAAG	58.8
MSL-410	GATCGTGGATACACCTACCGTG	56.5
MSL-411	GAGATAGGCTGGCTCCCAAG	56.0

Table 4: Table of sequencing primers

Primer name	Sequence	T_m (°C)
ST-4	GTGCGCAACACAGAGAAACG	57.2
ST-5	CGGGCTGAGCTTCCTGC	57.4
ST-10	TAATACGACTCACTATAGGG	46.8
ST-14	GGAAACAGCTATGACCATG	50.1
AS-79	GGCCGTGAGTTGGTTCTCCAG	59.5
AS-84	CTGGCCGCTGGCCTCAGAG	61.8
AS-85	CATGTTCTGGCGTACCTCGC	57.9
TK-88	CCCAGTCACGACGTTGTAAAACG	58.6
TK-89	AGCGGATAACAATTTCACACAGG	55.6
MR-106	TTGTTTGAGCATTCGGCCTGT	57.3
MR-109	AGGATGAGTGATGGCGCAGCGCC	65.7
MST-112	TCTCTGGGGCTCTGACCTTGGC	62.0
MST-120	GCACAAACAGCCCGGGTGATGAG	62.5
MST-154	CAATCGGGCACCGGTGAGGTGGCG	67.9
ML-240	GCCCAGTCAGGGTGTTCCTG	59.1
ML-251	CTCTGGGATGATTTCGGCATG	55.4
ML-252	TTCATCGTACTCCTCATCCGTG	55.8
ST-280	TTTTTTTTTTTTTTTTTTTTTTTTTTAAAATGCATCTAACTACC ACAAAG	58.8
ST-286	ATCCCTCGAGGGTCCCATTCGC	62.2
MSL-358	GGGCTTGAATTTGCGTTGCAAG	58.2
MSL-410	GATCGTGGATACACCTACCGTG	56.5
MSL-411	GAGATAGGCTGGCTCCCAAG	56.0
MSL-469	CAATGCCCTGATCTTGCTTG	53.9
MSL-471	CTGAGAGCCCTGTTGTTGATG	55.2

Site-directed mutagenesis of a full-length plasmid

The mutagenesis of plasmids #324, #377 and #398 was adapted from a protocol by Jena Bioscience for Pfu-X. Primers were designed as described by Liu & Naismith (2008). A volume of 50 µl was used per PCR reaction.

Reagent	Stock Concentration	Final Concentration
Pfu-X Buffer	10×	1×
dNTPs	10 mM	0.4 mM
Forward Primer	25 µM	0.4 µM
Reverse Primer	25 µM	0.4 µM
Template DNA	100 ng/µl	100 ng
Pfu-X Polymerase	2.5 U/µl	2.5 U
$ddH_2O_{RNase\text{-}free}$	--	--

PCR Program		
Temperature	**Time**	**Cycles**
94°C	02:00	1×
94°C	00:30	25×
50°C	00:45	
72°C	15:00	
72°C	30:00	1×
16°C	∞	

Template plasmid was digested with DpnI for 1 hour at 37°C and transformed into either *E. coli* HB101 or DH5α.

Taq polymerase PCR for pGEM®-T cloning

A fragment between NS4 and NS7 was amplified from plasmid pT7:MNV\3'RZ (#245) to insert into a pGEM®-T vector. The fragment was amplified using Taq polymerase to introduce adenine overhangs.

Reagent	**Stock Concentration**	**Final Concentration**
ThermoPol Reaction Buffer	10×	1×
dNTPs	10 mM	0.2 mM
Forward Primer (MSL-410)	25 µM	0.5 µM
Reverse Primer (MSL-411)	25 µM	0.5 µM
Template DNA	40 ng/µl	40 ng
Taq DNA Polymerase	5 U/µl	1 U
$ddH_2O_{RNase\text{-}free}$	--	--

PCR Program		
Temperature	**Time**	**Cycles**
95°C	00:30	1×
95°C	00:30	25×
51°C	00:45	
68°C	01:30	
68°C	05:00	1×
16°C	∞	

The PCR product was run by gel electrophoresis, extracted and purified using the QIAquick® Gel Extraction Kit. The fragment was ligated into pGEM®-T using the pGEM®-T Vector Systems kit.

Taq polymerase PCR for determining cloned insert presence after ligation reaction and transformation of plasmids in bacterial colonies

Cloned inserts were checked for their presence in the plasmid by way of a colony PCR using Taq DNA polymerase (NEB). Samples were taken either directly from the bacterial colony and added to the reaction mix, or 1 µl from a mini-prep was added. A suitable plasmid was selected as a positive control depending on the primers used for the tested samples.

Reagent	**Stock Concentration**	**Final Concentration**
ThermoPol Reaction Buffer	10×	1×
dNTPs	10 mM	0.2 mM
Forward Primer	25 µM	0.5 µM
Reverse Primer	25 µM	0.5 µM
Template DNA	100 ng/µl	100 ng
Taq DNA Polymerase	5 U/µl	1 U
$ddH_2O_{RNase\text{-}free}$	--	--

Temperature and elongation times were adjusted as necessary depending on size and primer melting temperatures, although a typical program was run as follows:

PCR Program		
Temperature	**Time**	**Cycles**
95°C	02:00	1×
95°C	00:45	25×
54°C	00:30	
68°C	01:00	
68°C	05:00	1×
16°C	∞	

Samples were visually analysed in a Tris-acetate-EDTA (TAE) buffer agarose gel separated by gel electrophoresis.

A PCR amplification technique was used on cDNA samples following reverse transcription of extracted viral RNA. This utilised Pfu-X Polymerase (Jena Bioscience). The method can be found in the subsection "Preparation of a cDNA copy of MNV genome for sequencing" as the technique differed from both the Pfu-X based mutagenesis PCR and Taq polymerase amplification PCRs listed here.

Restriction digestion with NEB enzymes

Restriction digests were performed as per NEB protocol. All digests were performed with their specified NEBuffer and temperature (see list of Enzymes from NEB) for 1 hour. Those enzymes denoted as "Time-Saver qualified" where 5-15 minutes is specified as sufficient, were digested for 1 hour as recommended to ensure complete digestion.

Reagent	**Stock Concentration**	**Final Concentration**
Plasmid DNA	Varied	1 µg
NEBuffer	10×	1×
NEB Restriction Enzyme	Varied	10 U
$ddH_2O_{RNase\text{-}free}$	--	--

Reactions were typically performed in a volume of 50 µl however smaller volumes of 20 µl were sometimes used to minimise enzyme usage when large DNA masses were not required. Enzyme volume was always kept below 10% of the reaction volume to prevent star activity.

Gel electrophoresis

Plasmids and nucleotide fragments were run by gel electrophoresis for visual analysis. Samples were loaded into a preformed 1× TAE, 1% agarose gel with MIDORI Green Xtra (NIPPON Genetics EUROPE) placed within a 1× TAE buffer-filled electrophoresis chamber. A GeneRuler™ 1 kb Plus DNA Ladder was also loaded.

Samples of DNA were typically run at 120 V for 20 min. Longer times were used when visualising the separation of larger fragments, or to allow for an easy gel extraction. Usually this did not exceed 40 min. Samples of RNA were typically run at 120 V for 8-10 min. The gel tray was washed with an NaOH solution prior to pouring the gel to minimise the presence of RNases. Gels were visualised using the GelDoc FastGene Blue/Green LED Transilluminator from NIPPON Genetics EUROPE.

Purification of fragments from a TAE gel

Some DNA samples were run by gel electrophoresis for the purpose of fragment isolation and purification. Once run and visualised as previously described, the desired fragment was excised from the gel. Three extraction methods from commercially manufactured kits were used.

Montage® Gel Extraction Kit

The gel fragment was placed in a Montage® Gel Extraction Kit column and centrifuged for 10 min at 5,000 × g. The gel slurry was collected and could be sent for sequencing.

QIAquick® Gel Extraction Kit

The mass of the gel slice was determined and for every 100 mg of agarose gel, 300 µl of Buffer QG was added. The gel slice and buffer mix was incubated at 50°C, vortexed intermittently for 10 min or until the gel slice dissolved. For every 100 mg of agarose gel, 100 µl isopropanol was added and mixed. The mixture was applied to the QIAquick® column and centrifuged for 1 min at 17,900 × g to bind the DNA. The flow-through was discarded. The column was washed with 750 µl of Buffer PE and centrifuged for 1 min at 17,900 × g. The flow-through was discarded and the column was further centrifuged dry for an additional 1 min at 17,900 × g.

The DNA was eluted by placing the column into a clean 1.5 ml microcentrifuge tube and adding 50 µl of $ddH_2O_{RNase/DNase\text{-}free}$ to the centre of the column membrane and centrifuging for 1 min at 17,900 × g. The concentration was measured by NanoDrop.

NucleoSpin® Gel and PCR Clean-up kit from Macherey-Nagel

Purification was performed with the NucleoSpin® Gel and PCR Clean-up kit from Macherey-Nagel with some minor adjustments from the manufacturer's protocol.

The mass of the gel slice was determined and for every 100 mg of agarose gel, 200 µl of Buffer NTI was added. The gel slice and buffer mix was incubated at 50°C, vortexed intermittently for 5-10 min or until the gel slice dissolved. The sample was loaded into an assembled NucleoSpin® column with collection tube, up to 700 µl. The column was centrifuged for 30 s at 11,000 × g and the flow-through discarded. Any remaining sample volume was loaded into the column until all of the sample had been centrifuged over the column.

The column was washed with 700 µl of Buffer NT3, centrifuged for 30 s at 11,000 × g and the flow-through discarded. The column was washed again with 650 µl of Buffer NT3, centrifuged for 30 s at 11,000 × g and the flow-through discarded. The column was centrifuged again with no added buffer for 1 min at 11,000 × g to remove all remaining buffer. The DNA was eluted by placing the column into a clean 1.5 ml microcentrifuge tube and adding 20 µl of Buffer NE, incubating for 5 min at RT and centrifuging for 1 min at 11,000 × g. The eluate was reapplied to the column, incubated for 1 min and centrifuged for 1 min at 11,000 × g. The eluate was again reapplied to the column, incubated for 1 min and centrifuged for 1 min at 11,000 × g. The final eluate was used for further cloning.

Ligation of a restriction digest product to a vector

A purified restriction digest insert product was ligated into a purified restriction digest vector using T4 DNA ligase from NEB. A mass of 50 ng purified vector was ligated in a total volume of 20 µl in a ratio of typically 5:1 to purified insert. The insert mass was calculated using the NEBioCalculator® that uses the formula:

$$required\ mass\ insert\ (ng) = desired\ molar\ ratio \frac{insert}{vector} \times mass\ of\ vector\ (ng) \times \frac{insert\ length\ (bp)}{vector\ length\ (bp)}$$

A volume of 2 µl T4 DNA Ligase Buffer (10×) was carefully mixed with the calculated vector and insert volumes, T4 DNA Ligase, and $ddH_2O_{RNase/DNase\text{-}free}$ up to the total volume of 20 µl. For sticky end ligations, the mixture was incubated at 4°C overnight and for 10-20 min at RT the following day prior to transformation. Blunt end ligations were incubated at 4°C overnight and for 1-2 hours at RT the following day prior to transformation. The ligation reactions were not heat inactivated, contrary to the NEB protocol. The ligated plasmids were chilled on ice and 5 µl were transformed into competent *E. coli*. Remaining ligated plasmids were stored at 4°C overnight.

Control ligation reactions were performed of vector DNA only and insert DNA only, substituting $ddH_2O_{RNase/DNase\text{-}free}$ in a volume equal to the missing DNA. This provided a background colony number once transformed. Should minimal transformed colonies be recovered, 10-15 µl remaining ligated plasmid were transformed or the ligation reaction was repeated. Molar ratios were adjusted for repeat ligations in the event of high background colony numbers, or repeated minimal transformed colony numbers.

Ligation of a PCR product to a pGEM®-T vector

A purified Taq polymerase PCR product was ligated into pGEM®-T using the pGEM®-T Vector Systems kit. Control ligations were not performed to reduce costs. Resulting ligations were used in a colony PCR, restriction digest and finally sent for sequencing to ensure the presence of the insert. The ligation was performed as per protocol from Promega.

Reagent	**Volume (µl)**
2× Rapid Ligation Buffer, T4 DNA Ligase	5.0
pGEM®-T Vector (50 ng)	1.0
PCR product (17 ng/µl)	3.0
T4 DNA Ligase	1.0

The reagents were carefully mixed by pipetting and incubated overnight at 4°C. The ligation was transformed into DH5α *E. coli* and plated on LB-Agar with 100 mM IPTG and 40 mg/ml X-β-Gal for blue/white screening. Plates were incubated at 37°C overnight and white colonies were selected for colony PCR.

Phenol-chloroform extraction

One volume of chloroform-saturated phenol was added to a pre-determined volume of aqueous DNA. The mixture was briefly vortexed and centrifuged at 12,000 × g for 5 min. The upper aqueous phase was removed and added to a clean microcentrifuge tube. One volume of chloroform was added to the aqueous DNA and briefly vortexed. The mixture was centrifuged at 12,000 × g for 5 min. The upper aqueous phase was removed and added to a clean microcentrifuge tube to which 579 µl 100% ethanol, 1 µl Glycoblue and 20 µl 3 M NaOAc (pH 5.2) was also added. The mixture was vortexed and precipitated at -80°C for at least 1 hour.

The mixture was allowed to thaw and centrifuged at 4°C, 12,000 × g for 20 min. The supernatant was discarded and the DNA pellet washed with 70% ethanol at 4°C, 12,000 × g for 20 min. The supernatant was discarded and the DNA pellet allowed to dry. Dry DNA was suspended in 50 µl of $ddH_2O_{RNase/DNase\text{-}free}$.

Transformation of a plasmid into competent *Escherichia coli*

A volume of prepared plasmid (100 ng from a pure preparation, 10 µl from a PCR sample) was added to competent bacteria cells (either *E. coli* HB101 or DH5α), gently mixed and incubated on ice for 20 min. The cells were shocked for 2 min at 42°C, cooled on ice and incubated at 37°C with agitation in an added volume of SOC medium for 30 min. Transformed bacteria were plated on LB-Amp agar and colonies picked for plasmid preparation.

Plasmid mini-preparation

A volume of transformed *E. coli* was grown in a volume of LB-Amp medium overnight. A volume of 1.5 ml was centrifuged at 10,000 × g for 30 sec. The supernatant was discard and the cell pellet was suspended in 100 µl S1 solution (Macherey-Nagel). The bacterial cells were lysed with 200 µl of solution S2 (Macherey-Nagel), carefully mixed by inversion and incubated for 5 min on ice. The solution was then neutralised with 150 µl S3 solution (Macherey-Nagel) and carefully mixed by inversion. The solution for incubated for 5 min on ice. The DNA-containing supernatant was pipetted

into a clean microcentrifuge tube and the cell debris was discarded. One volume of 100% isopropanol was added, the mixture briefly vortexed and precipitated at -80°C for at least 1 hour.

The mixture was allowed to thaw and centrifuged at 4°C, 12,000 × g for 20 min. The supernatant was discarded and the DNA pellet washed with 70% ethanol at 4°C, 12,000 × g for 20 min. The supernatant was discarded and the DNA pellet allowed to dry. Dry DNA was suspended in 50 µl of $ddH_2O_{RNase/DNase\text{-}free}$.

Plasmid midi-preparation

Larger plasmid preparations were purified using the Nucleobond® PC 100 kit from Macherey-Nagel from a bacterial culture of 100-200 ml. *E. coli* HB101 were grown overnight in LB-Amp medium. The bacteria were centrifuged at 4°C, 4,500 × g for 15 min. The bacterial pellet was suspended in 8 ml buffer S1, lysed with 8 ml buffer S2 at RT for 2-3 min, and neutralised with 8 ml buffer S3 on ice for 5 min. The Nucleobond® column was equilibrated with 2.5 ml buffer N2 and the filtered lysate left to bind by gravity flow. The column was washed with buffer 10 ml N3 and the DNA eluted with 5 ml N5.

Plasmid DNA was precipitated with the addition of 3.5 ml isopropanol and centrifugation at 4°C, 5,000 × g for 30 min. The DNA pellet was washed with 70% ethanol and centrifuged at RT, 5,000 × g for 10 min and the ethanol discarded. The pellet was dried at 37°C until all ethanol had evaporated. The pellet was suspended in 50 µl $ddH_2O_{RNase/DNase\text{-}free}$.

Preparation of m^7G-capped MNV RNA for transfection

The RNA-based reverse genetics plasmid containing the WT MNV-1.CW1 genome (#245, pT7:MNV\3'RZ) was a gift provided by Prof. Ian Goodfellow. Plasmids containing 10-20 µg of the full MNV-1.CW1 genome and its various mutations were first linearised with restriction enzyme NheI and purified by phenol-chloroform extraction.

Linearised plasmid was *in vitro* transcribed using the MAXIscript T7 IVT kit as per protocol in a total volume of 40 µl with a DNA template of 3-4 µg, of which the concentration was measured by NanoDrop. All reagents were gently mixed together and incubated at 37°C for 2 hours. The DNA template was digested with 1 µl DNase I as per protocol at 37°C for 30 min.

The RNA was purified using the Direct-zol™ RNA MiniPrep Kit. To the IVT RNA, 100 µl TRI Reagent® was added and incubated at RT for 5 min. To this mixture, 100 µl 100% ethanol was added, mixed and placed over the Direct-zol™ column. The column was centrifuged at 10,000 × g for 30 s at RT. The column was washed with 400 µl RNA PreWash Buffer (10,000 × g for 30 s at RT) and again with 700 µl RNA Wash Buffer (10,000 × g for 30 s at RT). The column was centrifuged dry at 10,000 × g for 30 s at RT. The RNA was eluted with 69 µl $ddH_2O_{RNase/DNase\text{-}free}$ and centrifugation at 10,000 × g for 30 s at RT. Concentration was determined by NanoDrop.

The purified RNA was capped using the ScriptCap™ m^7G Capping System in a total volume of 100 µl. The RNA was denatured at 65°C for 5-10 min and immediately stored on ice. To the denatured RNA, the following reagents were added:

Reagent	Volume (µl)
10× Capping Buffer	10.0
10 mM GTP	10.0
2 mM SAM	5.0
RNase Inhibitor	2.5
Capping Enzyme	4.0

The reaction was carefully mixed and incubated for 1.5 hours at 37°C.

Preparation of a cDNA copy of MNV genome for sequencing

A volume of 1 ml TRI Reagent® was added to 1 ml P3 virus stock and incubated for 5 min at RT. A volume of 1 ml 100% ethanol was added and the mixture was placed over the Zymo-Spin™ column and centrifuged (10,000 × g for 30 s at RT). The column was washed with 400 µl PreWash Buffer and centrifuged (10,000 × g for 30 s at RT). The column was washed with 700 µl Wash Buffer and centrifuged (10,000 × g for 30 s at RT). The column was centrifuged dry at 10,000 × g for 30 s at RT. The RNA was eluted in 50 µl $ddH_2O_{RNase/DNase\text{-}free}$. The concentration of RNA was measured by NanoDrop.

The isolated genomic RNA was used to synthesise a cDNA copy of the genome suitable for amplification by PCR. This was performed using the SuperScript™ II Reverse Transcriptase kit from Invitrogen™. Up to 5 µg of isolated RNA was added to 2 pM reverse primer ST-280, 1 mM dNTPs and $ddH_2O_{RNase/DNase\text{-}free}$ up to a volume of 12.5 µl. The RNA mixture was allowed to denature for 5 min at 65°C and immediately cooled on ice. Further reagents of 1× FS Buffer, 10 mM DTT and 20 U RNaseOut Inhibitor were mixed together in a volume of 6.5 µl and carefully added to the denatured RNA mixture. The 19 µl mixture was incubated for 2 min at 42°C. The SuperScript™ II Reverse Transcriptase enzyme was added at a volume of 1 µl containing 200 U, to the reaction mix. The reaction was incubated for 50 min at 42°C. The enzyme was inactivated for 15 min at 70°C and left to cool briefly at RT. The concentration of DNA was approximated by NanoDrop.

The cDNA was amplified using Pfu-X Polymerase. A positive control of pRevGen-MNV-1 (#27) and a negative control of $ddH_2O_{RNase/DNase\text{-}free}$ was used.

Reagent	Stock Concentration	Final Concentration
Pfu-X Buffer	10×	1×
dNTPs	10 mM	200 µM
Forward Primer (MST-112)	25 µM	0.4 µM
Reverse Primer (ST-280)	25 µM	0.4 µM
cDNA	100 ng/µl	100 ng
Pfu-X Polymerase	2.5 U/µl	1.25 U
$ddH_2O_{RNase\text{-}free}$	--	--

PCR Program		
Temperature	**Time**	**Cycles**
94°C	02:00	1×
94°C	00:30	30×
53°C	00:45	
72°C	05:20	
72°C	15:00	1×
16°C	∞	

The sample was purified by gel electrophoresis using 1× TAE, 1% agarose gel with MIDORI Green Xtra (NIPPON Genetics EUROPE) and the 3,315 bp fragment extracted. Extra care was taken as to minimise TAE agarose gel that did not contain DNA. The gel fragment was placed in a Montage® Gel Extraction Kit column and centrifuged for 10 min at 5,000 × g. A sample of gel slurry was sent for sequencing by LGC Genomics using primers MR-106, MST-120, ML-240, ST-280 and MSL-358 to ensure full coverage for capsid sequencing.

A minimum of 100 ng cDNA was used as template, however more was occasionally used for a repeat if the TAE gel showed a low concentration product.

Amino acid alignments

Sequences were obtained from the National Center for Biotechnology Information (NCBI) of the National Institutes of Health (NIH) database GenBank®. Seventeen sequences were compared spanning GI to GVII.

Table 5: Table of GenBank® accession numbers

Virus	Genogroup	GenBank® Accession Number
Norwalk (1968)	GI	JX023285.1
Chiba (1987)	GI	AB042808.1
Southampton (1993)	GI	L07418.1
Norwalk-like (1998)	GI	AF093797.1
Hawaii (1971)	GII	U07611.2
MD145 (1987)	GII	AY032605.1
Camberwell (1994)	GII	AF145896.1
Sydney (2012)	GII	JX459908.1
Japan Kao (2019)	GII	LC771966.1
Norovirus GII.17 (2015)	GII	NC_039475.1
Bovine, Adam (2006)	GIII	NC_029645.1
Lake Macquarie (2010)	GIV	NC_029647.1
Cat (2010)	GIV	JF781268.1
MNV-1.CW1 (2002)	GV	DQ285629.1
MNV-CR6 (2005)	GV	EU004676.1
Dog (2018)	GVI	MN908340.1
Bat (2016)	GVII	MF373609.1

Norovirus sequences were manually aligned from the cleavage site. All GI and GII amino acid cleavage sites were determined from the published HNoV cleavage site data (Belliot *et al.*, 2003). The GV cleavage sites have also been previously published (Sosnovtsev *et al.*, 2006). Published locations for the cleavage sites of noroviruses GIII, GIV, GVI and GVII could not be found. Therefore these sites were inferred based upon their similar sequences from P4-P2' compared to other norovirus genogroups, as well as the NS protein sequences as a whole.

Cell culture

Culturing of cells

Cells were cultured in either DMEM-5 (BV-2) or DMEM-10 (Huh7$^{mCD300lf\text{-}Sec61b}$), passaging every 3-4 days. BV-2 cells were scraped whereas Huh7$^{mCD300lf\text{-}Sec61b}$ cells were washed with 1× PBS, trypsinised with trypsin/EDTA and neutralised with growth medium. Cells were incubated at 37°C, 5% CO_2 and 95% RH.

Determining viral titre by $TCID_{50}$/ml

BV-2 cells were seeded in a 96-well plate at a concentration of 1×10^4 cells/well, 180 µl per well. Virus was titrated from a starting addition of 20 µl per well, 10-fold down each row of wells. The plate was incubated for 4 days post-infection or until a colour-change could be observed. Titre was determined using the Reed-Münch method.

Determining viral titre by plaque assay

Huh7$^{mCD300lf\text{-}Sec61b}$ cells were seeded in a 6-well plate at a concentration of 2×10^5 cells per well, a day prior to infection, in DMEM-10. Medium was removed and replaced with inoculum. Inoculum was prepared as a viral 10-fold dilution series in a sodium phosphate buffer (pH 7.4) of which 500 µl was used to infect the cell monolayer. The inoculum was incubated on the cells for 1 hour at 37°C, 5% CO_2 and 95% RH, removed and replaced with MEM/Avicel. Assays were incubated at 37°C, 5% CO_2 and 95% RH for 48 hours. The MEM/Avicel overlay was removed, the cells washed with 1× PBS and stained for 15 min with 1 mg/ml Erythrosine B in 1× PBS. Plaques were counted and PFU/ml calculated per plate.

Generation of recombinant viruses by transfection of RNA into Huh7$^{mCD300lf\text{-}Sec61b}$

Huh7$^{mCD300lf\text{-}Sec61b}$ cells were seeded at a concentration of 2×10^5 cells per well in a 6-well tissue culture plate in DMEM-10. The cells were incubated for 24 hours at 37°C, 5% CO_2 and 95% RH. The cells were transfected at a confluence of 70-90%. Transfections were performed with Lipofectamine™ MessengerMAX™ and a transfection method adapted from the manufacturer's instructions.

A volume of 3.75 µl Lipofectamine™ MessengerMAX™ was added to 100 µl pre-warmed Opti-MEM™ (Gibco™) and incubated at RT for 10 min. A calculated volume containing 2500 ng m^7G-capped RNA to 100 µl Opti-MEM™. The RNA/ Opti-MEM™ mixture was added to the Lipofectamine™/ Opti-MEM™ mixture and incubated at RT for 5 min.

Growth medium from the previously seeded Huh7$^{mCD300lf\text{-}Sec61b}$ cells was removed and replaced with 800 µl Opti-MEM™. The Lipofectamine™ incubated RNA was added dropwise to the Huh7$^{mCD300lf\text{-}Sec61b}$ cells and incubated for 3-4 hours 37°C, 5% CO_2 and 95% RH. The transfection inoculum was removed and replaced with 2 ml DMEM-10 and incubated for 48 hours at 37°C, 5% CO_2 and 95% RH. The transfection was observed by fluorescence microscopy regularly from 4-48 hours.

Virus preparations

Transfection lysate (P0) of 1 ml was blind-passaged to a 50% confluent T75 flask of BV-2 cells. The flask was incubated for 24-48 hours at 37°C, 5% CO_2 and 95% RH, until CPE was observed. The flask was then frozen at -80°C to lyse any remaining cells. Virus was aliquoted only after centrifugation of thawed lysate at 4500 × g. Passaging further was performed after calculating the freeze-thaw $TCID_{50}$/ml. Subsequent infections were performed with an MOI of approximately 0.5 until a P3 stock was generated.

All experimental work was carried out using a P4 stock. A P4 stock was grown in the same fashion; however, several T150 flasks of 50% confluent BV-2 cells were infected at an MOI of 0.5. After a 24-48 hour infection, remaining cells were lysed at -80°C. Cell debris was removed by centrifugation at 4500 × g. Lysate supernatant was purified by ammonium sulphate precipitation at 40%, 4°C overnight. Virus was pelleted by centrifugation at 10,000 × g for 15 min at 4°C. Supernatant was discarded and the viral pellet was suspended in an appropriate volume of sodium phosphate buffer. The virus was sterile-filtered and aliquoted into volumes suitable for experiments.

Microscopy and image processing

Cells were observed prior to and during both transfection and infection. Simple light microscopy was used to determine if BV-2 and Huh7$^{mCD300lf\text{-}Sec61b}$ cells were suitable for either infection of transfection immediately prior to an experiment. Cells were also monitored throughout passaging.

Fluorescence microscopy was used to monitor both the infection and transfection of Huh7$^{mCD300lf\text{-}Sec61b}$ cells. For the purposes of data collection, assessing the percentage of cells showing a GFP shift into the nucleus, multiple fields of view within the sample were captured. The captures were at 10× magnification. A GFP and brightfield view captured for every field of view. From each image, each cell with a GFP-positive nucleus was counted using the software Fiji (based on the software ImageJ). The total number of cells was also counted. A percentage of each field of view was then determined.

Results

RNA-based MNV reverse genetics system with a reporter for infection

The RNA-based MNV reverse genetics system is based upon a single plasmid (#245: pT7:MNV\3'RZ) that contains the entire MNV genome under the control of a T7 promotor (**Figure 5**). Infectious viral genome is generated by *in vitro* RNA transcription and a functional 3' end is achieved by linearising the plasmid with the restriction endonuclease NheI by letting the polymerase fall off its template. Mutations can then be introduced by site-directed mutagenesis in the plasmid containing the viral genomic cDNA.

Site-directed mutagenesis

Site-directed mutagenesis can be achieved by amplifying the plasmid with two overlapping primers containing the mutation(s), insertions or deletions at their respective 5' ends (Liu & Naismith, 2008). Practically however, it is difficult to perform the mutagenesis on the entire plasmid, as plasmids containing viral genomes are usually very long, in this case >11 kb. Hence, the efficiency of generating long PCR amplicons without unwanted mutations is very low and would require extensive sequence analysis to rule out any unwanted mutations in the entire genome. To perform site-directed mutagenesis, three subcloning strategies were devised, breaking up the genomic MNV-1.CW1 plasmid into smaller fragments flanked by unique restriction sites to subclone the mutated region back into the main reverse genetics plasmid containing the full genome.

Generating constructs for subcloning

The generation of mutations anywhere in the MNV genome, bar the six base HindIII recognition site, can be easily achieved with a simple site-directed mutagenesis within an intermediate plasmid for simple cloning into pT7:MNV\3'RZ (#245). The first subcloning construct, pGEM-T-NS5/NS6, (#377) contained the genome region NS5-NS6 flanked by partial 3' NS4 and 5' NS7 regions. The second subcloning construct, pBluescriptSK(-)fragment[GV-CW1-NS], (#398) contained the genome region NS1-NS7 (partial 5' end). The third subcloning construct, pT7:MNV-DEcoRV-PmlI, (#324) contained the genome regions NS6 (partial 3' end), NS7, ORF2, ORF3 and ORF4.

The following subcloning plasmids can be used to perform any mutation by site-directed mutagenesis within the MNV-1.CW1 genome. The only region where no mutation can be introduced is the six nucleotide HindIII recognition site. The indicated restriction enzyme sites can be used to digest and ligate the desired mutation back into the main reverse genetics plasmid, pT7:MNV\3'RZ (#245).

Table 6: Table of subcloning plasmids for back-insertion to pT7:MNV\3'RZ (#245)

Plasmid #	Plasmid name	Genome region	Restriction sites for back-insertion
#377	pGEM-T-NS5/NS6	NS5, NS6, partial 3' NS4 from BamHI, partial 5' NS7 to HindIII	BamHI, HindIII
#398	pBluescriptSK(-)fragment [GV-CW1-NS]	NS1-2, NS3, NS4, NS5, NS6, partial 5' NS7 to HindIII	SpeI, HindIII **n.b.* the reverse orientation
#324	pT7:MNV-DEcoRV-PmlI	NS7, ORF2, ORF3, ORF4, partial 3'NS6	HindIII, NheI **n.b.* HindIII is located within NS7 making the partial NS6 region and the first 120 nucleotides of NS7 incapable of back-insertion

Mutation in the active site of the viral protease NS6

Although a negative infection but positive transfection control plasmid, pT7:MNV\3'RZ(NS7-F/S) (#246), was already available, a true negative control that should not permit the proteolytic cleavage and therefore functional NS protein production was not. A mutation in the active site of NS6 was thus introduced by site-directed mutagenesis after the subcloning of NS5 and NS6 into pGEM-T (**Figure 7**). The resulting plasmid pT7:MNV\3'RZ(NS6-C139A) (#376) was used in further reverse genetics experiments.

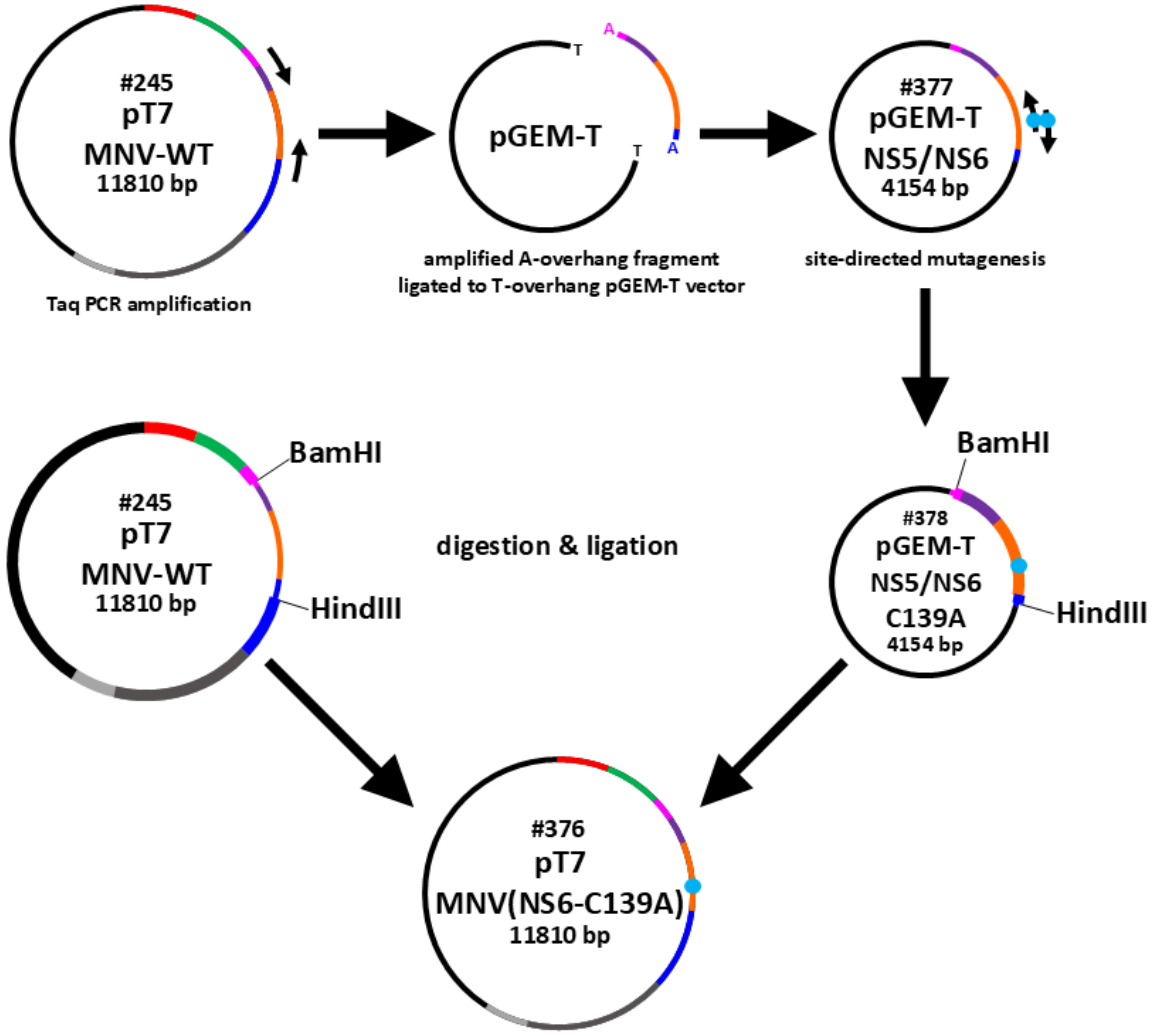

Figure 7: Site-directed mutagenesis and cloning techniques for the generation of an MNV reverse genetics plasmid with a mutation in NS6

A Taq-amplified fragment of plasmid pT7:MNV\3'RZ (#245) with primers MSL-410 and MSL-411 was ligated to pGEM-T to create plasmid pGEM-T-NS5/NS6 (#377). Site-directed mutagenesis was performed on this plasmid generating pGEM-T-MNV1.CW1-NS6-C139A (#378) with the mutation cloned back into #245 using dual restriction digests with enzymes BamHI and HindIII. This reverse genetics plasmid was named pT7:MNV\3'RZ(NS6-C139A). Reverse genetics plasmids are indicated as: NS1-2 (red), NS3 (green), NS4 (pink), NS5 (purple), NS6 (orange), NS7 (dark blue), VP1 (yellow), VP2 (grey), mutation (light blue), and plasmid backbone (black).

Mutation of the NS polyprotein protease cleavage site

For the investigation into the NS6 protease cleavage sites, a further two intermediate plasmids were generated (**Figure 8A**) for the insertion of a small protein between two NS proteins, and the site-directed mutagenesis of the protease cleavage sites. Most of ORF1 was cloned into pBluescriptSK(-) (#322) generating plasmid pBluescriptSK(-)fragment[GV-CW1-NS] (#398). This smaller plasmid permitted site-directed mutagenesis. These mutations could be cloned back into pT7:MNV\3'RZ generating plasmids #456–#463 (see **Table 1: Table of plasmids**).

A plasmid, pUC18-CW1[NS1-2/3-HA/FLAG-NotI/NdeI-FseI/EcoNI] (#399), containing a 96 bp insert of the sequence for tags HA and FLAG, restriction sites NotI and NdeI, and the five amino acids at the beginning of NS3 and end of NS1-2, sandwiched between NS1-2 and NS3 was obtained from BioCat GmbH. This fragment (**Figure 8B**) was cloned into the intermediate plasmid pBluescriptSK(-)fragment[GV-CW1-NS] (#398) to utilise the EcoNI site. This kept the cost of a synthesised pUC18 plasmid low. Subsequent cloning back into pT7:MNV\3'RZ generated reverse genetics plasmid pT7:MNV\3'RZ-NS1-2/NS3(HA/FLAG) (#406). The generation of the second intermediate plasmid of a smaller size, pBluescriptSK(-)fragment[GV-CW1-NS]-NS1-2/NS3(HA/FLAG) (#404), also permitted a straightforward site-directed mutagenesis and cloning to change the sequence of a protease cleavage site (plasmids #421 and #422, see **Table 1: Table of plasmids**).

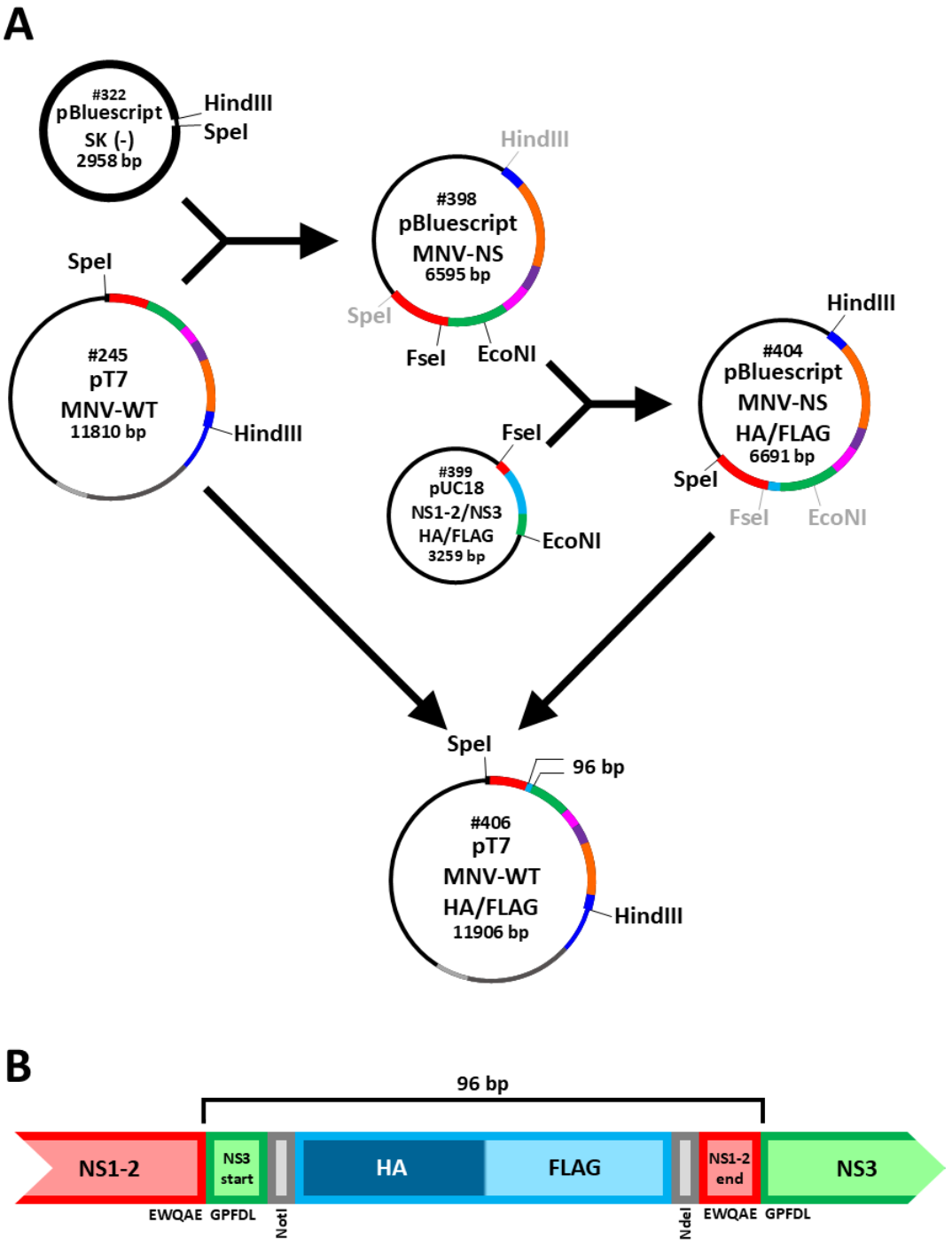

Figure 8: Cloning techniques for the generation of an MNV reverse genetics plasmid with an insertion between NS1-2 and NS3

(A) Cloning of a 96 bp insert between NS1-2 and NS3. A pT7:MNV\3'RZ (#245) fragment was cloned into pBluescriptSK(-) (#322) using dual restriction digests with enzymes HindIII and SpeI. This generated a plasmid suitable for future site-directed mutagenesis, named pBluescriptSK(-)fragment[GV-CW1-NS] (#398). A fragment from a BioCat GmbH synthesised plasmid, pUC18-CW1[NS1-2/3-HA/FLAG-NotI/NdeI-FseI/EcoNI] (#399) was cloned into #398 using dual restriction digests with enzymes FseI and EcoNI. This new plasmid, also suitable for future site-directed mutagenesis, was named pBluescriptSK(-)fragment[GV-CW1-NS]-NS1 2/NS3(HA/FLAG) (#404). A final dual restriction digests with enzymes HindIII and SpeI cloned the introduced insertion back into #245. (B) Design of a 96 bp insert inserted between NS1-2 and NS3. The sequence for both HA and FLAG tags are flanked either side by unique restriction sites of NotI (with an additional single base keeping all codons intact) and NdeI, permitting future cloning of another sequence. Further flanking of the first 15 bp of the NS3 sequence and last 15 bp of NS1-2 keep the translated polyprotein protease sites intact.

Mutation in the VP1

Mutations in the VP1 of MNV-1 were introduced using the same technique described in (Creutznacher *et al.*, 2022; Lane, 2021). Primers were designed according to the methods described by Liu & Naismith (2008), generating a plasmid that was sequenced to check for the desired mutation and cloned back into pT7:MNV\3'RZ. Multiple of these full-length plasmids with different VP1 mutations were generated (**Figure 9**). Two of these plasmids, pT7:MNV\3'RZ-D410A (#340) and pT7:MNV\3'RZ-D440A (#341) contained the divalent cation binding site mutations D410A and D440A respectively. These mutations were successfully recovered after transfection and passaging, resulting in observable $TCID_{50}$ titres. The desired mutations were present after sequencing of the amplified, reverse transcribed, extracted genomic RNA from P3. All experimentation was performed using a buffered P4 stock, passaged from the sequenced P3.

Three other mutations were introduced, namely D440C, S504C and Y250A, present in plasmids pT7:MNV\3'RZ-D440C (#356), pT7:MNV\3'RZ-S504C (#395) and pT7:MNV\3'RZ-Y250A (#348) respectively. Transfection after linearisation and *in vitro* transcription resulted in an observable $TCID_{50}$ titre in BV-2 cells. The stock obtained for D440C did not result in the mutation being present in the sequenced viral capsid taken from a P2. The desired mutation, if it had been present, was intended for

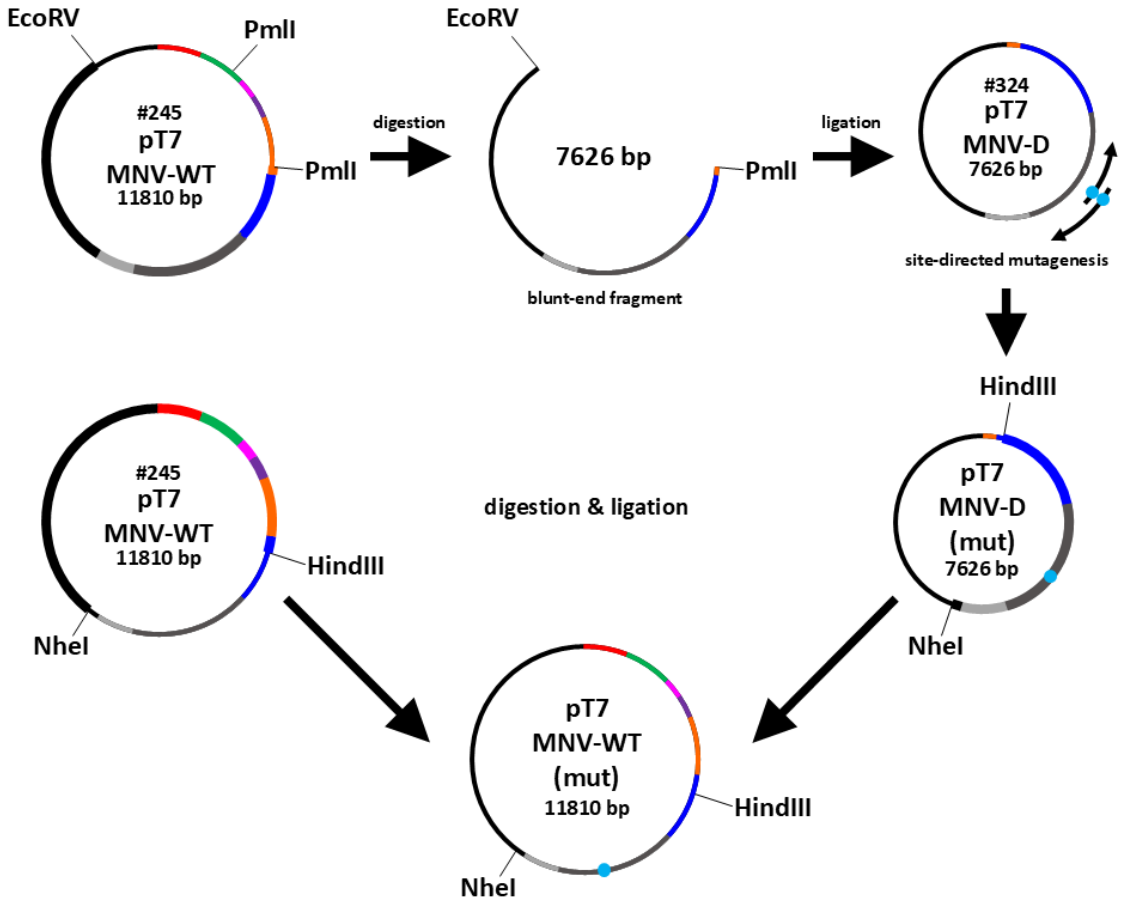

Figure 9: Site-directed mutagenesis and cloning techniques for the generation of an MNV reverse genetics plasmid with a mutation in ORF2

Plasmid pT7:MNV\3'RZ (#245) was digested with enzymes EcoRV and PmlI creating a blunt-ended fragment that was ligated to create plasmid pT7:MNV-DEcoRV-PmlI (#324). Site-directed mutagenesis was performed on this plasmid with the mutation cloned back into #245 using dual restriction digests with enzymes HindIII and NheI. This technique generated reverse genetics plasmids pT7:MNV\3'RZ-D410A (#340), pT7:MNV\3'RZ-D440A (#341), pT7:MNV\3'RZ-D440C (#356), pT7:MNV\3'RZ-S504C (#395) and pT7:MNV\3'RZ-Y250A (#348). Reverse genetics plasmids are indicated as: NS1-2 (red), NS3 (green), NS4 (pink), NS5 (purple), NS6 (orange), NS7 (dark blue), VP1 (yellow), VP2 (grey), mutation (light blue), and plasmid backbone (black).

use in cysteine labelling. The S504C mutation was present however this project was abandoned. The titre of Y250A was too low to obtain sufficient RNA for a successful reverse transcription reliably. This mutation, if found to be present after sequencing, could be used for experimentation in relation to bile acid binding. The VP1 residue 250 is present in the bile acid binding pocket with mutant proteins already having been produced for binding analysis (Nelson *et al.*, 2018).

In summary, cloning strategies were successfully used to generate MNV-1.CW1 reverse genetics plasmids with a mutation in the active site of NS6; a small protein insertion between NS1-2 and NS3; an intermediate permitting the site-directed mutagenesis of sites within ORF1; and VP1 mutations D410A and D440A.

Reverse genetics in Huh7$^{mCD300lf\text{-}Sec61b}$ protease reporter cells

Previous data from the lab had shown that recombinantly expressed MNV-1 generated from Huh7$^{mCD300lf\text{-}Sec61b}$ cells yielded the same titres as its WT counterpart and that there were not major titre differences expected between naturally susceptible cell lines and the recombinant Huh7$^{mCD300lf\text{-}Sec61b}$ cells. The reproducibility of this norovirus reverse genetics system in Huh7$^{mCD300lf\text{-}Sec61b}$ cells and whether there is a change in titre after passaging was investigated.

Recombinant WT MNV-1.CW1 can be rescued and passaged on BV-2 cells

Transfection of capped MNV-1.CW1 RNA into Huh7$^{mCD300lf\text{-}Sec61b}$ cells generates a recombinant virus that is infectious in naturally susceptible BV-2 cells. The recombinant virus can be passaged and titrated on BV-2 cells. The technique is reproducible and robust resulting in transfection titres varying from a 10^5-10^7 $TCID_{50}$/ml range (**Figure 10**). Further passages are typically around 10^7 $TCID_{50}$/ml but can be pushed higher with careful CPE monitoring.

In conclusion, the reverse genetics system in Huh7$^{mCD300lf\text{-}Sec61b}$ cells is robust and reproducible. Occasional low titres at P0 are quickly overcome during passaging.

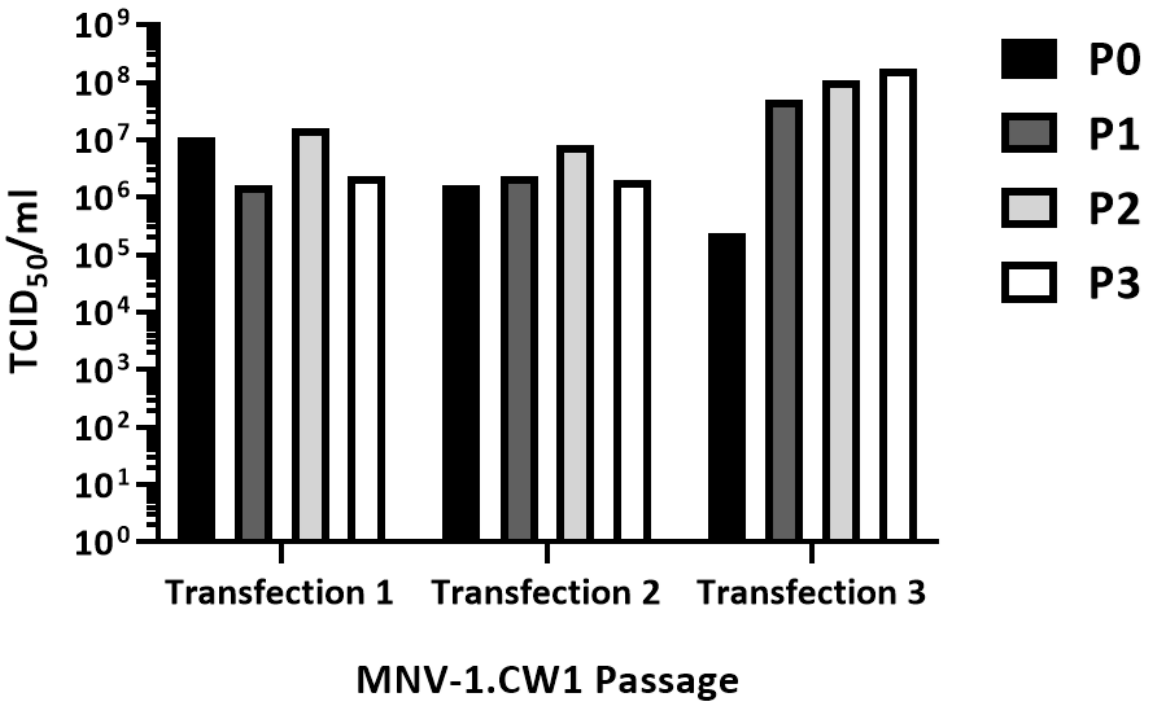

Figure 10: Recombinant MNV-1.CW1 can be passaged on BV-2 cells

Three independent MNV-1.CW1 transfection lysates (P0) were passaged on BV-2 cells up to a third passage (P3). Infections were freeze-thawed, aliquoted and freeze-thawed before titration by $TCID_{50}$ on BV-2 cells.

Transfection of Huh7$^{mCD300lf\text{-}Sec61b}$ cells with an intact WT protease sequence causes a GFP shift to the nuclei

Transfected Huh7$^{mCD300lf\text{-}Sec61b}$ cells were observed over a 48 hour period by fluorescence microscopy (**Figure 11**). Multiple fields of view were observed per transfection across four time-points over multiple separate transfections. Percentage of GFP-illuminated nuclei was determined per field of view (**Figure 11A**). Titre at 48 hours post-transfection was also calculated (**Figure 11B**). Percentage of GFP-illuminated nuclei varied greatly between each field of view but the overall pattern for both WT and the mutant RdRp F/S was some, but a largely minimal shift at four hours post-transfection, with only a slight increase by eight hours. The most noticeable shift from cytoplasm to nucleus could be observed at 24 hours post-transfection. This was mostly then further reduced by 48 hours post-transfection.

Differences between the WT and RdRp F/S are subtle but can be noted after 24 hours post-transfection. A WT transfection has a relatively compact shift of between 15-40%, 24 hours post-transfection. This shift is higher and more broad for the mutant RdRp F/S, ranging between 25-70%, possibly due to a lack of CPE as there would be a loss of infected cell signal in the productive WT infection. Only looking at nuclear shift, WT and RdRp F/S are indistinguishable, thus this reporter system cannot distinguish between single or multiple rounds of infection.

As expected, introducing a mutation into the protease (NS6) active site of MNV-1.CW1 at C139A prevents any GFP-illumination of the Huh7$^{mCD300lf\text{-}Sec61b}$ nucleus. No field of view at any time point over the 48 hour period was observed to have a GFP-positive nucleus. Multiple separate transfections with freshly prepared RNA failed to show any evidence of a shift to illumination of the nucleus with GFP, confirming that the reporter is highly specific.

In summary, this shows an optimised RNA-based norovirus reverse genetics system with a real-time GFP reporter measuring protease activity. The reporter is a clear indication for successful RNA transfection and viral NS protein synthesis, but it is not reminiscent for productive infection.

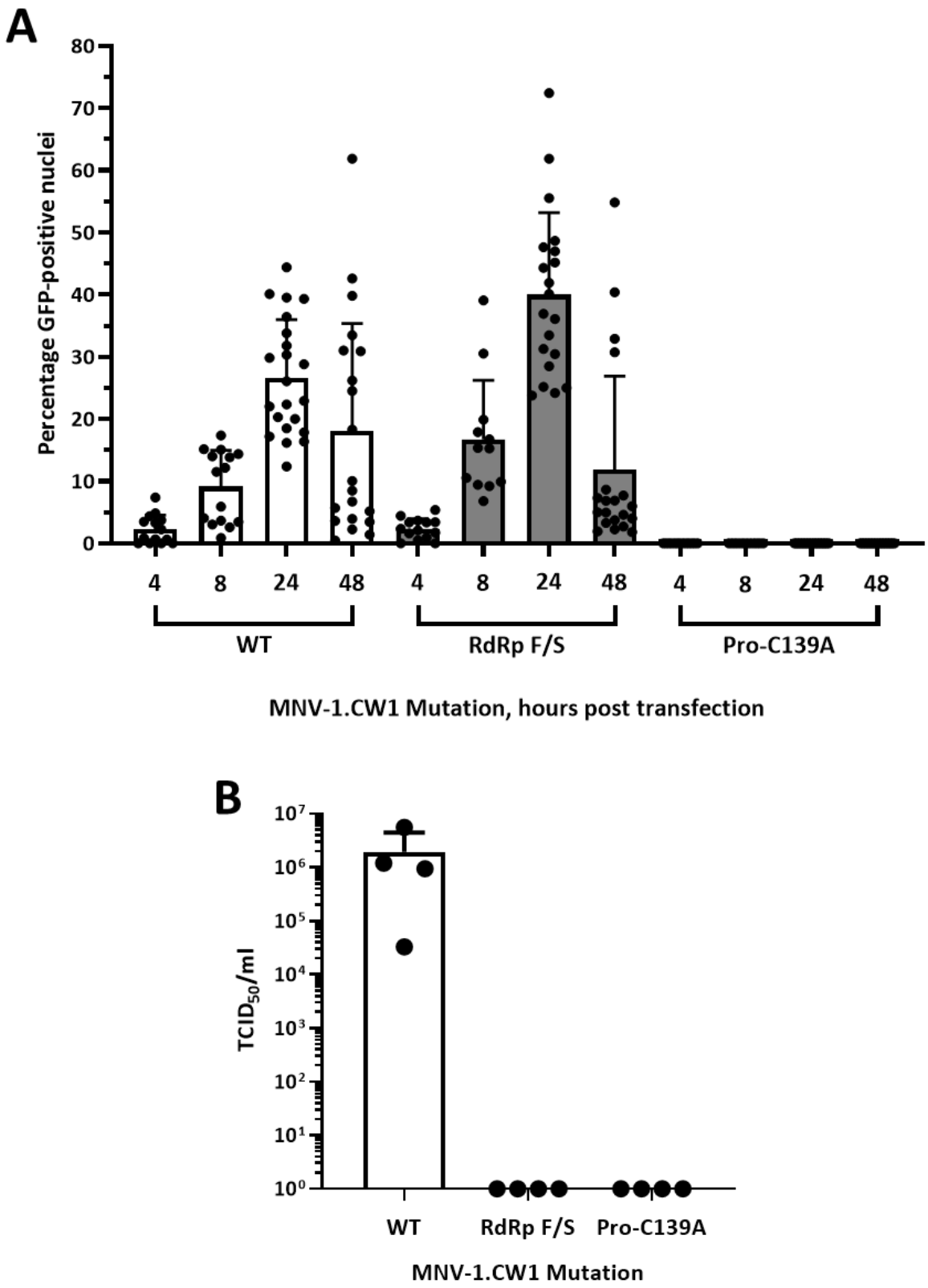

Figure 11: Nuclear shift in Huh7$^{mCD300lf\text{-}Sec61b}$ cells transfected with MNV-1.CW1 RNA

(A) Percentage of GFP nuclear shift in Huh7$^{mCD300lf\text{-}Sec61b}$ cells transfected with MNV-1.CW1 WT (white), RdRp F/S (grey) and protease mutation C139A (black) RNA over a 48 hour period. Percentages calculated from multiple fields of view observed through fluorescence microscopy. (B) Reverse genetics transfection titres (P0) by $TCID_{50}$ on BV-2 cells, from recovered transfections performed on Huh7$^{mCD300lf\text{-}Sec61b}$ cells. Error bars indicate standard deviation.

Norovirus protease cleavage sites

Protease cleavage sites have been analysed to identify motifs and patterns necessary for inserting a gene of interest into the polyprotein.

"Early" protease cleavage sites (NS1-2/NS3 and NS3/NS4) are mostly conserved across multiple genogroups

Amino acid sequences of 17 representative norovirus strains spanning seven genogroups were aligned and compared from their respective protease cleavage sites, showing ten amino acids before (P10-P1) and ten amino acids after the reported cleavage (P1'-P10') (**Figure 12**). The norovirus genogroups GIII, GIV, GVI and GVII protease cleavage sites have been inferred based upon NS protein sequence similarities and cleavage site similarities, as no experimental data confirming cleavage at these positions had been reported. All sequences have been aligned from the point of cleavage. The cleavage sites are indicated with "/". A table of the full GenBank® accession numbers (**Table 5: Table of GenBank® accession numbers**) can be found in "Materials and Methods" under "Amino acid alignments".

Within genogroups (of those with multiple strains analysed), conservation is high and mostly identical. Only minor differences can be seen P4-P2' and involve chemically similar amino acids. Between genogroups is where more obvious differences can be observed. Between GI and GII, NS1-2/NS3, P4-P2', the most drastic change is at the P3 position, where a positively charged histidine or a negatively charged glutamic acid is present respectively. This position is different for GV (murine) and GVII (bat) where a glutamine is present. Unusually, an aspartic acid is present at P1 for GV where this is consistently a glutamine for all other analysed genogroups. The last major changes for NS1-2/NS3 is for GIII (bovine). The post-cleavage site is highly conserved whereas positions P4 and P3 are cysteine and valine respectively. This is the only genogroup analysed where a major change is present at P4, with cysteine being slightly polar, although can be categorised as hydrophobic. A serine is present at P2' in GVI (canine) where this is consistently a proline with its unique ring structure across other genogroups.

The NS3/NS4 protease cleavage site is mostly conserved across genogroups. The major changes occur at P3 where the only conservation is within genogroups. An unusual glutamic acid is present at P1 in GIV (feline) and GVI (canine). The P1' and P2' positions are less conserved, even within genogroups and genotypes. This is of particular note for GIII and GV. A hydrophobic alanine is present at P1' for GIII where a similar structure is not present for any other analysed genogroup. For GV these positions are either the polar asparagine or serine followed by the positive lysine.

In conclusion, the P4-P2' cleavage site recognition region is mostly conserved for NS1-2/NS3 and NS3/NS4 with minor differences being chemically similar amino acids. Major differences typically occur at the P3 position.

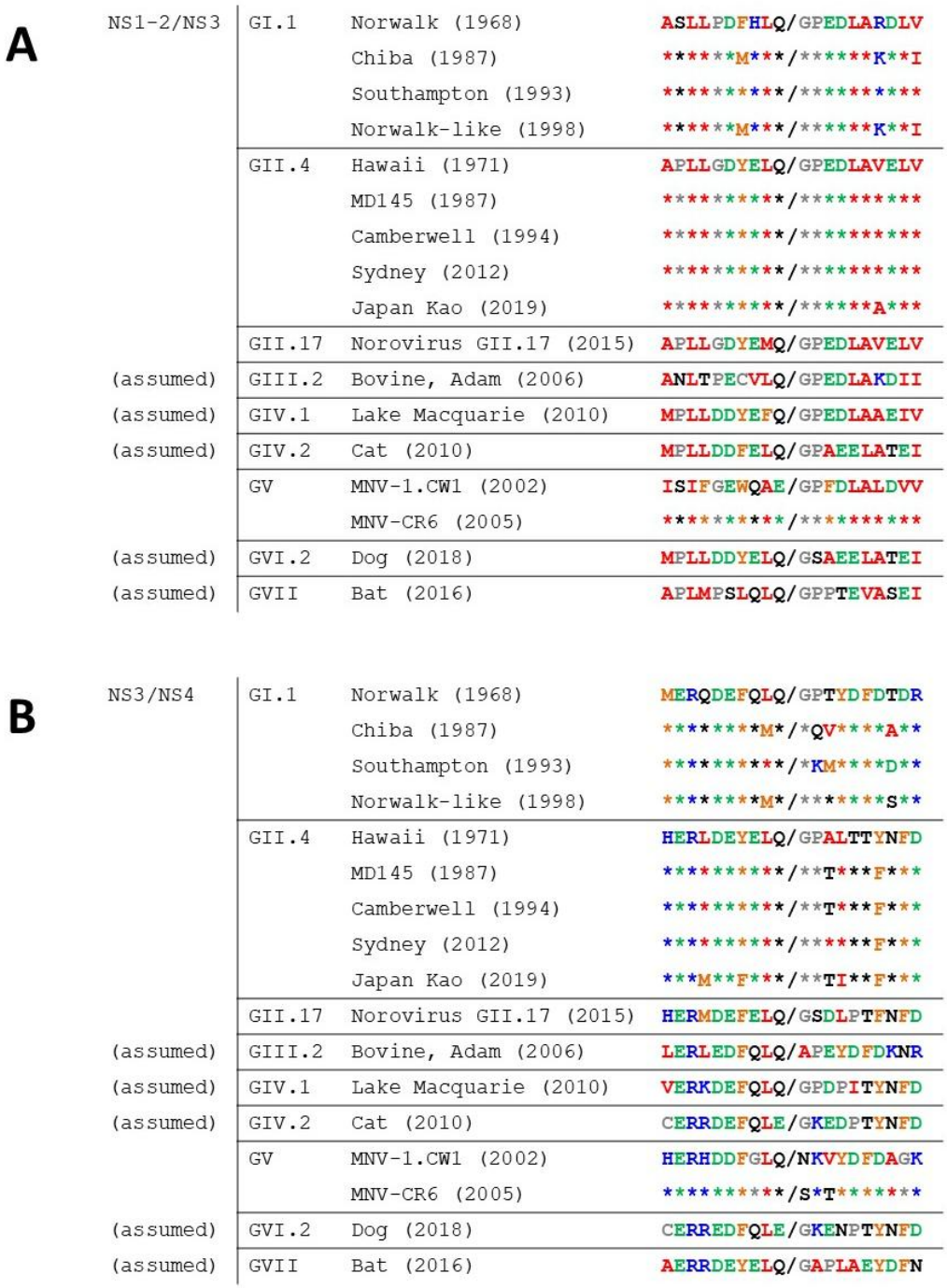

Figure 12: Alignments of protease cleavage sites at NS1-2/NS3 and NS3/NS4

Norovirus amino acid sequence alignments for multiple strains spanning GI-GVII for protease cleavage sites (A) NS1-2/NS3 and (B) NS3/NS4. Cleavage sites for GIII, GIV, GVI and GVII are assumed. Amino acid properties are indicated as: positive (blue); negative (green); polar uncharged (black); short-chain hydrophobic (red); long-chain or ring-structure hydrophobic (yellow); and special (grey). Point of cleavage is indicated with "/". Identical amino acids within genotypes are indicated with "*".

"Late" protease cleavage sites are conserved across multiple genogroups

Analogous to the early cleavage sites, respective protease cleavage sites for NS4/NS5, NS5/NS6 and NS6/NS7 are shown for the respective norovirus strains (**Figure 13**). The protease cleavage site at NS4/NS5 (**Figure 13A**) is mostly conserved. Functional variation does however occur at P3 and P2. The P3 position varies wildly with only some consistency seen within a genogroup. The P2 position is slightly more conservative in variation within GII but varies greatly across genogroups. The histidine present at P2 in Norwalk-like (GI) is the only positive charge in this position of those analysed. The other interesting outlier is Norwalk (GI) being the sole sequence analysed with a hydrophobic amino acid at P3 and a rigid proline at P2. A proline is also found at P3 in GIII but the remainder of the site is typical. All variation occurs at the end of NS4 rather than the beginning of NS5 with the one exception being the alanine presence in place of a glycine at P1' in GVII (bat). The remainder of the site is again very typical.

A

NS4/NS5	GI.1	Norwalk (1968)	QMVPSDAVPE/GKNKGKTKKG
		Chiba (1987)	NVELPT*TS*/**********
		Southampton (1993)	HTEIPS*TM*/******N***
		Norwalk-like (1998)	TIELPT*SH*/**********
	GII.4	Hawaii (1971)	VVSSDDIKVE/GKKGKNKTGR
		MD145 (1987)	********T*/**********
		Camberwell (1994)	********T*/**********
		Sydney (2012)	********T*/*******S**
		Japan Kao (2019)	II**K***E*/**********
	GII.17	Norovirus GII.17 (2015)	TIDSRDIKVE/GKKGKNKSGR
(assumed)	GIII.2	Bovine, Adam (2006)	SDTEMPAPQE/GKEKKAQAPT
(assumed)	GIV.1	Lake Macquarie (2010)	EIVESNLEEE/GKKKGKNKQG
(assumed)	GIV.2	Cat (2010)	VIEPEDFEDE/GKKGKSKKGR
	GV	MNV-1.CW1 (2002)	DDDDGWYHSE/GKKGKNKKGR
		MNV-CR6 (2005)	**N*******/****R**R**
(assumed)	GVI.2	Dog (2018)	VIMPEDFEDE/GKKGKTKKGR
(assumed)	GVII	Bat (2016)	RPVWCDWDME/AKGKTKTGRG

B

NS5/NS6	GI.1	Norwalk (1968)	VDYNEKINFE/APPTLWSRVT
		Chiba (1987)	******LS**/*********V
		Southampton (1993)	*******S**/**********
		Norwalk-like (1998)	***T*******/****M*****
	GII.4	Hawaii (1971)	VDYNEKLSFE/APPSIWSRIV
		MD145 (1987)	*****R****/**********
		Camberwell (1994)	**********/**********
		Sydney (2012)	*******N**/**********
		Japan Kao (2019)	*******D**/**********
	GII.17	Norovirus GII.17 (2015)	VDYNERIDFE/APPSVWSRIV
(assumed)	GIII.2	Bovine, Adam (2006)	VDYNEVIEFQ/APPSIWSRIQ
(assumed)	GIV.1	Lake Macquarie (2010)	VDYNEKLDFE/APASIWARIV
(assumed)	GIV.2	Cat (2010)	VDYNERIQFE/APASIWSRIV
	GV	MNV-1.CW1 (2002)	VDYGEKINFE/APVSIWSRVV
		MNV-CR6 (2005)	**********/******T***
(assumed)	GVI.2	Dog (2018)	VDYNEKIQFE/APASIWSRIV
(assumed)	GVII	Bat (2016)	IDYKEEIRFE/APASVWARIV

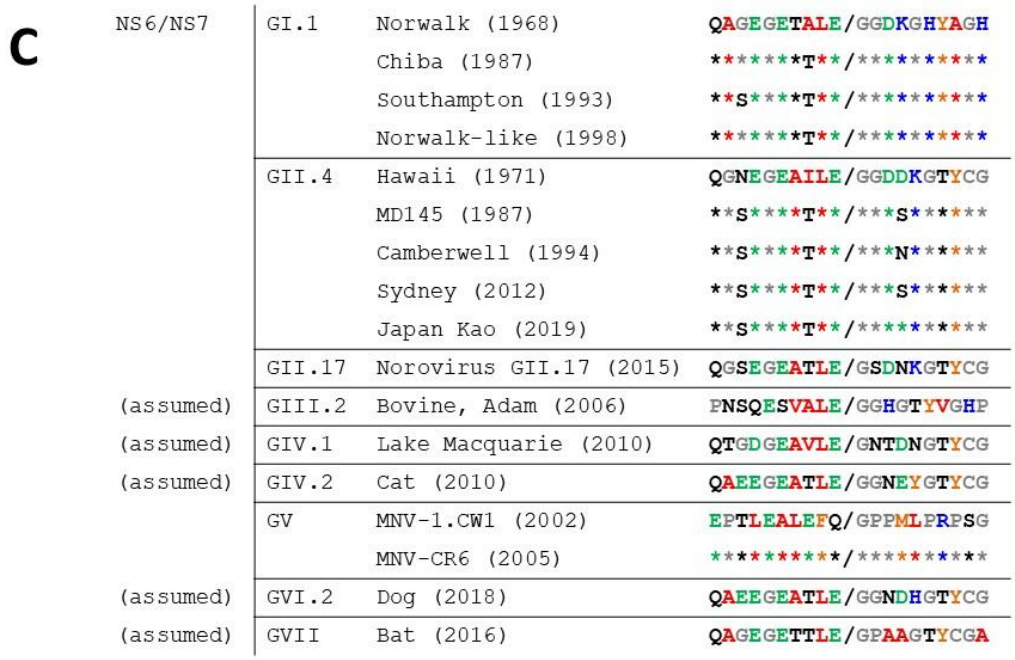

Figure 13: Alignments of protease cleavage sites at NS4/NS5, NS5/NS6 and NS6/NS7

Norovirus amino acid sequence alignments for multiple strains spanning GI-GVII for protease cleavage sites (A) NS4/NS5, (B) NS5/NS6 and (C) NS6/NS7. Cleavage sites for GIII, GIV, GVI and GVII are assumed. Amino acid properties are indicated as: positive (blue); negative (green); polar uncharged (black); short-chain hydrophobic (red); long-chain or ring-structure hydrophobic (yellow); and special (grey). Point of cleavage is indicated with "/". Identical amino acids within genotypes are indicated with "*".

The NS5/NS6 protease cleavage site is highly conserved across all analysed genogroups (**Figure 13B**). Variations are either minor, replacing a residue with a functionally similar one, or at P3 where the consensus is either a residue of negative charge or polar uncharged. The one break from the status quo at this position is an arginine present at P3 in GVII (bat). An unusual glutamine is present at P1 in GIII (bovine).

The NS6/NS7 protease sites are also highly conserved (**Figure 13C**). The P1' and P2' positions vary only for GII.17 and GIV at P2' with a polar and uncharged residue rather than a glycine or proline. The P4 positions are either polar or short hydrophobic amino acids. The P2 and P1 positions are leucine and glutamic acid respectively. The exception is for the MNVs (GV) where they are another hydrophobic amino acid, phenylalanine, and the polar glutamine respectively. More variation is present at P3, although this again is restricted to either a polar amino acid or a short hydrophobic amino acid. The outliers to this are again the MNVs where a negatively charged glutamic acid is present.

Substitution of the MNV-1.CW1 P4-P2' protease cleavage sites to a HNoV "early" cleavage site does not impact GFP nuclear shift in Huh7$^{mCD300lf\text{-}Sec61b}$ cells but does impact recovery titres

Each protease cleavage site in MNV-1.CW1 was mutated prior to IVT to a HNoV GII "early" protease cleavage amino acid sequence. This sequence of FELQ/GP is found in the reporter-system construct of the Huh7$^{mCD300lf\text{-}Sec61b}$ cell line. It is one of the similar sequences present in GI and GII noroviruses at the NS1-2/NS3 and NS3/NS4 cleavage sites. This specific sequence can be found at the NS3/NS4 site of Norovirus Japan Kao (GII). Partial-sequence mutations were also made keeping the P2-P1' sequence as LQ/G. Individual amino acid changes from the WT are noted with the use of lower case.

All eight mutants were transfected into Huh7$^{mCD300lf\text{-}Sec61b}$ cells with WT, RdRp F/S and Pro-C139A RNA transfections used as controls. Each transfection was monitored over a 48 hour period with multiple fields of view used to determine GFP-positive nuclei percentage (**Figure 14**). Shift of GFP from the cytoplasm to the nucleus showed little change in pattern when compared to the controls except in a few instances. The NS4/NS5 felq/Gp showed very few GFP-positive nuclei, however issues were noted with the RNA preparation. This result has been shown for completion purposes however no conclusions should be drawn from these results.

The NS4/NS5 felq/GK indicated a high percentage of GFP-positive nuclei at 48 hours post-transfection when this is not the case for either the WT or RdRp F/S controls, or any of the other mutants. The other most notable difference comes from the NS2/NS3 felq/GP mutant where GFP-positive nuclei were low at 24 hours post-transfection when compared to both controls. All mutants however, showed clear evidence of MNV protease production due to a clear observance of multiple GFP-positive nuclei.

No mutant had a recoverable titre at 48 hours post-transfection, except for NS2/NS3 felq/GP. This was measured by $TCID_{50}$ on BV-2 cells giving a result of 1.19×10^6 $TCID_{50}$/ml. The WT titre for this experiment was 1.19×10^5 $TCID_{50}$/ml.

In conclusion, mutation of the protease cleavage sites in MNV-1 to an HNoV "early" site did not impact protease cleavage, per se. However, recovery of infectious MNV from an RNA transfection with a protease cleavage site mutation was only possible from a full FELQ/GP present at the NS2/NS3. This suggests that either the timing of polyprotein processing is affected leading to a block in infection, or there are other effects associated with the specific mutation not related to polyprotein processing. The cleavage site between NS2 and NS3 has been identified to tolerate a heterologous cleavage site with loss of titre. Further analysis would now be needed to confirm reproducibility and sequence integrity of this newly generated recombinant virus.

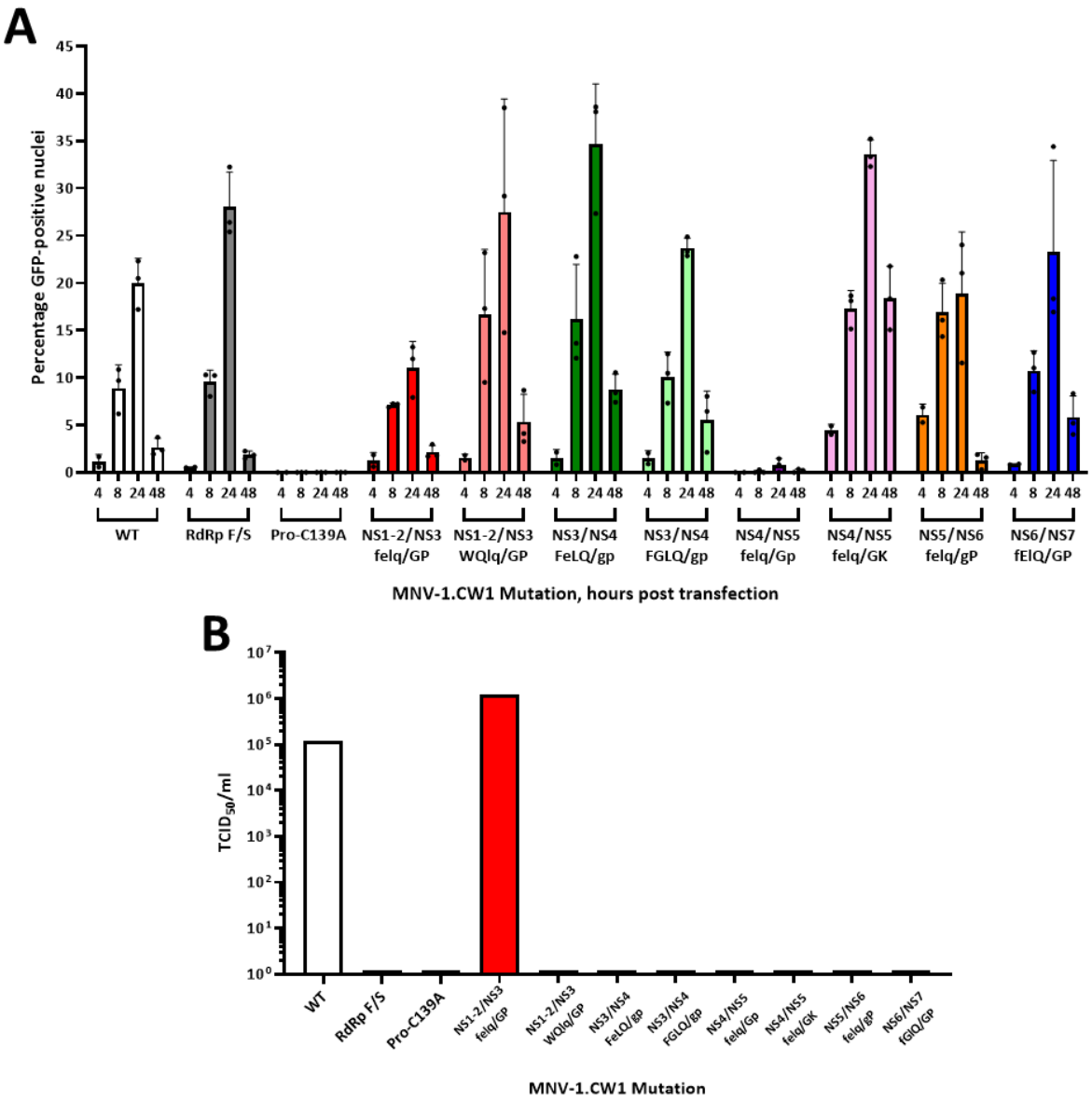

Figure 14: Nuclear shift in Huh7$^{mCD300lf\text{-}Sec61b}$ cells transfected with MNV-1.CW1 protease cleavage site mutations

(A) Percentage of GFP nuclear shift in Huh7$^{mCD300lf\text{-}Sec61b}$ cells transfected with MNV-1.CW1 WT (white), RdRp F/S (grey), protease mutation C139A (black), NS1-2/NS3 felq/GP (red), NS1-2/NS3 WQlq/GP (light red), NS3/NS4 FeLQ/gp (green), NS3/NS4 FGLQ/gp (light green), NS4/NS5 felq/Gp (purple), NS4/NS5 felq/GK (pink), NS5/NS6 felq/gP (orange) and NS6/NS7 fElQ/GP (blue) RNA over a 48 hour period. Percentages calculated from multiple fields of view observed through fluorescence microscopy. Error bars indicate standard deviation. (B) Reverse genetics transfection titres (P0) by $TCID_{50}$ on BV-2 cells, from recovered transfections performed on Huh7$^{mCD300lf\text{-}Sec61b}$ cells. Recombinant MNV-1.CW1 transfections of WT, RdRp F/S, protease mutation C139A, NS1-2/NS3 felq/GP, NS1-2/NS3 WQlq/GP, NS3/NS4 FeLQ/gp, NS3/NS4 FGLQ/gp, NS4/NS5 felq/Gp, NS4/NS5 felq/GK, NS5/NS6 felq/gP and NS6/NS7 fElQ/GP shown using identical colour scheme.

Small peptide insertions between MNV-1.CW1 NS1-2 and NS3 did not impede protease function in Huh7$^{mCD300lf\text{-}Sec61b}$ cells transfected with genomic norovirus RNA

Having identified a protease cleavage site that recognises alterations, the site was investigated for its ability to tolerate insertions. For this, a small sequence contained an HA and FLAG tag was inserted, also containing flanking restriction sites for future insertion of alternative reporter genes. The protease cleavage site (AE/GP) was copied (shown previously in **Figure 8B**) to ensure an unaltered NS1-2 and NS3. This mutation is denoted "HA-FLAG". Site-directed mutagenesis introduced two amino acid changes (AE to LQ) to the copied, second cleavage site to create an MNV/HNoV hybrid protease cleavage site (LQ/GP). This mutation is denoted "HA-FLAG (LQGP)".

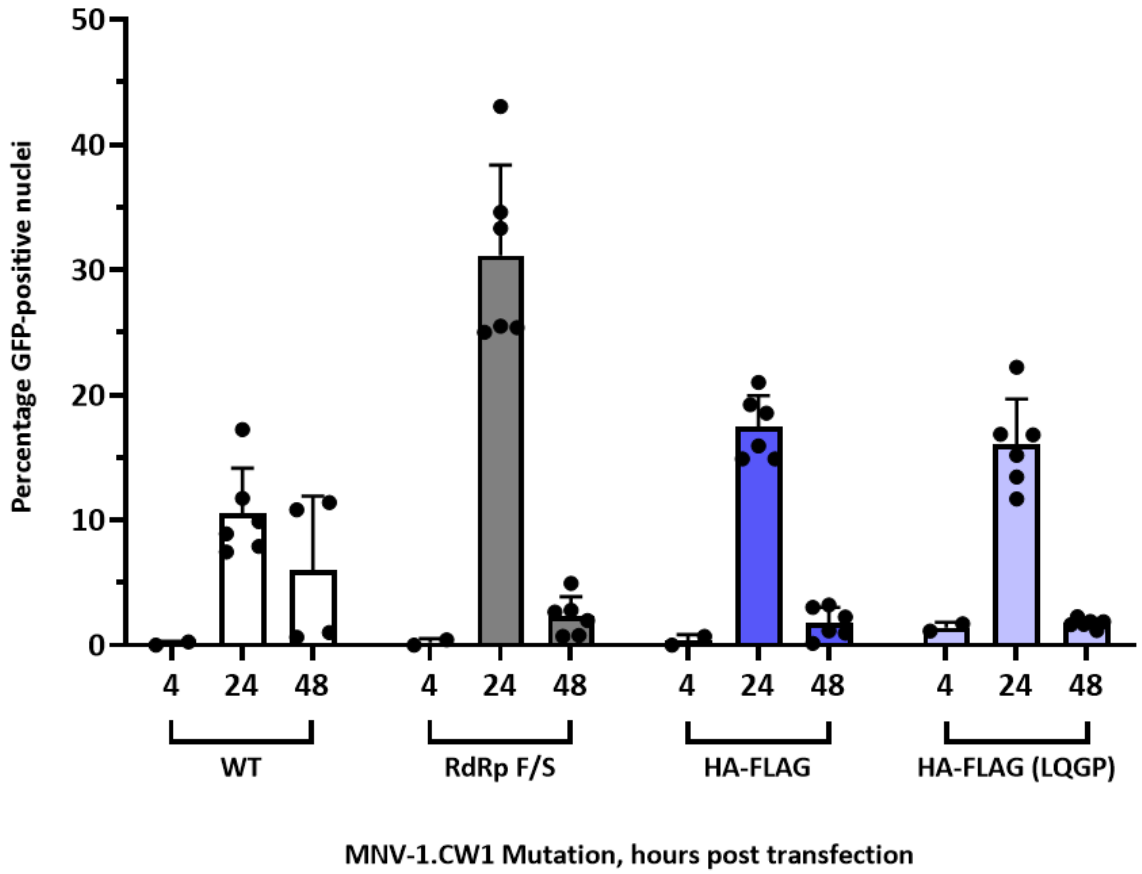

Figure 15: Nuclear shift in Huh7$^{mCD300lf\text{-}Sec61b}$ cells transfected with MNV-1.CW1 NS1-2/NS3 insertion mutations

Percentage of GFP nuclear shift in Huh7$^{mCD300lf\text{-}Sec61b}$ cells transfected with MNV-1.CW1 WT (white), RdRp F/S (grey), NS1-2/NS3 HA-FLAG insertion mutant (dark blue) and NS1-2/NS3 HA-FLAG (LQGP) insertion mutant (light blue) RNA over a 48 hour period. Percentages calculated from multiple fields of view observed through fluorescence microscopy. Error bars indicate standard deviation.

Nuclear shift was analysed over a 48 hour period after a transfection of WT and mutant RNAs of MNV-1.CW1 containing the insertions (**Figure 15**). As expected, both WT and RdRp F/S transfections showed high overall nuclear GFP illumination at 24 hours post-transfection and the RdRp F/S when compared to the WT transfected cells showed a higher percentage of cells had positive nuclei.

Both insert mutants of HA-FLAG and HA-FLAG (LQGP) demonstrated a near identical phenotype when compared to one another. Both showed their highest GFP-positive nuclei at 24 hours post-transfection with a reasonably narrow range at no more than 20%. This is very similar to the fields of view noted from the WT transfected cells and showed that the insertion did not affect protease function. Both insert mutants differed from the WT by 48 hours post-transfection showing closer similarities to the RdRp F/S transfected cells. Only a small percentage of cells showed GFP-positive nuclei at 48 hours without the slightly larger range that could be observed for the WT at the same time point.

MNV-1.CW1 virions tolerate a small peptide insertion with a unique protease cleavage site

In order to determine if the insertion lead to infectious virions, the transfection lysate was passaged onto Huh7$^{mCD300lf\text{-}Sec61b}$ cells and infectious titres were determined (**Figure 16**).

Transfection lysates were applied to fresh Huh7$^{mCD300lf\text{-}Sec61b}$ cells and monitored regularly for up to 72 hours post-infection under a fluorescence microscope (**Figure 16A**). Nuclei positive for GFP were observed in WT-infected cells from 12 hours with consistent fluorescence between 24-48 hours post-infection. At 30 hours post-infection, approximately 50% of cells in observed fields of view showed a shift of GFP to the nuclei. The infection was stopped after 48 hours due to very few remaining live cells still attached to the flask.

After titration by $TCID_{50}$ on BV-2 cells (**Figure 16B**), recombinant WT virus had a titre of 1.76×10^8 $TCID_{50}$/ml. Neither the RdRp F/S control nor the HA-FLAG mutant at any time point, in any field of view showed a GFP-positive nucleus. Neither the RdRp F/S control nor the HA-FLAG mutant produced a titre by $TCID_{50}$, nor was cytopathic effect (CPE) observed.

The insertion mutant with a single adjusted protease cleavage site, HA-FLAG (LQGP) showed GFP-positive nuclei from 24 hours post-infection with the majority of these nuclei being present from 48 hours post-infection. Less than 10% of nuclei were positive for GFP at 48 and 54 hours post-infection. At 72 hours post-infection the infection was terminated and titrated by $TCID_{50}$. Recombinant MNV-1.CW1 NS1-2/NS3 HA-FLAG (LQGP) was subsequently passaged to P3 on BV-2.

In summary, a short genomic protein sequence can be inserted between the NS1-2 and NS3 MNV-1 genome without disrupting protease production after transfection into Huh7$^{mCD300lf\text{-}Sec61b}$ cells. The subsequent passaging of transfection lysates on Huh7$^{mCD300lf\text{-}Sec61b}$ cells yields no nuclear shift nor titre for a simple insertion of HA-FLAG, but limited nuclear shift. Infectious virions were only recovered for HA-FLAG (LQGP) at a reduced titre compared to WT. Additional analysis and in particular sequencing of the entire genome is required to determine if potential compensatory mutations have developed which would explain the delayed rescue.

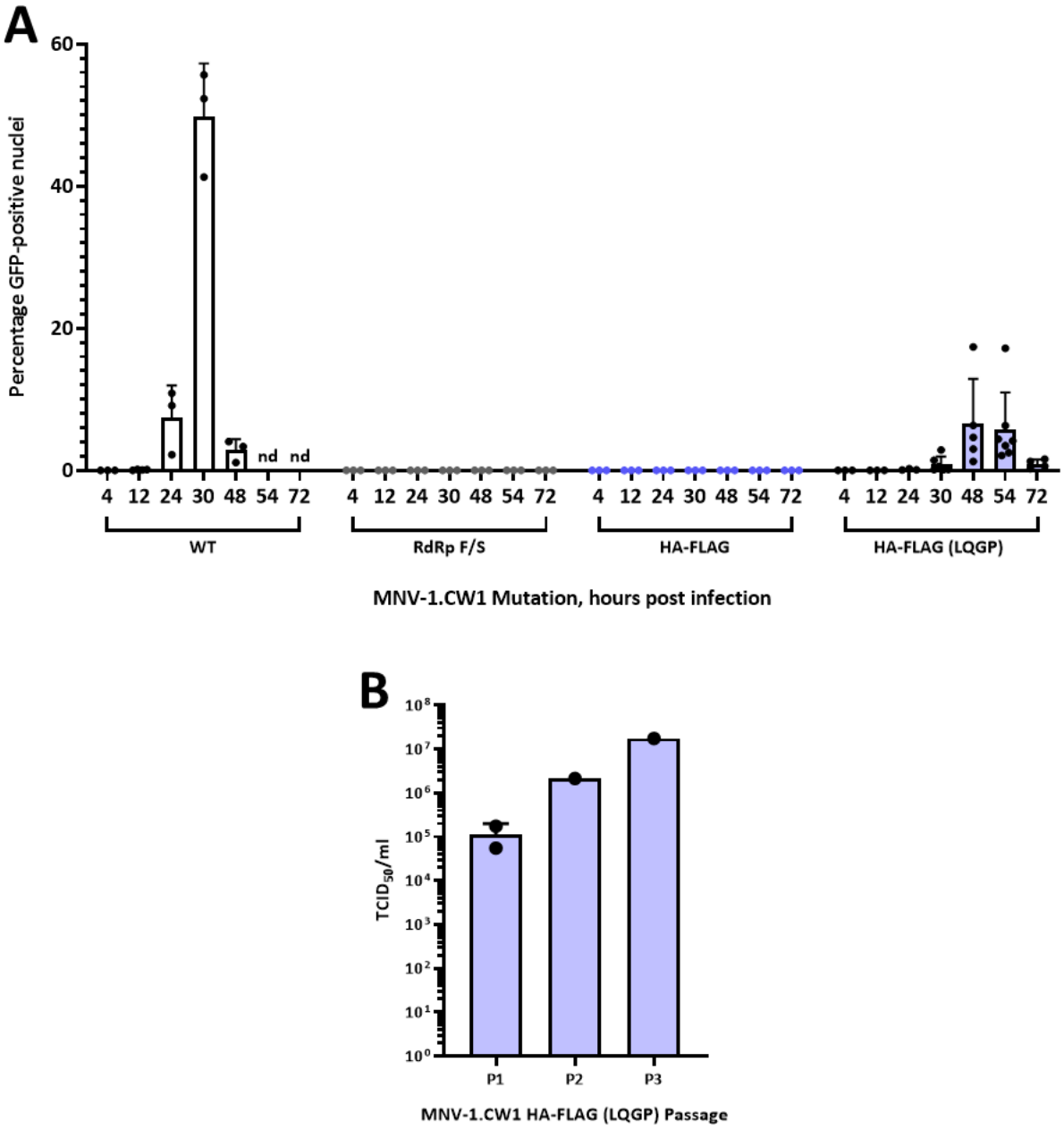

Figure 16: Nuclear shift in Huh7$^{mCD300lf\text{-}Sec61b}$ cells infected with MNV-1.CW1 NS1-2/NS3 insertion mutations' lysate

(A) Percentage of GFP nuclear shift in Huh7$^{mCD300lf\text{-}Sec61b}$ cells infected with MNV-1.CW1 WT (white), RdRp F/S (grey), NS1-2/NS3 HA-FLAG insertion mutant (dark blue) and NS1-2/NS3 HA-FLAG (LQGP) insertion mutant (light blue) transfection lysates over a 72 hour period. Infection with WT at time points 54 hours and 72 hours not determined (nd). Percentages calculated from multiple fields of view observed through fluorescence microscopy. Error bars indicate standard deviation. (B) Recombinant MNV-1.CW1 NS1-2/NS3 HA-FLAG (LQGP) passaging titres (P1-P3) by $TCID_{50}$ on BV-2 cells, from passages performed on Huh7$^{mCD300lf\text{-}Sec61b}$ (P1) and BV-2 cells (P2 and P3). Error bars indicate standard deviation.

Role of ions and bile acid in MNV infection using reverse genetics

For the study of the role of divalent cations in MNV infection, recombinant MNVs had to be generated with defined amino acid changes in the viral capsid. Recombinant WT MNV-1.CW1 and two MAb escape mutations had previously been generated in previous thesis work (Lane, 2021). A detailed assessment of quality control had yet to be described.

Generation of recombinant viruses

The experimental setup was assessed across the individual steps for quality control (**Figure 17**). Reverse genetics plasmid pT7:MNV\3'RZ and derivatives thereof were linearised at the end of the poly-A tail. Before *in vitro* transcription, a purification of the DNA was performed by phenol-chloroform extraction. Samples from after the linearisation and after the purification were run by gel electrophoresis (**Figure 17A**). This was to observe that the single-site restriction digest was complete and that the DNA had not been damaged during the purification.

Two distinct patterns were observed after a phenol-chloroform extraction. The expected and typical bands can be observed as represented by Prep. A, where both bands are of the same length at 11.8 kb pairs with no other band present. The thicker band after purification is due to more DNA loaded onto the gel despite the same volume, from the increase in concentration after purification. An unexpected pattern was occasionally observed to varying degrees of intensity. After some purifications, a band with a length of approximately 7 kb is observed, indicated here on Prep. B with the black arrow. At this low concentration in comparison to the desired band length, no influence was caused on the following *in vitro* transcription. What the exact cause for this band was could not be concluded. Contamination was ruled out as the same reagents were used at the same time for multiple extractions. These reagents were also replaced with independent stocks, however the same issue persisted. More intense lower bands, if observed, were more common in extractions that had taken more time (such as ten performed at once over the usual three or four) or been performed in hotter laboratory conditions (such as during the summer months). If a second band is observed, it is always of the same 7 kb length.

Once the linearised DNA was purified, it was *in vitro* transcribed. The RNA was then purified and finally capped ready for transfection. Samples at each stage were taken and run by gel electrophoresis. Two of such preparations are shown in **Figure 17B**. No RNA ladder was available so the GeneRuler™ 1 kb Plus DNA Ladder was used for comparison but could not be used to determine band length. Prep. X shows a typical and expected band pattern. Band intensity decreases as the concentration of the preparation decreases despite the same volume taken. A band with low intensity running slower than desired is visible after IVT and running a little faster after purification. This band is not visible after capping. The main RNA band is of a consistent size throughout.

Another example is what can occur during an RNA preparation is shown by Prep. Y. Both preparations, X and Y were performed at the same time from comparable DNA preparations. Neither initial DNA preparation showed any abnormality when run by gel electrophoresis. Both DNA preparations were of a similar concentration and the same DNA mass was used as template in IVT. After IVT, a band is visible but obvious smearing is evident. After purification some remnants of a band can be observed with the smear more intense by comparison. After capping only a faint smear is observed with no band. This is an example of RNA degradation. Transfection of this preparation did not yield notable nuclear shift nor a $TCID_{50}$ titre.

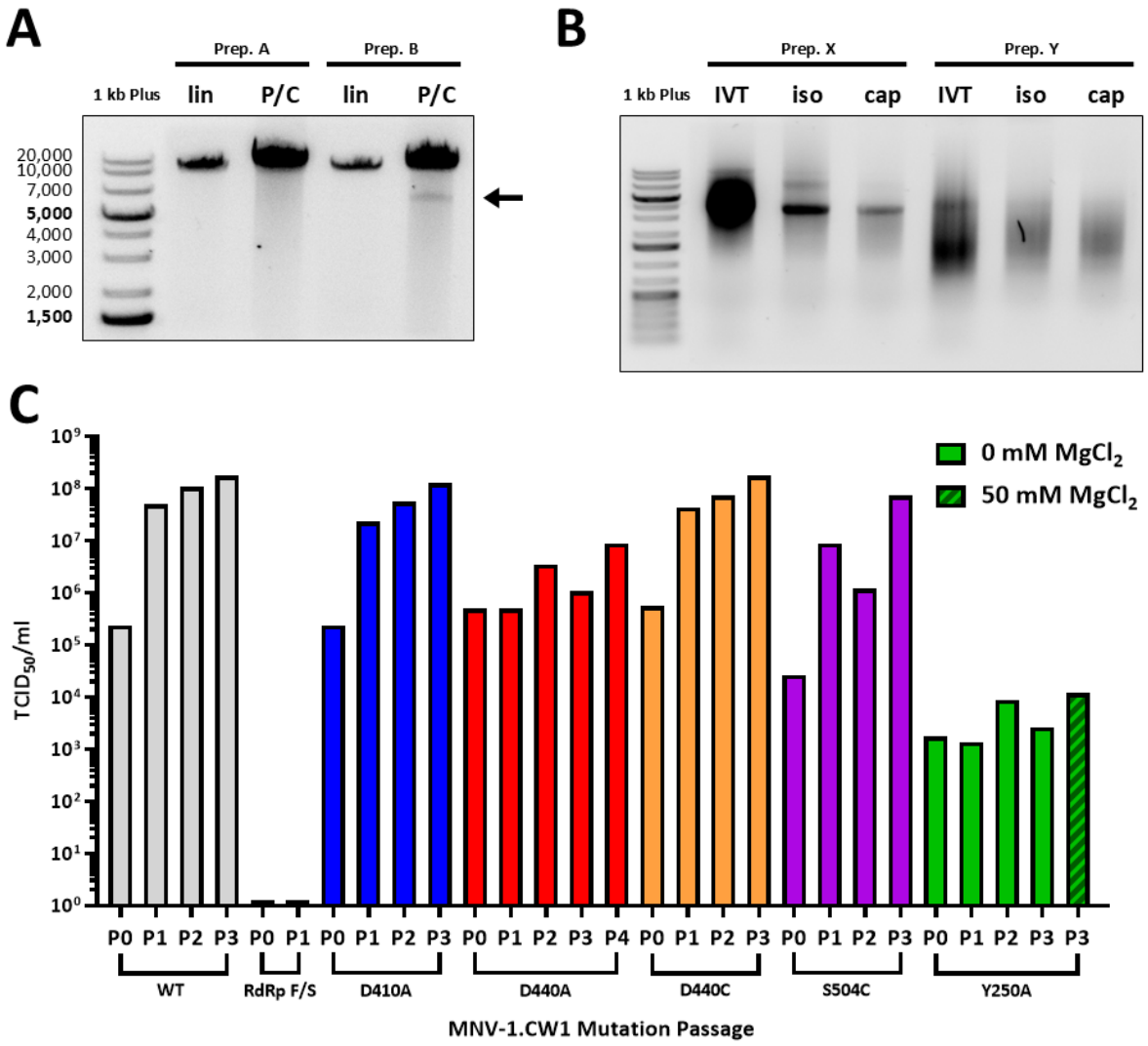

Figure 17: Plasmid linearisation with RNA preparation prior to transfection and recovered recombinant MNV-1.CW1 reverse genetics and passaging titres

(A) Two independent linearised (lin) and phenol-chloroform extracted (P/C) plasmid preparations (Prep.) run by gel electrophoresis prior to *in vitro* transcription for transfection. The arrow indicates a shorter fragment of approximately 7,000 bp that is occasionally observed after a phenol-chloroform extraction of linearised pT7:MNV\3'RZ (#245) or its derivatives. The marker GeneRuler™ 1 kb Plus DNA Ladder is shown with lengths indicated. (B) Two independent preparations (Prep.) of *in vitro* transcribed (IVT), purified or isolated (iso) and capped (cap) linearised pT7:MNV\3'RZ (#245) or its derivatives run by gel electrophoresis. Prep. X shows a typical pattern and Prep. Y the pattern of a degraded preparation after mishandling. The marker GeneRuler™ 1 kb Plus DNA Ladder is shown with no lengths indicated as they are not representative. (C) Reverse genetics transfection titres (P0) and passaging titres (P1-P4) by $TCID_{50}$ on BV-2 cells, from recovered transfections performed on Huh7$^{mCD300lf\text{-}Sec61b}$ cells. Recombinant MNV-1.CW1 transfections of WT (grey), RdRp F/S (black), D410A (blue), D440A (red), D440C (yellow), S504C (purple) and Y250A (green). Recombinant D440C sequenced at P2 later found to be D440R. Recombinant Y250A also passaged to a P3 in the presence of 50 mM $MgCl_2$, indicated with dashing.

Viral lysates from RNA transfections into Huh7$^{mCD300lf\text{-}Sec61b}$ cells were recovered and passaged on BV-2 cells over multiple passages (**Figure 17C**). Titres generally increased with every passage with WT virus reaching between 10^7-10^8 $TCID_{50}$/ml. The control mutant RdRp F/S containing a frame-shift in the RdRp as expected did not produce infectious virus, nor could the lysate be passaged. Mutations of the capsid protein at D410A, D440C and S504C resulted in a passaging behaviour not dissimilar to that of WT virus.

Other capsid mutations resulted in lower titres after multiple passages. Mutation D440A reached between 10^6-10^7 $TCID_{50}$/ml and Y250A reached between 10^3-10^4 $TCID_{50}$/ml. The addition of 50 mM $MgCl_2$ to a second P3 of Y250A was not sufficient to raise this titre substantially.

Recombinant mutants were sequenced at P3 from a cDNA sample derived from RNA extracted from viral lysate. Mutant Y250A RNA was not extracted due to a low viral titre. This mutation was therefore not confirmed. The mutations D410A and D440A were confirmed in their respective viral samples with no other mutations present in the VP1. All experiments using viruses with these mutations were performed using an ammonium sulphate precipitated P4 stock in a sodium phosphate buffer, generated directly from the sequenced P3 stock.

The desired mutation of D440C was sequenced at P2 with the intention of sequencing at a P3 should subsequent stocks been necessary for experimentation. Sequencing data that was returned showed this mutation to actually be D440R with no other mutations present in the VP1. No mixed data for residue 440 was observed. A further sequencing of the P3 was not performed as D440R was not a needed mutation for subsequent planned experiments. The mutation S504C was confirmed, sequencing at P2 and P3. Further experimentation with this recombinant MNV was not pursued.

In summary, five recombinant MNV-1 viruses, with mutations in respective functional sites, were generated. Mutations in the divalent cation binding sites did not have a major impact on infectivity. The recombinant virus with the mutation in the bile acid binding site on the other hand, was rescuable but very low in yield. This mutation, Y250A, was therefore excluded from functional analysis for now.

Functional analysis of recombinant MNV

Binding of Mg^{2+} to D440 but not D410 prevents neutralisation from MAb A6.2

As has been shown in previous studies, MNV-1.CW1 can be neutralised by MAb A6.2 by approximately three logs, PFU/ml. When controlled for divalent cation presence before and during infection, the addition of Mg^{2+} increases viral titre by a half log (**Figure 18A**). The neutralisation of MNV-1.CW1 is prevented with the addition of higher concentrations of Mg^{2+} simultaneous to the addition of MAb A6.2 and infection.

For the MNV mutant with only the D440 cation-binding residue remaining, MNV-1.CW1-D410A, the virus is neutralised by the addition of MAb A6.2 by approximately four logs (**Figure 18B**). The addition of increasing concentrations of Mg^{2+} slightly increases viral titre, although not to the comparable significance of the WT. Viral titres are restored to non-neutralised levels with the addition of higher concentrations of Mg^{2+}.

The MNV mutant with only the D410 cation-binding residue remaining, MNV-1.CW1-D440A, showed a near identical slight but significant increase in viral titre with the addition of increasing Mg^{2+} concentrations (**Figure 18C**). Contrary to both the WT and D410A viruses, D440A titres could not be restored by $MgCl_2$, to non-neutralised levels with simultaneous MAb A6.2 addition during infection. Even the highest $MgCl_2$ concentration tested was still three to four logs below that of a typical infection titre.

The binding of a divalent cation to D440 is necessary to escape the neutralising MAb A6.2 during MNV-1.CW1 infection. In conclusion, the divalent cation impact on MNV-1.CW1 infection is residue-dependant.

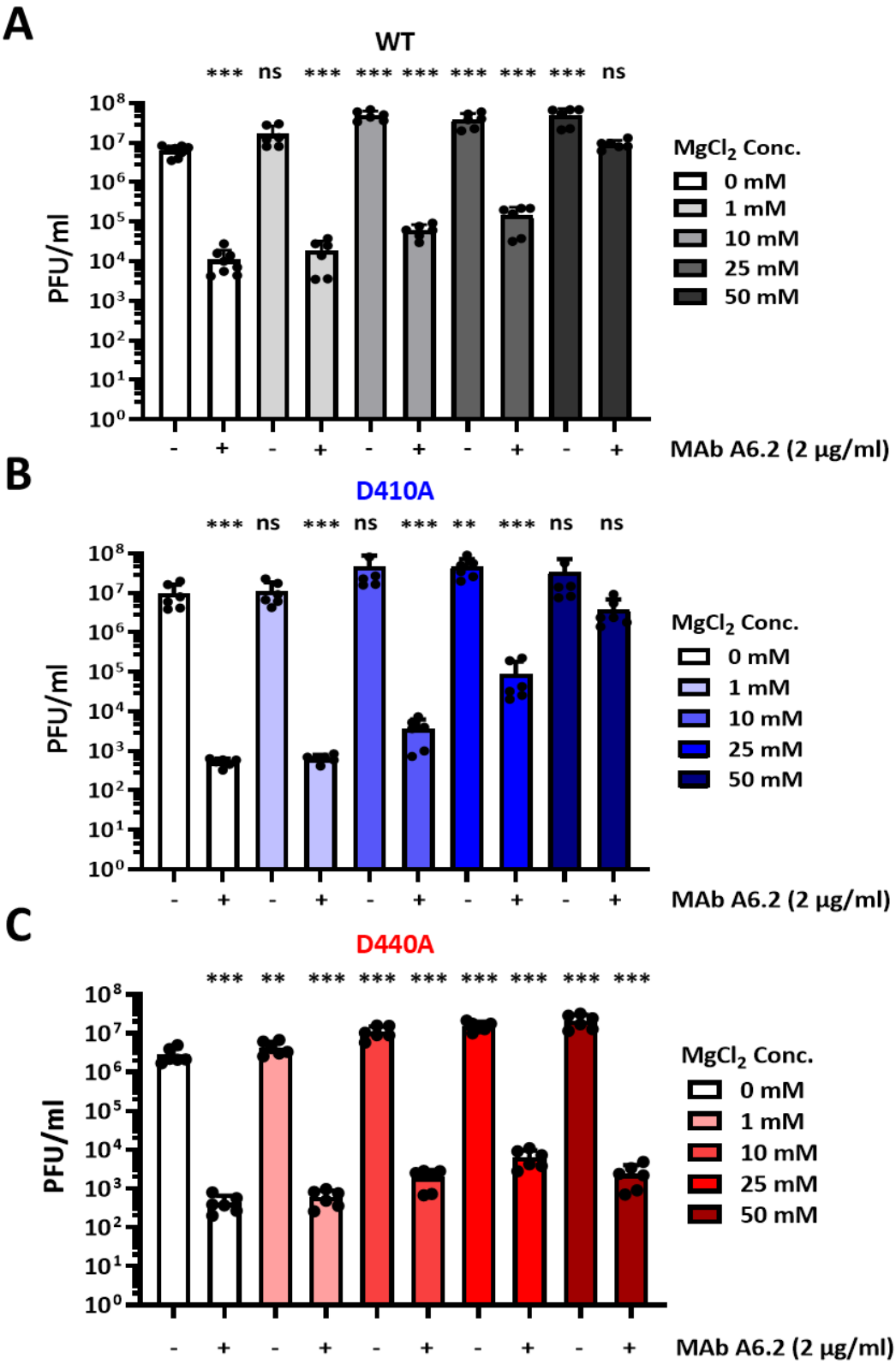

Figure 18: Comparison of recombinant WT, D410A and D440A MNV infection in increasing $MgCl_2$ concentrations in the presence of neutralising antibody A6.2

(A) WT MNV-1.CW1 plaque assay infection on Huh7$^{mCD300lf\text{-}Sec61b}$ in the presence of MAb A6.2 and increasing $MgCl_2$ concentrations. Performed by M. Chaika. (B) D410A MNV plaque assay infection on Huh7$^{mCD300lf\text{-}Sec61b}$ in the presence of MAb A6.2 and increasing $MgCl_2$ concentrations. (C) D440A MNV plaque assay infection on Huh7$^{mCD300lf\text{-}Sec61b}$ in the presence of MAb A6.2 and increasing $MgCl_2$ concentrations. Error bars indicate standard deviation. Statistical analysis performed in Prism 10; lognormal Brown-Forsythe and Welch ANOVA with multiple comparisons. P value: 0.12 (ns), 0.033 (*), 0.002 (**), <0.001 (***).

Mg^{2+} and GCDCA act synergistically to prevent MNV neutralisation by MAb A6.2

A synergistic effect of Mg^{2+} and bile acid was investigated in Huh7$^{mCD300lf\text{-}Sec61b}$ cells (**Figure 19**). When controlling for divalent cations, the presence of 500 µM GCDCA did not prevent neutralisation by MAb A6.2 (**Figure 19A**). A low $MgCl_2$ concentration of only 1 mM as also shown above is not sufficient to prevent the effects of MAb A6.2. When both GCDCA and 1 mM $MgCl_2$ are present during infection, viral titres increase by two logs and only one log below that of a typical infection. Titres are increased and neutralisation is prevented under a high $MgCl_2$ concentration regardless of GCDCA presence.

Similar observations were made on BV-2 cells where the combination of both 1 mM $MgCl_2$ and GCDCA nearly restored the titre to a typical WT level (**Figure 19B**). What is observable on BV-2 that is not on Huh7$^{mCD300lf\text{-}Sec61b}$ is the effect of GCDCA on both infections in the presence of and without MAb A6.2. Some significant increase in titre can be observed with the addition of 500 µM GCDCA. This is not the case on Huh7$^{mCD300lf\text{-}Sec61b}$ were Mg^{2+} is required to have any observable effect. At the higher $MgCl_2$ concentration on BV-2 cells, slightly higher titres can be observed in the presence of GCDCA over just the 50 mM $MgCl_2$.

Persistent strain, MNV-CR3, was also tested acquiring similar albeit subtler results when compared to MNV-1.CW1 (**Figure 19C**). Neutralisation with MAb A6.2 only dropped titres by approximately two logs, however the combination of 1 mM $MgCl_2$ and 500 µM GCDCA while in the presence of MAb A6.2 increased titres by a log. This cannot be observed for neutralised infections with the addition of either GCDCA or 1 mM $MgCl_2$.

A low concentration of $MgCl_2$, insufficient to prevent neutralisation by MAb A6.2 alone, permits the escape of MNV-1.CW1 when also in the presence of GCDCA. When controlling for divalent cation concentration, GCDCA alone cannot prevent neutralisation by MAb A6.2.

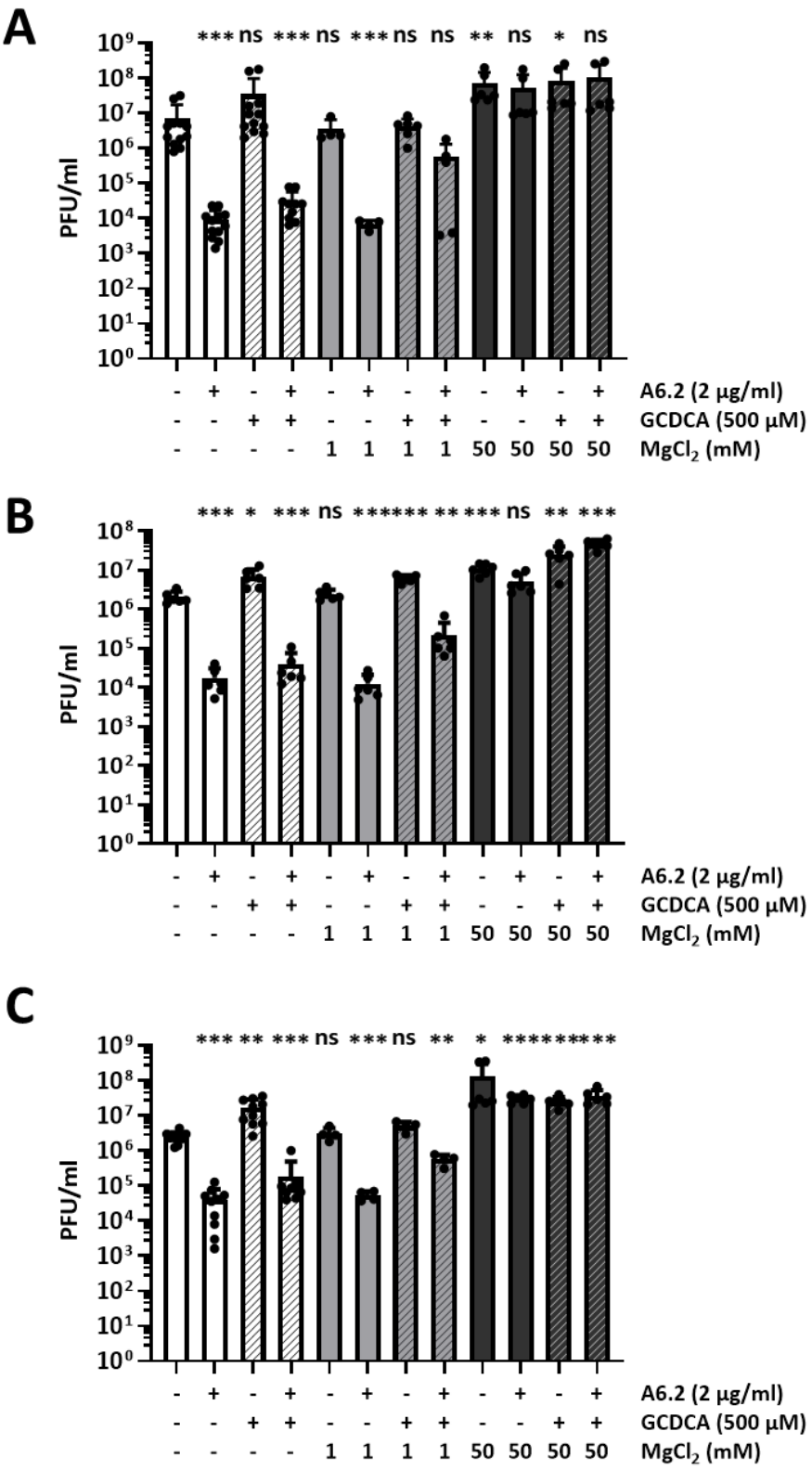

Figure 19: MNV infection in the presence of MAb A6.2, GCDCA and $MgCl_2$

(A) MNV-1.CW1 plaque assay infection on Huh7$^{mCD300lf\text{-}Sec61b}$ cells in the presence of neutralising MAb A6.2, 500 µM GCDCA and both 1 mM and 50 mM $MgCl_2$. Performed by M. Chaika. (B) MNV-1.CW1 plaque assay infection on BV-2 cells in the presence of neutralising MAb A6.2, 500 µM GCDCA and both 1 mM and 50 mM $MgCl_2$. (C) MNV-CR3 plaque assay infection on Huh7$^{mCD300lf\text{-}Sec61b}$ cells in the presence of neutralising MAb A6.2, 500 µM GCDCA and both 1 mM and 50 mM $MgCl_2$. Error bars indicate standard deviation. Statistical analysis performed in Prism 10; lognormal Brown-Forsythe and Welch ANOVA with multiple comparisons. P value: 0.12 (ns), 0.033 (*), 0.002 (**), <0.001 (***).

Mg^{2+} presence during MNV infection prevents neutralisation with polyclonal Ab

Neutralisation assays were performed using polyclonal Ab on Huh7$^{mCD300lf\text{-}Sec61b}$ (**Figure 20**). Polyclonal Ab reduces the titre of MNV-1.CW1 by approximately one to two logs. Neither GCDCA nor a low $MgCl_2$ concentration were sufficient to prevent neutralisation with polyclonal Ab. A higher concentration of $MgCl_2$ did prevent neutralisation by polyclonal Ab but the simultaneous addition of GCDCA has no effect in titre.

In conclusion, low Mg^{2+} concentrations permit GCDCA to prevent MNV neutralisation by MAb A6.2.

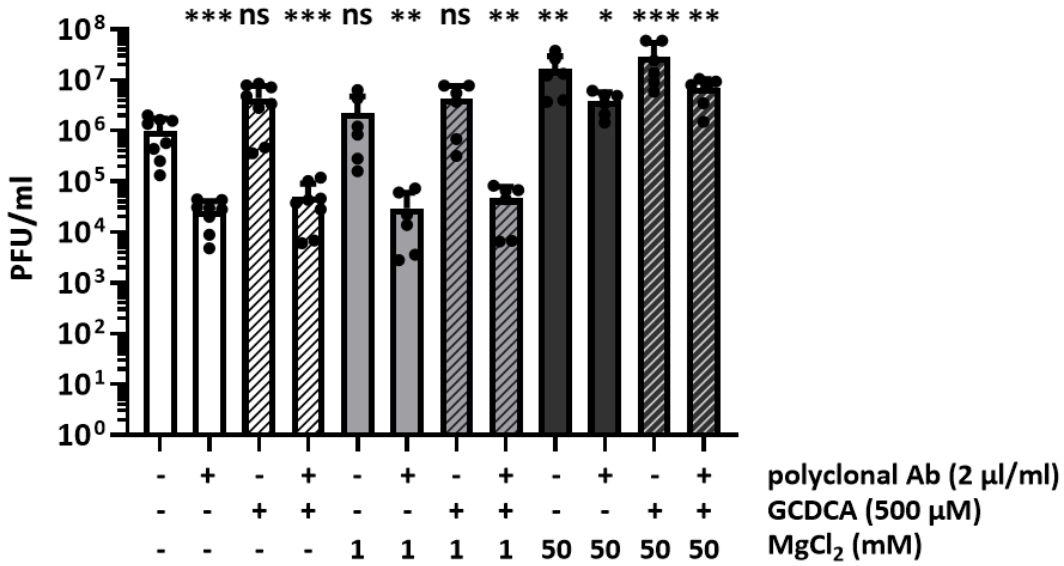

Figure 20: MNV polyclonal antibody neutralisation assay in the presence of GCDCA and $MgCl_2$

MNV-1.CW1 plaque assay infection on Huh7$^{mCD300lf\text{-}Sec61b}$ in the presence of neutralising polyclonal Ab, 500 µM GCDCA and both 1 mM and 50 mM $MgCl_2$. Error bars indicate standard deviation. Statistical analysis performed in Prism 10; lognormal Brown-Forsythe and Welch ANOVA with multiple comparisons. P value: 0.12 (ns), 0.033 (*), 0.002 (**), <0.001 (***).

Discussion

This study has explored the flexibility of the MNV-1.CW1 genome with regards to ORF1: implementing an integrated cellular GFP reporter into an RNA-based MNV reverse genetics system and monitoring protease production from transfected m^7G-capped RNA; and identifying a tolerant insertion site within the genome that may permit the addition of a protein. The role of divalent cations on MAb antibody escape and their synergistic effect with bile acid has been investigated. The cloning method and site-directed mutagenesis system established here provides a foundation for the future study and genetic engineering of MNV.

Establishment of a scalable mutagenesis platform

A scalable reverse genetics mutagenesis platform was established that allows site-directed mutations and flexible insert of protein-coding sequences at multiple positions in the MNV genome. This can be performed using modular plasmids and strategically chosen restriction sites, with cloning feasibility primarily limited by site availability and cost.

Both pT7:MNV-DEcoRV-PmlI (#324) and pBluescriptSK(-)fragment[GV-CW1-NS] (#398) permit site-directed mutagenesis. This allows for mutations to be introduced at any site within the MNV-1.CW1 genome, with an exception at the HindIII restriction site, as this site is used for subcloning. Any mutated sites can be easily cloned back into the WT reverse genetics plasmid pT7:MNV\3'RZ. Changes to six bases in the NS7 RdRp making up the HindIII recognition site is not possible with this current setup.

Further investigation into the insertion of a protein-coding gene can be carried out with the use of pT7:MNV\3'RZ-NS1-2/NS3(HA/FLAG) (#406) as the current small insert is flanked by two unique restriction sites. This should allow for the insertion of sequences for other desired proteins and act as a starting framework for future study. The intermediate precursor plasmid pBluescriptSK(-)fragment[GV-CW1-NS]-NS1-2/NS3(HA/FLAG) (#404) has also been used to generate a mutation in a protease site opening up avenues for further exploration.

Should other protease sites be of further interest, this cloning technique could be adapted with plasmid synthesis costs dependant largely on the size of the inserted protein rather than the MNV genome. For example, plasmid pBluescriptSK(-)fragment[GV-CW1-NS] (#398) could be used, but different restriction enzyme sites within the MNV-1.CW1 genome would need to be used to insert a protein-coding gene between two other NS proteins, not explored here. For simplicity, these sites are recommended:

Table 7: Table of suggested restriction enzymes

Protease cleavage site	Preceding restriction enzyme	Proceeding restriction enzyme	Remarks
NS1-2/NS3	FseI	EcoNI	Explored here, 510 bp
NS3/NS4	MfeI	AflII	520 bp
NS4/NS5	BamHI	BsgI or SphI	No unique sites present in NS5. 465 bp or 774 bp respectively, assess costs.
NS5/NS6	BamHI	BsgI or SphI	No unique sites present in NS5. 465 bp or 774 bp respectively, assess costs.
NS6/NS7	SphI	HindIII	312 bp

Technical optimisations

Gel electrophoresis can be used to gauge the quality of DNA and RNA prior to a transfection. Bands can be observed to be of a consistent length over the preparation from linearisation of the plasmid, to IVT to capping. It is particularly crucial to observe bands in an RNA gel prior to transfection, to determine whether an issue arising with the transfection may be due to the RNA preparation itself rather than a cellular or viral factor. Bands of RNA can be observed to run slower than an expected band and

this is likely due to folding of the RNA in multiple conformational states. This upper band is no longer visible after capping due to the denaturation step prior to the addition of the capping reagents (Edelmann *et al.*, 2014).

Gel electrophoresis is essential in identifying more major issues with a preparation such as a degradation. In many linearisations of plasmid pT7:MNV\3'RZ (#245) and its derivatives, a band of approximately 7 kb can sometimes be observed. What this band is composed of is not clear. Contaminations have been ruled out suggesting a quirk with the structure of this linear plasmid in particular combined with a handling issue. This band is mostly observed after: an extraction performed in warmer laboratory conditions; inexperience resulting in extended time period where the DNA is not on ice; or when physically processing a larger quantity at once also resulting in extended periods where the DNA is not on ice.

Handling or contamination issues due to the use of non-RNase-free plastics may have caused the resulting degeneration of RNA preparations. The running of both these DNA and RNA sample sets by gel electrophoresis are crucial. If the linearised DNA preparation exhibits an unwanted lower band of a high intensity, it is wise to repeat the procedure rather than risk a low quality and low concentration RNA preparation, unsuitable for transfection. Although the RNA preparation cannot be fully compared until after capping, extra samples could be taken at the different steps and compared using an RNA ladder to identify issues in degradation or band length. Comparison to an RNA ladder was not performed here as this was not available. Comparison prior to transfection should be performed, as the capped RNA should be of a sufficient quantity and quality to ensure a successful transcription and translation in the cell.

Mutagenesis sites

Some mutations performed in the VP1 of the MNV-1.CW1 genome are recoverable as infectious viruses, and can be passaged as WT in BV-2 cells. Specifically D410A, D440C (sequenced as D440R), and S504C behave, in terms of infectivity, as a WT recombinant virus. Other mutations in the VP1, originally generated through passaging with MAbs (Kolawole, Li, *et al.*, 2014) have previously been expressed by this reverse genetics system (Creutznacher *et al.*, 2022; Lane, 2021). The VP1 mutation shown in this study to be sensitive to Mg^{2+}-dependant MAb escape, D440A, although recoverable and able to be passaged, does not reach WT-like titres. This D440A mutation and the D440C mutation sequenced as D440R by the second passage may indicate sensitivity in this region.

Other VP1 mutations in and around the GCDCA binding pocket were attempted with only one, Y250A, resulting in a recoverable virus. The small titre was however too small to obtain an adequate genome mass suitable for reverse transcription and sequencing. Other possible mutations of Y250D, R437D and R437A were attempted (data not shown) but resulted in no titre and were abandoned. These sites were selected as the VP1 with these mutations have been analysed in regards to bile acid binding (Nelson *et al.*, 2018). This may demonstrate that the structure of the VP1 is particularly sensitive in this bile acid binding region and its integrity is crucial to the viral capsid in regards to infection.

Of the two mutations in this region that were recoverable, D440A and Y250A, the former is adjacent but not an integral structure of the pocket, and the latter is a minor change of a long hydrophobic amino acid to a shorter one. These mutations are likely disruptive enough to stunt infectivity, but not entirely sufficient to cause the capsid to be unstable. Attempting to change a long and hydrophobic tyrosine to a negatively changed aspartic acid likely causes structural interactions that fail the capsid. The arginine at residue 437 is negatively charged and is again likely very structurally relevant. Changing this to a positive amino acid (aspartic acid) or to a hydrophobic one (alanine) is likely destabilising the capsid structure.

The mutation that was most surprising was an attempted D440C. This was initially attempted with the intention of using an infectious virus and not just a virus-like particle or isolated VP1 to perform cysteine labelling. The site was chosen as it is exposed and a D440A mutation had already been recovered. This

indicated the residue was accommodating of modifications. Interestingly the transfection resulted in an infectious virus and behaved similarly in terms of a high passage titre to WT. Either the desired mutation or a reversion to WT was expected. If not either of these then another negative amino acid in glutamic acid was expected. Once sequenced, it was clear that this residue was in fact a positively charged arginine. No other mutations were present. Why a mutation to a very different amino acid is not only possible but preferred is certainly, for lack of a better term, a little odd. How the viral capsid accommodates this change would be an interesting topic to pursue and may require crystallisation which is beyond the scope of this project.

What can be drawn from these results is that the recovery of MNV-1.CW1 recombinant mutants is robust. Mutations that can exist, even if slow growing or stunted, can be passaged and used for further experimentation. Those mutations likely unfavourable to the structure of the viral capsid and therefore unlikely to ever physically exist in anything other than a theoretical model, cannot be recovered.

Limitations of the GFP reporter system

The GFP reporter system requires the presence of viral protease for the observation of a shift of GFP from the ER to the nucleus in Huh7$^{mCD300lf\text{-}Sec61b}$ cells (Lingemann, 2020). This system can be therefore used to determine when translation of the polyprotein occurs. Transfected RNA is translation-ready and can be immediately utilised by the cellular machinery to produce the polyprotein in which NS6 protease is present.

This particular reverse genetics system methods has already been described (Wobus *et al.*, 2023) and the reporter system explained (Lingemann, 2020). The system has permitted for the generation of both WT and mutant MNV-1.CW1 to be used in GCDCA studies (Creutznacher *et al.*, 2022), however a detailed breakdown of the nuclear shift pattern with NS protein mutant controls needed to be established. Understanding at what time points a WT transfection shows sign of a shift and to what extent, and comparing this to intentional mutations resulting in no recoverable titre, a general idea of whether mutations introduced elsewhere for the purpose of other experiments express any differences.

The presence of protease can be reliably first observed from eight hours post-transfection. This is logical and fits within MNV replication cycle times (Wobus *et al.*, 2004). The greatest shift in GFP is observed 24 hours post-transfection. Evidence of CPE is obvious by this time-point, but most cells are not dead. By 48 hours, very few cells are intact. Polyprotein is clearly made by the cellular machinery from the point of transfection as a nuclear shift is observable from four to eight hours from transfected RdRp F/S RNA. The proportion of shifted cells when compared to WT is higher at eight and 24 hours post-transfection, with this higher percentage due to the death of cells from viral release in the WT transfection. This indicates that at up to 24 hours, there is still a sufficient quantity of translation-ready transfected RNA to produce NS6 protease. One can infer that this same transfected RNA will be available for protein production from ORF2.

Aside from a few outliers at 48 hours post-transfection, nuclear shift is low in RdRp F/S transfected cells. There is little NS6 protease remaining and little to no transfected RNA remains for translation. Any shift after 24 hours is due to protease produced by newly synthesised RNA. The synthesis of progeny RNA is not possible in the transfected RdRp F/S due to the premature STOP introduced in NS7 by the frame-shift.

The lower shift and CPE presence in the WT transfection from 24 hours is indicative of virus production. Polyprotein production is high up to 24 hours from the transfected RNA, but this transitions to production from viral RNA from 24 hours until cell death. Most cells by 48 hours are detached with any remaining in the latter stages of a nuclear shift with atypical cell membranes.

Importantly the changing of one residue in the active site of the NS6 protease (C139A), completely prevents a nuclear shift at any time-point. This is due to a lack of a functional protease, as the mutation

was intended. The lack of a functional protease also prevents the generation of an infectious virus. This is evident by the lack of observable CPE and a titre of 0 $TCID_{50}$/ml 48 hours post-transfection.

Manipulation of the protease cleavage sites in the NS polyprotein

Amino acid sequences for multiple norovirus genogroups were compared. Importantly, the P4, P2, P1, P1' and P2' were observed to be highly conserved in both "early" and "late" cleavage sites. The P3 site shows more variation. This may be due to, as noted by Emmott *et al.* (2015), a more subtle interaction of P3 in the protease-complex. Regardless of "early" or "late" cleavage, a trend appears across the cleavage sites. Pre-cleavage, position P4 is typically hydrophobic and position P1 is typically negative. Post-cleavage at P1' and P2', special amino acid structures are present as well as positive charges.

Although more variation does exist at the "early" cleavage sites observed, functionality of the amino acids remains similar. "Late" sites appear very conserved, even across genogroups and especially post-cleavage. However, P2 does show some interesting variation at the NS4/NS5 site. This is illustrative of the variation generally at the end of NS4, in particular that of the GI.1 sequences compared. Despite this, P4 and P1 remain conserved. The beginning of NS5 is very positively charged with the post-cleavage site being highly conserved. This may be an indicator of "late" cleavage.

It appears that "early" and "late" protease cleavage sites are conserved across genotypes. Some more minor variation typically appears pre-cleavage, keeping functionally similar antibodies in place, in particular P4 and P1. This is more noticeable for "early" sites with this variation suggesting some design flexibility should this be an area of future study. Here, manipulation of the NS1-2/NS3 protease cleavage site may open the possibility for a small peptide sequence to be genomically carried over multiple passages.

A six amino acid sequence (P4-P2') across the protease cleavage sites in MNV-1.CW1 was mutated to FELQ/GP and --LQ/GP. Neither sequence is present naturally in MNV-1.CW1 however this is the site found for NS3/NS4 in HNoV Japan Kao (GII) and is present in the Huh7$^{mCD300lf\text{-}Sec61b}$ reporter system. As noted by May *et al.* (2014), this is an "early" cleavage site. The purpose of this experiment was to attempt to further understand how and where cleavage can be altered in an MNV-1 reverse genetics system.

With a straightforward method of simply substituting bases for an, up to five amino acid change, the testing of a foreign cleavage site and its tolerated position could be determined. This approach aimed to eliminate other complicating factors such as packaging issues, small protein interactions, or protein misfolding which may arise should an NS protein sequence insertion be attempted. With this more simple information, it may be possible to concentrate on a particular site using a specific cleavage site sequence for use in a potential small-protein insertion mutant.

What was shown through these mutations is that no difference was made to protease function at any site that was either partially or fully mutated. The one exception to this was at NS4/5-felq/Gp, however this was later determined to be an issue with degradation in the transfected RNA. What was clear after titration was none but one of these mutations resulted in an infectious virus as compared to WT. The full mutation at NS2/3-felq/GP resulted in not only a titre, but one that is comparable to a WT. This mutant could not be tested due to a small volume and contaminating transfected RNA, but should be passaged further with a sample to be taken for sequencing analysis to confirm or deny the presence of the mutation in the MNV-1 genome. The fact that this is the only one of multiple transfections to result in an infectious virus is however suggestive that this site and sequence could be usable for further NS protein manipulation.

It should not be too surprising that an "early" site is more accommodating of a change to another "early" sequence already proven to function with an MNV protease. Across the norovirus genogroups, "late" sites are highly conserved. There will be two main reasons for this conservation. The first being that the NS proteins themselves are conserved, providing individually critical functions. The second is that their

cleavages from the polyprotein must occur after the cleavages of NS1-2 and NS3. This "late" cleavage may be crucial to the function of NS4, NS5, NS6 and NS7.

An "early" site NS protein may be located in the genome and use such a site so as to be cleaved earlier and be made available for a range of functions throughout the replication cycle. The functions of NS1 and NS2, both before and after caspase cleavage, and NS3 are not determined. Publications have suggested that NS1-2 may be used in glycolysis (Hafner *et al.*, 2024) as well as lipid recruitment and replication (Hung *et al.*, 2023). The function of NS3 may be chaperoning (Han *et al.*, 2018; Li *et al.*, 2018) or cell death (Wang *et al.*, 2023; Yen *et al.*, 2021) related. The function of NS4, the NS protein sharing both an "early" and a "late" cleavage site is also as yet unknown, possibly inhibiting protein secretion by disassembly the Golgi apparatus (Sharp *et al.*, 2010, 2012), is involved in replication (Doerflinger *et al.*, 2017), or assists apoptosis by NS3 (Yen *et al.*, 2021). These proteins may have broader functions that may vary across genotypes. This may permit some sequential flexibility.

This study has explored the flexibility of the MNV genome with regards to ORF1. The manipulation of the protease cleavage sites by swapping each site individually to a known, robust HNoV site expands a little upon what we already understand regarding protease cleavage (Emmott *et al.*, 2015; May *et al.*, 2014). This study has identified that the NS1-2/NS3 cleavage site seems to accommodate a change whereas the others do not. This may be due to more variation (although conserved within genogroups) of the site across genogroups. The NS1, NS2 and NS3 proteins may accept change due to their, as of yet unknown, varied functions. This may also have been simply due to a swapping of an "early" for another "early" cleavage sequence.

The mutations performed here are however narrow in scope and so the exact reasons for why the NS1-2/NS3 site may permit a change or an insertion cannot be concluded. What can be concluded is that the NS1-2/NS3 site gives a basis upon which to approach the insertion of a sequence coding for a protein of interest.

An insertion of a small protein sequence of only 96 nucleotides or 32 amino acids was performed between NS1-2 and NS3. This encompassed the sequence for HA and FLAG proteins as well as expanded, duplicated protease cleavage sites. A near identical insertion was made but with mutations in the second cleavage site that are found in HNoV and the Huh7$^{mCD300lf\text{-}Sec61b}$ reporter system. This eliminated a repeat in both the nucleic acid sequence and the protein sequence, but retained a sequence known to be recognised by MNV-1.CW1 protease. These mutations were performed with the intention of understanding whether insertions between the NS proteins would impact protease cleavage and if infectious viral progeny would be produced.

Transfections were observed for functional protease expression by way of nuclear shift in Huh7$^{mCD300lf\text{-}Sec61b}$ cells. Transfected mutant behaviour was similar to that of the WT transfection at 24 hours post-transfection with some CPE observed. This was different behaviour from that seen from the RdRp F/S control mutant where a higher proportion of cells are positive for protease but no CPE is observed. This similarity with the WT however had changed by 48 hours post-transfection. Although some CPE in the insertion mutants could be observed, it was not to the extent of the WT transfection and the proportion of cells positive for protease was at the similar low level that was observed for the RdRp F/S control mutant. It should be noted that no CPE is typically observed in RdRp F/S transfections. Importantly no titre from $TCID_{50}$ in BV-2 cells could be obtained after the 48 hour transfection.

These preliminary results show that translation of the polyprotein is not inhibited by the insertion, nor the subsequent folding and function of the protease as nuclear shift is present. The presence of CPE at 24 hours indicates virulence factors are expressed from the transfected and assumably translated RNA. It is possible that assembled capsid proteins are expressed, however a lack of titre indicates that potential virions are void of a packaged genome or the insertion damages the genome making it non-replicable. A lack of nuclear shift at 48 hours suggests a lack of reinfection that was observed in the WT. The phenotype was similar to that of the RdRp F/S control.

Although no titre was obtained 48 hours post-transfection from either HA-FLAG insertion mutations, their 24 hour phenotypes suggested a behaviour of an infectious virus. It was possible that some virus was active in these samples but the threshold to observe a titre by $TCID_{50}$ was too high for the very low viral quantity present. Passaging on Huh7$^{mCD300lf\text{-}Sec61b}$ cells and observing for a shift of the GFP signal to the nucleus would indicate a functional protease and therefore a translated genome from an active virus.

Lysates from the transfections were passaged on fresh Huh7$^{mCD300lf\text{-}Sec61b}$ cells and observed over 72 hours by fluorescence microscopy. The infection from the WT lysate showed a prominent nuclear shift after 24 hours with 50% of cells showing a shift at 30 hours post-infection. At 48 hours, the majority of cells were dead and the infection was terminated. A high titre of 1.76×10^8 $TCID_{50}$/ml was obtained. Neither the RdRp F/S control nor the standard HA-FLAG insert mutant ever showed a nuclear shift after infection with the transfection lysate. Titres of 0 $TCID_{50}$/ml were obtained for both.

Some GFP nuclear shift was observed in the infection with HA-FLAG (LQGP) transfection lysate. This was a small percentage of cells with most of the shift coming at 48 hours averaging at under 10% for total cells. The infection was terminated after 72 hours and a titre of 1.76×10^5 $TCID_{50}$/ml was obtained. This demonstrates that there was some active virus present in the transfection lysate and was somewhat replicable over a single passage.

These results indicate that the NS1-2/NS3 cleavage site is a reasonable site to attempt further insertion mutation experiments. What was demonstrated here is that the sequence of protease cleavage at this site is important. A repetition here failed to result in an infectious product, however a mutation in the repeated site so as to change the expressed amino acid sequence permitted viable progeny.

The slower nuclear shift response after infection may indicate not only protease function, but possibly the functions of NS1, NS2 and NS3. These early NS proteins, that are not currently understood to have any one defined function, may be involved in some capacity in replication and translation. A disruption with their cleavage from the polyprotein may be sufficient to slow the infection and stunt viral progeny and is a possible explanation for the delayed and lower nuclear shift percentage.

Attempting to insert a small protein between two NS proteins failed to result in an infectious virus despite evidence of protease production within the cell. Mutating the duplicated cleavage site to LQ/GP resulted in no titre after transfection, but the passaging of the lysate did result in signs of infection and a titre. This passage was of a small volume and low titre, rendering isolation of sufficient P1 genome mass suitable for reverse translation and sequencing difficult. The small protein insertion was also too small to have been observable by western blot and was used only as a proof of principle. Neither the genomic sequence, nor protein expression could be confirmed. However, the fact that this mutation (HA-FLAG LQGP) resulted in nuclear shift and a titre after infection with lysate, and its duplicated protease site insert mutant (HA-FLAG) counterpart did not, suggests that a reversion or removal of the full mutation was unlikely. A different phenotype of a delayed nuclear shift and a difference in titre by three logs compared to WT is also supportive that mutant HA FLAG (LQGP) may be a retainable mutation in MNV-1.CW1. This could be utilised as a first step in the generation of an infectious and easily passaged MNV with a small inserted NS protein.

This is not the only site that has been shown to accept an insertion. A very recent publication showed a 51 nucleotide total insertion at the NS4/NS5 cleavage site (Olson *et al.*, 2025). This copied the relevant nucleotides coding for the amino acid cleavage site (P4-P2') and an insert of a small, 11 amino acid protein called HiBiT. No easy-access cloning sites were included within the insertion. Another recent publication also introduced a HiBiT tag in a recombinant HNoV using a zebrafish reverse genetics model (Kotaki *et al.*, 2025). The NS4/NS5 cleavage site was not disrupted, nor was any other, as the HiBiT sequence was inserted between P7 and P6 of the NS4, near the 3' terminus of the NS protein.

This study and the recent publications differ in the type of cleavage chosen. This study chose an "early" cleavage site and exchanged it for another in the knowledge that this cleavage sequence is recognised

by MNV protease. The study performed by Olson *et al.* (2025) chose a "late" site, copying it to permit an insertion. This site is poorly processed (Emmott *et al.*, 2015) but this may work to an advantage. The exact function of NS4 is currently unknown. It may have multiple functions or it may be partially functional when not cleaved from NS5 (VPg). It is only in late transcription that the VPg is required and a delayed cleavage may not be an issue for either the function of NS4 or NS5. The study by Kotaki *et al.* (2025) took an alternative approach in not disrupting the cleavage site at all, thus tagging the NS4 with the luminescence marker.

The insertion mutants were not as robust as a WT with the NS4/NS5 mutant showing a loss in function after two to four passages (Olson *et al.*, 2025). No evidence was given with regards to the genome sequences. In this study, an infectious insertion mutant was only achieved after a round of passaging and the genome sequence was not confirmed. The luminescence of the HiBiT protein-tagged NS4 was maintained for at least five passages in zebrafish (Kotaki *et al.*, 2025). In future both the NS1-2/NS3 and the NS4/NS5 sites should be explored. Insertions at either site with optimisation to ensure a more robust infectious virus could be invaluable to track infection via a tag or fluorescence. Achieving robust insertion mutants at both sites could provide insight into the functions of NS proteins 1-4.

Overall, this study has shown limited but useful flexibility within ORF1 of the MNV-1.CW1 genome. The NS1-2/NS3 protease site, an "early" site, emerged as the only cleavage junction that consistently tolerated sequenced exchange or insertion. Together with recent evidence that the "late" NS4/NS5 site can also accept small inserts, these findings identify two promising regions that can tolerate useful insertions such as fluorescence or luminescence markers.

Synergistic effect of bile acid and divalent metal cations on antibody escape

Two residues shown to bind divalent cations were previously identified by Nelson *et al.* (2018) as D410 and D440. Using a method of recombinant mutant MNV generation by reverse genetics (Wobus *et al.*, 2023) that has been tested to generate stable VP1 mutants (Lane, 2021), two divalent cation non-binder mutants were generated. These were D410A and D440A with their VP1 sequences confirmed at a third passage. The replacing of an aspartic acid to an alanine permits both residues to be tested for their functions by removing said function.

In neutralisation assays in the presence of $MgCl_2$, binding of the cation to D410 only (MNV.1-CW1-D440A) could not prevent neutralisation by MAb A6.2. Allowing for the binding of divalent cations to D440 only (MNV.1-CW1-D410A), neutralisation could be prevented. From these rather distinct results, it can be concluded that binding of divalent cations to residue D440 but not D410 is required to permit an escape from MAb neutralisation.

The exact reasons for why one residue that binds divalent cations but does not assist in antibody escape exists and another is clearly essential in mediating escape is not at first glance entirely clear. One must look at the VP1 as an overall structure and relate this new information that was previously explored with regards to GCDCA function by Creutznacher *et al.* (2022). The VP1 dimer exhibits the receptor and antibody binding loop structures at the most distal regions. These when binding to the receptor are pushed in canon to be rigid by the C'D' loop movement upwards (Nelson *et al.*, 2018; M. B. Sherman *et al.*, 2019). The C'D' loop movement can be enabled by the binding of GCDCA into the pocket (Nelson *et al.*, 2018). Residue D440 is located in close proximity to the GCDCA binding pocket. It is possible that the binding of a divalent cation in this region initiates the same conformational change as observed by the binding of GCDCA, forcing the A'B' and E'F' loops into a preferably receptor-binding, closed conformation.

Both GCDCA and Mg^{2+} have been shown to bind VP1 (Nelson *et al.*, 2018). This binding stabilises the VP1 (M. B. Sherman *et al.*, 2019) and permits a rotation of the dimer by 90°. This conformational change or rotation and distal loop rigidity permits a more efficient receptor binding and prevents MAb binding (Williams *et al.*, 2021a). Neutralisation studies have shown this to be the case in cell culture for GCDCA (Creutznacher *et al.*, 2022).

Importantly, previous studies investigating GCDCA function in MNV have typically not indicated whether divalent cation concentration has been accounted for, measured, or set to a standard or base level. This investigation identified this discrepancy. When concentrating the virus stock for experimentation, a set buffer was used, adjusting ion concentrations to a minimising standard. Assessment of $MgCl_2$ addition in relation to GCDCA could then be made.

In isolation, GCDCA addition could not prevent neutralisation by MAbs. The addition of low $MgCl_2$ concentrations, that are not sufficient to prevent neutralisation alone, are necessary to permit the antibody escape effects of GCDCA that were previously observed. This is evidence of an assistive relationship between divalent cations and bile acid in MNV infection.

Similar effects from exposure to physiological concentrations of $MgCl_2$ can be observed when MNV is in the presence of polyclonal Abs. Such concentrations are sufficient to prevent neutralisation by polyclonal Abs, however GCDCA was found not to be beneficial. Unlike with the addition of small $MgCl_2$ concentrations to an MNV infection with MAbs, small divalent cations concentrations were not sufficient to prevent neutralisation with polyclonal Abs. This is supportive of divalent cations being an essential component in causing a conformational change in the VP1. Infection increase is caused by improving the binding affinity to mCD300lf and reducing the binding affinity to neutralising Abs.

Both neutralisation studies performed with MAb A6.2 and polyclonal Abs allow us to see that both GCDCA and divalent cations are involved in preventing neutralisation, but that there are nuances to their utilisation by the virus. Divalent cations are a crucial component. Their presence during infection despite the presence of either a MAb or polyclonal Abs, increases infectivity and prevents neutralisation. The presence of GCDCA however is not necessary and cannot rescue infection alone. The addition of divalent cations is necessary, at a concentration too low to prevent neutralisation in isolation, and then a synergistic effect with GCDCA is seen. This is not the case for the tested concentrations for polyclonal Ab, however a slighter higher concentration may be necessary, but this was not tested. One can conclude that the presence of a divalent cation is crucial to the neutralisation escape of MNV from MAbs and polyclonal Abs, with GCDCA being merely an assistive factor.

Murine norovirus utilises the environment of the gut to its advantage in order to escape the host immune response. These environmental factors of a low pH, the presence of bile acids, and the presence of metal ions causes a structural change in the capsid. The P2-subdomain loops structures close, move upwards and become rigid, with the P-domain as a whole rotating and contracting onto the S-domain (M. Sherman *et al.*, 2024). This rigidity and closing of the loop structures prevents the binding of a neutralising MAb. Specifically this study has shown that the binding of Mg^{2+} to residue D440 is required to permit escape from MAbs.

The presence of GCDCA only as shown in previous studies to prevent MAb neutralisation (Creutznacher *et al.*, 2022; Williams *et al.*, 2021a) has here been shown not to be the case. When controlling for metal ions, GCDCA alone cannot prevent neutralisation. However, a small metal ion concentration, not sufficient to prevent neutralisation itself, can assist GCDCA in MAb escape. This work and studies by other groups have shown that divalent cations, and to a lesser extent GCDCA, block MAb binding by causing a conformational change (M. Sherman *et al.*, 2024; Song *et al.*, 2020; Williams *et al.*, 2021b) not too dissimilar to that found in antibody escape mutants (M. B. Sherman *et al.*, 2025).

An RNA-based reverse genetics system was successfully employed to generate recombinant MNVs containing VP1 mutations D410A and D440A. Neutralisation assays have shown the binding of a divalent cation to D440 is necessary to escape the neutralising MAb A6.2 during MNV-1.CW1 infection. When controlling for divalent cation concentration, GCDCA alone cannot prevent neutralisation by MAb A6.2, however a low concentration of $MgCl_2$, insufficient to prevent neutralisation by MAb A6.2 in isolation, permits the escape of MNV-1.CW1 when also in the presence of GCDCA.

Using reverse genetics, this work demonstrates that escape from neutralising MAb A6.2 depends on the binding of a divalent cation to VP1 residue D440, with GCDCA alone being insufficient to drive this conformational change. A synergistic effect of Mg^{2+} and bile acid was shown with $MgCl_2$ being the major component and GCDCA as a supporting factor.

Conclusion

This study focussed on two major aims. Firstly to expand and optimise an RNA-based MNV reverse genetics system with a reporter for infection. This was successfully achieved and used to identify tolerant insertion sites suitable for the insertion of a small peptide sequence, as well as the generation of infectious recombinant MNVs with mutations in the major capsid protein VP1. The constructs produced provide a cloning pipeline for future mutagenesis projects and expand the toolkit for dissecting MNV biology using reveres genetics. Parts of this system are published in collaboration (Wobus *et al.*, 2023), and a second first-author manuscript focussing on the reporter is in preparation.

The second aim of this project was to utilise the reverse genetics system to analyse the role of ions and bile acid in MNV infection and antibody escape. This was successful and the story contributed to a publication showing that GCDCA stabilises the MNV-1 P-dimers, which directly impact antibody and receptor binding *in vitro* and in infection assays (Creutznacher *et al.*, 2022) and a pre-print (Maass *et al.*, 2024). A third first-author manuscript focusing on the synergistic effect of GCDCA and divalent cations on antibody escape is close to submission.

References

Ahmed, S. M., Hall, A. J., Robinson, A. E., Verhoef, L., Premkumar, P., Parashar, U. D., Koopmans, M., & Lopman, B. A. (2014). Global prevalence of norovirus in cases of gastroenteritis: A systematic review and meta-analysis. *The Lancet Infectious Diseases*, *14*(8), 725–730. https://doi.org/10.1016/S1473-3099(14)70767-4

Amodio, E., De Grazia, S., Genovese, D., Bonura, F., Filizzolo, C., Collura, A., Di Bernardo, F., & Giammanco, G. M. (2022). Clinical and Epidemiologic Features of Viral Gastroenteritis in Hospitalized Children: An 11-Year Surveillance in Palermo (Sicily). *Viruses*, *15*(1), 41. https://doi.org/10.3390/v15010041

Atmar, R. L., Ettayebi, K., Ramani, S., Neill, F. H., Lindesmith, L., Baric, R. S., Brinkman, A., Braun, R., Sherwood, J., & Estes, M. K. (2024). A Bivalent Human Norovirus Vaccine Induces Homotypic and Heterotypic Neutralizing Antibodies. *Journal of Infectious Diseases*, *229*(5), 1402–1407. https://doi.org/10.1093/infdis/jiad401

Belliot, G., Sosnovtsev, S. V., Mitra, T., Hammer, C., Garfield, M., & Green, K. Y. (2003). In Vitro Proteolytic Processing of the MD145 Norovirus ORF1 Nonstructural Polyprotein Yields Stable Precursors and Products Similar to Those Detected in Calicivirus-Infected Cells. *Journal of Virology*, *77*(20), 10957–10974. https://doi.org/10.1128/jvi.77.20.10957-10974.2003

Blasi, E., Barluzzi, R., Bocchini, V., Mazzolla, R., & Bistoni, F. (1990). Immortalization of murine microglial cells by a v-raf / v-myc carrying retrovirus. *Journal of Neuroimmunology*, *27*(2–3), 229–237. https://doi.org/10.1016/0165-5728(90)90073-V

Burroughs, J. N., & Brown, F. (1978). Presence of a Covalently Linked Protein on Calicivirus RNA. *Journal of General Virology*, *41*(2), 443–446. https://doi.org/10.1099/0022-1317-41-2-443

Chaudhry, Y., Nayak, A., Bordeleau, M. E., Tanaka, J., Pelletier, J., Belsham, G. J., Roberts, L. O., & Goodfellow, I. G. (2006). Caliciviruses differ in their functional requirements for eIF4F components. *Journal of Biological Chemistry*, *281*(35), 25315–25325. https://doi.org/10.1074/jbc.M602230200

Chaudhry, Y., Skinner, M. A., & Goodfellow, I. G. (2007). Recovery of genetically defined murine norovirus in tissue culture by using a fowlpox virus expressing T7 RNA polymerase. *Journal of General Virology*, *88*(8), 2091–2100. https://doi.org/10.1099/vir.0.82940-0

Cheetham, S., Souza, M., Meulia, T., Grimes, S., Han, M. G., & Saif, L. J. (2006). Pathogenesis of a Genogroup II Human Norovirus in Gnotobiotic Pigs. *Journal of Virology*, *80*(21), 10372–10381. https://doi.org/10.1128/jvi.00809-06

Chhabra, P., de Graaf, M., Parra, G. I., Chan, M. C. W., Green, K., Martella, V., Wang, Q., White, P. A., Katayama, K., Vennema, H., Koopmans, M. P. G., & Vinjé, J. (2019). Updated classification of norovirus genogroups and genotypes. *Journal of General Virology*, *100*(10), 1393–1406. https://doi.org/10.1099/JGV.0.001318

Chiang, J. Y. L. (2013). Bile Acid Metabolism and Signaling. In *Comprehensive Physiology* (Vol. 3, Issue 3, pp. 1191–1212). Wiley. https://doi.org/10.1002/cphy.c120023

Clarke, I. N., & Lambden, P. R. (2000). Organization and Expression of Calicivirus Genes. *The Journal of Infectious Diseases*, *181*(s2), S309–S316. https://doi.org/10.1086/315575

Cohen, J. I., Rosenblum, B., Ticehurst, J. R., Daemer, R. J., Feinstone, S. M., & Purcell, R. H. (1987). Complete nucleotide sequence of an attenuated hepatitis A virus: comparison with wild-type virus. *Proceedings of the National Academy of Sciences*, *84*(8), 2497–2501. https://doi.org/10.1073/pnas.84.8.2497

Cohen, J. I., Ticehurst, J. R., Feinstone, S. M., Rosenblum, B., & Purcell, R. H. (1987). Hepatitis A virus cDNA and its RNA transcripts are infectious in cell culture. *Journal of Virology*, *61*(10), 3035–3039. https://doi.org/10.1128/jvi.61.10.3035-3039.1987

Cohen, J. I., Ticehurst, J. R., Purcell, R. H., Buckler-White, A., & Baroudy, B. M. (1987). Complete nucleotide sequence of wild-type hepatitis A virus: comparison with different strains of hepatitis A virus and other picornaviruses. *Journal of Virology*, *61*(1), 50–59. https://doi.org/10.1128/jvi.61.1.50-59.1987

Conley, M. J., McElwee, M., Azmi, L., Gabrielsen, M., Byron, O., Goodfellow, I. G., & Bhella, D. (2019). Calicivirus VP2 forms a portal-like assembly following receptor engagement. *Nature*, *565*(7739), 377–381. https://doi.org/10.1038/s41586-018-0852-1

Cotton, B. T., Hyde, J. L., Sarvestani, S. T., Sosnovtsev, S. V., Green, K. Y., White, P. A., & Mackenzie, J. M. (2017). The Norovirus NS3 Protein Is a Dynamic Lipid- and Microtubule-Associated Protein Involved in Viral RNA Replication. *Journal of Virology*, *91*(3). https://doi.org/10.1128/jvi.02138-16

Creutznacher, R., Maass, T., Dülfer, J., Feldmann, C., Hartmann, V., Lane, M. S., Knickmann, J., Westermann, L. T., Thiede, L., Smith, T. J., Uetrecht, C., Mallagaray, A., Waudby, C. A., Taube, S., & Peters, T. (2022). Distinct dissociation rates of murine and human norovirus P-domain dimers suggest a role of dimer stability in virus-host interactions. *Communications Biology*, *5*(1). https://doi.org/10.1038/s42003-022-03497-4

Daughenbaugh, K. F., Fraser, C. S., Hershey, J. W. B., & Hardy, M. E. (2003). The genome-linked protein VPg of the Norwalk virus binds eIF3, suggesting its role in translation initiation complex recruitment. *The EMBO Journal*, *22*(11), 2852–2859. https://doi.org/10.1093/emboj/cdg251

Deerain, J. M., Aktepe, T. E., Trenerry, A. M., Ebert, G., Hyde, J. L., Charry, K., Edgington-Mitchell, L., Xu, B., Ambrose, R. L., Sarvestani, S. T., Lawlor, K. E., Pearson, J. S., White, P. A., & Mackenzie, J. M. (2024). Murine norovirus infection of macrophages induces intrinsic apoptosis as the major form of programmed cell death. *Virology*, *589*, 109921. https://doi.org/10.1016/j.virol.2023.109921

Doerflinger, S. Y., Cortese, M., Romero-Brey, I., Menne, Z., Tubiana, T., Schenk, C., White, P. A., Bartenschlager, R., Bressanelli, S., Hansman, G. S., & Lohmann, V. (2017). Membrane alterations induced by nonstructural proteins of human norovirus. *PLoS Pathogens*, *13*(10). https://doi.org/10.1371/journal.ppat.1006705

Dunham, D. M., Jiang, X., Berke, T., Smith, A. W., & Matson, D. O. (1998). Genomic mapping of a calicivirus VPg. *Archives of Virology*, *143*(12), 2421–2430. https://doi.org/10.1007/s007050050471

Edelmann, F. T., Niedner, A., & Niessing, D. (2014). Production of pure and functional RNA for in vitro reconstitution experiments. *Methods*, *65*(3), 333–341. https://doi.org/10.1016/j.ymeth.2013.08.034

Emmott, E., Sweeney, T. R., & Goodfellow, I. (2015). A cell-based fluorescence resonance energy transfer (FRET) sensor reveals inter- and intragenogroup variations in norovirus protease activity and polyprotein cleavage. *Journal of Biological Chemistry*, *290*(46), 27841–27853. https://doi.org/10.1074/jbc.M115.688234

Ettayebi, K., Crawford, S. E., Murakami, K., Broughman, J. R., Karandikar, U., Tenge, V. R., Neill, F. H., Blutt, S. E., Zeng, X. L., Qu, L., Kou, B., Opekun, A. R., Burrin, D., Graham, D. Y., Ramani, S., Atmar, R. L., & Estes, M. K. (2016). Replication of human noroviruses in stem cell-derived human enteroids. *Science*, *353*(6306), 1387–1393. https://doi.org/10.1126/science.aaf5211

Goodfellow, I., Chaudhry, Y., Gioldasi, I., Gerondopoulos, A., Natoni, A., Labrie, L., Laliberté, J. F., & Roberts, L. (2005). Calicivirus translation initiation requires an interaction between VPg and eIF4E. *EMBO Reports*, *6*(10), 968–972. https://doi.org/10.1038/sj.embor.7400510

Graziano, V. R., Walker, F. C., Kennedy, E. A., Wei, J., Ettayebi, K., Strine, M. S., Filler, R. B., Hassan, E., Hsieh, L. L., Kim, A. S., Kolawole, A. O., Wobus, C. E., Lindesmith, L. C., Baric, R. S., Estes, M. K., Orchard, R. C., Baldridge, M. T., & Wilen, C. B. (2020). CD300lf is the primary physiologic receptor of murine norovirus but not human norovirus. *PLoS Pathogens*, *16*(4). https://doi.org/10.1371/journal.ppat.1008242

Hafner, A., Meurs, N., Garner, A., Azar, E., Kannan, A., Passalacqua, K. D., Nagrath, D., & Wobus, C. E. (2024). Norovirus NS1/2 protein increases glutaminolysis for efficient viral replication. *PLoS Pathogens*, *20*(7). https://doi.org/10.1371/journal.ppat.1011909

Haga, K., Fujimoto, A., Takai-Todaka, R., Miki, M., Doan, Y. H., Murakami, K., Yokoyama, M., Murata, K., Nakanishi, A., & Katayama, K. (2016). Functional receptor molecules CD300lf and CD300ld within the CD300 family enable murine noroviruses to infect cells. *Proceedings of the National Academy of Sciences of the United States of America*, *113*(41), E6248–E6255. https://doi.org/10.1073/pnas.1605575113

Han, K. R., Lee, J. H., Kotiguda, G. G., Jung, K. H., Chung, M. S., Kang, S., Hwang, S., & Kim, K. H. (2018). Nucleotide triphosphatase and RNA chaperone activities of murine norovirus NS3. *Journal of General Virology*, *99*(11), 1482–1493. https://doi.org/10.1099/jgv.0.001151

Hofmann, A. F. (1999). The Continuing Importance of Bile Acids in Liver and Intestinal Disease. *Archives of Internal Medicine*, *159*(22), 2647. https://doi.org/10.1001/archinte.159.22.2647

Hung, C. H., Yen, J. B., Chang, P. J., Chen, L. W., Huang, T. Y., Tsai, W. J., & Tsai, Y. C. (2023). Characterization of Human Norovirus Nonstructural Protein NS1.2 Involved in the Induction of the Filamentous Endoplasmic Reticulum, Enlarged Lipid Droplets, LC3 Recruitment, and Interaction with NTPase and NS4. *Viruses*, *15*(3). https://doi.org/10.3390/v15030812

Hussey, R. J., Coates, L., Gill, R. S., Erskine, P. T., Coker, S. F., Mitchell, E., Cooper, J. B., Wood, S., Broadbridge, R., Clarke, I. N., Lambden, P. R., & Shoolingin-Jordan, P. M. (2011). A structural study of norovirus 3C protease specificity: Binding of a designed active site-directed peptide inhibitor. *Biochemistry*, *50*(2), 240–249. https://doi.org/10.1021/bi1008497

Hyde, J. L., & Mackenzie, J. M. (2010). Subcellular localization of the MNV-1 ORF1 proteins and their potential roles in the formation of the MNV-1 replication complex. *Virology*, *406*(1), 138–148. https://doi.org/10.1016/j.virol.2010.06.047

Hyde, J. L., Sosnovtsev, S. V., Green, K. Y., Wobus, C., Virgin, H. W., & Mackenzie, J. M. (2009). Mouse Norovirus Replication Is Associated with Virus-Induced Vesicle Clusters Originating from Membranes Derived from the Secretory Pathway. *Journal of Virology*, *83*(19), 9709–9719. https://doi.org/10.1128/jvi.00600-09

Innis, B. L. (1994). Protection Against Hepatitis A by an Inactivated Vaccine. *JAMA: The Journal of the American Medical Association*, *271*(17), 1328. https://doi.org/10.1001/jama.1994.03510410040030

Jones, M. K., Grau, K. R., Costantini, V., Kolawole, A. O., De Graaf, M., Freiden, P., Graves, C. L., Koopmans, M., Wallet, S. M., Tibbetts, S. A., Schultz-Cherry, S., Wobus, C. E., Vinjé, J., & Karst, S. M. (2015). Human norovirus culture in B cells. *Nature Protocols*, *10*(12), 1939–1947. https://doi.org/10.1038/nprot.2015.121

Karst, S. M., Wobus, C. E., Lay, M., Davidson, J., & Virgin IV, H. W. (2003). STAT1-dependent innate immunity to a norwalk-like virus. *Science*, *299*(5612), 1575–1578. https://doi.org/10.1126/science.1077905

Katpally, U., Voss, N. R., Cavazza, T., Taube, S., Rubin, J. R., Young, V. L., Stuckey, J., Ward, V. K., Virgin, H. W., Wobus, C. E., & Smith, T. J. (2010). High-Resolution Cryo-Electron Microscopy Structures of Murine Norovirus 1 and Rabbit Hemorrhagic Disease Virus Reveal Marked Flexibility in the Receptor Binding Domains. *Journal of Virology*, *84*(11), 5836–5841. https://doi.org/10.1128/jvi.00314-10

Kolawole, A. O., Li, M., Xia, C., Fischer, A. E., Giacobbi, N. S., Rippinger, C. M., Proescher, J. B. G., Wu, S. K., Bessling, S. L., Gamez, M., Yu, C., Zhang, R., Mehoke, T. S., Pipas, J. M., Wolfe, J. T., Lin, J. S., Feldman, A. B., Smith, T. J., & Wobus, C. E. (2014). Flexibility in Surface-Exposed Loops in a Virus Capsid Mediates Escape from Antibody Neutralization. *Journal of Virology*, *88*(8), 4543–4557. https://doi.org/10.1128/jvi.03685-13

Kolawole, A. O., Smith, H. Q., Svoboda, S. A., Lewis, M. S., Sherman, M. B., Lynch, G. C., Pettitt, B. M., Smith, T. J., & Wobus, C. E. (2017). Norovirus Escape from Broadly Neutralizing Antibodies Is Limited to Allostery-Like Mechanisms. *MSphere*, *2*(5). https://doi.org/10.1128/mSphere.00334-17

Kolawole, A. O., Xia, C., Li, M., Gamez, M., Yu, C., Rippinger, C. M., Yucha, R. E., Smith, T. J., & Wobus, C. E. (2014). Newly isolated mAbs broaden the neutralizing epitope in murine norovirus. *Journal of General Virology*, *95*(PART 9), 1958–1968. https://doi.org/10.1099/vir.0.066753-0

Kotaki, T., Akieda, Y., Chen, Z., Onishi, M., Komatsu, S., Motooka, D., Omori, H., Tamiya, S., Kanai, Y., Minami, S., Kawagishi, T., Sakon, N., Sato, S., Ishitani, T., & Kobayashi, T. (2025). Recovery of infectious recombinant human norovirus using zebrafish embryos. *Proceedings of the National Academy of Sciences*, *122*(49). https://doi.org/10.1073/pnas.2526726122

Lane, M. S. (2021). *Glycochenodeoxycholic acid triggers murine norovirus escape from neutralising antibody recognition* [Master Thesis]. Universität zu Lübeck.

Leen, E. N., Baeza, G., & Curry, S. (2012). Structure of a murine norovirus NS6 protease-product complex revealed by adventitious crystallisation. *PLoS ONE*, *7*(6). https://doi.org/10.1371/journal.pone.0038723

Li, T.-F., Hosmillo, M., Schwanke, H., Shu, T., Wang, Z., Yin, L., Curry, S., Goodfellow, I. G., & Zhou, X. (2018). Human Norovirus NS3 Has RNA Helicase and Chaperoning Activities. *Journal of Virology*, *92*(5). https://doi.org/10.1128/jvi.01606-17

Lingemann, M. (2020). *New Tools to Study Murine Norovirus-Host Interactions* [Doctoral Thesis]. Universität zu Lübeck.

Liu, H., & Naismith, J. H. (2008). An efficient one-step site-directed deletion, insertion, single and multiple-site plasmid mutagenesis protocol. *BMC Biotechnology*, *8*, 91. https://doi.org/10.1186/1472-6750-8-91

Maass, T., Westermann, L. T., Sharotri, L., Blankenhorn, L., Lane, M. S., Chaika, M., Taube, S., Peters, T., & Mallagaray, A. (2024). NMR Reveals the Synergistic Roles of Bivalent Metal Ions in Norovirus Infections. *BioRxiv*. https://doi.org/10.1101/2024.07.10.602906

Marionneau, S., Ruvoën, N., Le Moullac–Vaidye, B., Clement, M., Cailleau–Thomas, A., Ruiz–Palacois, G., Huang, P., Jiang, X., & Le Pendu, J. (2002). Norwalk virus binds to histo-blood group antigens present on gastroduodenal epithelial cells of secretor individuals. *Gastroenterology*, *122*(7), 1967–1977. https://doi.org/10.1053/gast.2002.33661

May, J., Viswanathan, P., Ng, K. K.-S., Medvedev, A., & Korba, B. (2014). The P4-P2′ Amino Acids Surrounding Human Norovirus Polyprotein Cleavage Sites Define the Core Sequence Regulating Self-Processing Order. *Journal of Virology*, *88*(18), 10738–10747. https://doi.org/10.1128/jvi.01357-14

Meyers, G. (2007). Characterization of the Sequence Element Directing Translation Reinitiation in RNA of the Calicivirus Rabbit Hemorrhagic Disease Virus. *Journal of Virology*, *81*(18), 9623–9632. https://doi.org/10.1128/JVI.00771-07

Nakabayashi, H., Taketa, K., Miyano, K., Yamane, T., & Sato, J. (1982). Growth of human hepatoma cells lines with differentiated functions in chemically defined medium. *Cancer Research*, *42*(9), 3858–3863. http://www.ncbi.nlm.nih.gov/pubmed/6286115

Nelson, C. A., Wilen, C. B., Dai, Y. N., Orchard, R. C., Kim, A. S., Stegeman, R. A., Hsieh, L. L., Smith, T. J., Virgin, H. W., & Fremont, D. H. (2018). Structural basis for murine norovirus engagement of bile acids and the CD300lf receptor. *Proceedings of the National Academy of Sciences of the United States of America*, *115*(39), E9201–E9210. https://doi.org/10.1073/pnas.1805797115

Olson, M. C., Pierce, L. R., & Orchard, R. C. (2025). Development of a replication competent murine norovirus reporter system. *PLOS Pathogens*, *21*(5), e1012834. https://doi.org/10.1371/journal.ppat.1012834

Orchard, R. C., Wilen, C. B., Doench, J. G., Baldridge, M. T., McCune, B. T., Lee, Y. C. J., Lee, S., Pruett-Miller, S. M., Nelson, C. A., Fremont, D. H., & Virgin, H. W. (2016). Discovery of a proteinaceous cellular receptor for a norovirus. *Science*, *353*(6302), 933–936. https://doi.org/10.1126/science.aaf1220

Perry, J. W., Taube, S., & Wobus, C. E. (2009). Murine norovirus-1 entry into permissive macrophages and dendritic cells is pH-independent. *Virus Research*, *143*(1), 125–129. https://doi.org/10.1016/j.virusres.2009.03.002

Perry, J. W., & Wobus, C. E. (2010). Endocytosis of Murine Norovirus 1 into Murine Macrophages Is Dependent on Dynamin II and Cholesterol. *Journal of Virology*, *84*(12), 6163–6176. https://doi.org/10.1128/JVI.00331-10

Prasad, B. V. V., Hardy, M. E., Dokland, T., Bella, J., Rossmann, M. G., & Estes, M. K. (1999). X-ray Crystallographic Structure of the Norwalk Virus Capsid. *Science*, *286*(5438), 287–290. https://doi.org/10.1126/science.286.5438.287

Racaniello, V. R., & Baltimore, D. (1981). Cloned Poliovirus Complementary DNA Is Infectious in Mammalian Cells. *Science*, *214*(4523), 916–919. https://doi.org/10.1126/science.6272391

Raschke, W. C., Baird, S., Ralph, P., & Nakoinz, I. (1978). Functional macrophage cell lines transformed by abelson leukemia virus. *Cell*, *15*(1), 261–267. https://doi.org/10.1016/0092-8674(78)90101-0

Rohayem, J., Robel, I., Jäger, K., Scheffler, U., & Rudolph, W. (2006). Protein-Primed and De Novo Initiation of RNA Synthesis by Norovirus 3D pol . *Journal of Virology*, *80*(14), 7060–7069. https://doi.org/10.1128/jvi.02195-05

Roth, A. N., Helm, E. W., Mirabelli, C., Kirsche, E., Smith, J. C., Eurell, L. B., Ghosh, S., Altan-Bonnet, N., Wobus, C. E., & Karst, S. M. (2020). Norovirus infection causes acute self-resolving diarrhea in wild-type neonatal mice. *Nature Communications*, *11*(1). https://doi.org/10.1038/s41467-020-16798-1

Royet, A., Ruedas, R., Gargowitsch, L., Gervais, V., Habersetzer, J., Pieri, L., Ouldali, M., Paternostre, M., Hofmann, I., Tubiana, T., Fieulaine, S., & Bressanelli, S. (2024). Nonstructural protein 4 of human norovirus self-assembles into various membrane-bridging multimers. *Journal of Biological Chemistry*, 107724. https://doi.org/10.1016/j.jbc.2024.107724

Santiana, M., Ghosh, S., Ho, B. A., Rajasekaran, V., Du, W.-L., Mutsafi, Y., De Jésus-Diaz, D. A., Sosnovtsev, S. V., Levenson, E. A., Parra, G. I., Takvorian, P. M., Cali, A., Bleck, C., Vlasova, A. N., Saif, L. J., Patton, J. T., Lopalco, P., Corcelli, A., Green, K. Y., & Altan-Bonnet, N. (2018). Vesicle-Cloaked Virus Clusters Are Optimal Units for Inter-organismal Viral Transmission. *Cell Host & Microbe*, *24*(2), 208-220.e8. https://doi.org/10.1016/j.chom.2018.07.006

Schaffer, F. L., Ehresmann, D. W., Fretz, M. K., & Soergel, M. E. (1980). A Protein, VPg, Covalently Linked to 36S Calicivirus RNA. *Journal of General Virology*, *47*(1), 215–220. https://doi.org/10.1099/0022-1317-47-1-215

Sharp, T. M., Crawford, S. E., Ajami, N. J., Neill, F. H., Atmar, R. L., Katayama, K., Utama, B., & Estes, M. K. (2012). Secretory pathway antagonism by calicivirus homologues of Norwalk virus nonstructural protein p22 is restricted to noroviruses. *Virology Journal*, *9*. https://doi.org/10.1186/1743-422X-9-181

Sharp, T. M., Guix, S., Katayama, K., Crawford, S. E., & Estes, M. K. (2010). Inhibition of cellular protein secretion by norwalk virus nonstructural protein p22 requires a mimic of an endoplasmic reticulum export signal. *PLoS ONE*, *5*(10). https://doi.org/10.1371/journal.pone.0013130

Sherman, M. B., Smith, H. Q., Cox, F., Wobus, C. E., Lynch, G. C., Pettitt, B. M., & Smith, T. J. (2025). Murine norovirus allosteric escape mutants mimic gut activation. *Journal of Virology*. https://doi.org/10.1128/jvi.00219-25

Sherman, M. B., Williams, A. N., Smith, H. Q., Nelson, C., Wilen, C. B., Fremont, D. H., Virgin, H. W., & Smith, T. J. (2019). Bile Salts Alter the Mouse Norovirus Capsid Conformation: Possible Implications for Cell Attachment and Immune Evasion. *Journal of Virology*, *93*(19). https://doi.org/10.1128/JVI.00970-19

Sherman, M., Cox, F., Smith, H., Habib, M. H., Karst, S., Wobus, C. E., & Smith, T. J. (2024). The reversible activation of norovirus by metal ions. *Journal of Virology*. https://doi.org/10.1128/jvi.01735-23

Song, C., Takai-Todaka, R., Miki, M., Haga, K., Fujimoto, A., Ishiyama, R., Oikawa, K., Yokoyama, M., Miyazaki, N., Iwasaki, K., Murakami, K., Katayama, K., & Murata, K. (2020). Dynamic rotation of the protruding domain enhances the infectivity of norovirus. *PLoS Pathogens*, *16*(7). https://doi.org/10.1371/journal.ppat.1008619

Sosnovtsev, S., & Green, K. Y. (1995). RNA Transcripts Derived from a Cloned Full-Length Copy of the Feline Calicivirus Genome Do Not Require VpG for Infectivity. *Virology*, *210*(2), 383–390. https://doi.org/10.1006/viro.1995.1354

Sosnovtsev, S. V., Belliot, G., Chang, K.-O., Prikhodko, V. G., Thackray, L. B., Wobus, C. E., Karst, S. M., Virgin, H. W., & Green, K. Y. (2006). Cleavage Map and Proteolytic Processing of the Murine Norovirus Nonstructural Polyprotein in Infected Cells. *Journal of Virology*, *80*(16), 7816–7831. https://doi.org/10.1128/jvi.00532-06

Subba-Reddy, C. V., Goodfellow, I., & Kao, C. C. (2011). VPg-Primed RNA Synthesis of Norovirus RNA-Dependent RNA Polymerases by Using a Novel Cell-Based Assay. *Journal of Virology*, *85*(24), 13027–13037. https://doi.org/10.1128/jvi.06191-11

Sutherland, H., Conley, M. J., Emmott, E., Streetley, J., Goodfellow, I. G., & Bhella, D. (2021). The Cryo-EM Structure of Vesivirus 2117 Highlights Functional Variations in Entry Pathways for Viruses in Different Clades of the *Vesivirus* Genus. *Journal of Virology*, *95*(13). https://doi.org/10.1128/JVI.00282-21

Taniguchi, T., Palmieri, M., & Weissmann, C. (1978). Qβ DNA-containing hybrid plasmids giving rise to Qβ phage formation in the bacterial host. *Nature*, *274*(5668), 223–228. https://doi.org/10.1038/274223a0

Taube, S., Perry, J. W., Yetming, K., Patel, S. P., Auble, H., Shu, L., Nawar, H. F., Lee, C. H., Connell, T. D., Shayman, J. A., & Wobus, C. E. (2009). Ganglioside-Linked Terminal Sialic Acid Moieties on Murine Macrophages Function as Attachment Receptors for Murine Noroviruses. *Journal of Virology*, *83*(9), 4092–4101. https://doi.org/10.1128/JVI.02245-08

Taube, S., Rubin, J. R., Katpally, U., Smith, T. J., Kendall, A., Stuckey, J. A., & Wobus, C. E. (2010). High-Resolution X-Ray Structure and Functional Analysis of the Murine Norovirus 1 Capsid Protein Protruding Domain. *Journal of Virology*, *84*(11), 5695–5705. https://doi.org/10.1128/jvi.00316-10

Thorne, L. G., & Goodfellow, I. G. (2014). Norovirus gene expression and replication. *Journal of General Virology*, *95*(2), 278–291. https://doi.org/10.1099/vir.0.059634-0

Ticehurst, J. R., Racaniello, V. R., Baroudy, B. M., Baltimore, D., Purcell, R. H., & Feinstone, S. M. (1983). Molecular cloning and characterization of hepatitis A virus cDNA. *Proceedings of the National Academy of Sciences*, *80*(19), 5885–5889. https://doi.org/10.1073/pnas.80.19.5885

Van Dycke, J., Ny, A., Conceição-Neto, N., Maes, J., Hosmillo, M., Cuvry, A., Goodfellow, I., Nogueira, T. C., Verbeken, E., Matthijnssens, J., De Witte, P., Neyts, J., & Rocha-Pereira, J. (2019). A robust human norovirus replication model in zebrafish larvae. *PLoS Pathogens*, *15*(9). https://doi.org/10.1371/journal.ppat.1008009

Wang, G., Zhang, D., Orchard, R. C., Hancks, D. C., & Reese, T. A. (2023). Norovirus MLKL-like protein initiates cell death to induce viral egress. *Nature*, *616*(7955), 152–158. https://doi.org/10.1038/s41586-023-05851-w

Ward, V. K., McCormick, C. J., Clarke, I. N., Salim, O., Wobus, C. E., Thackray, L. B., Virgin, H. W., & Lambden, P. R. (2007). Recovery of infectious murine norovirus using pol II-driven expression of full-length cDNA. *Proceedings of the National Academy of Sciences*, *104*(26), 11050–11055. https://doi.org/10.1073/pnas.0700336104

Williams, A. N., Sherman, M. B., Smith, H. Q., Taube, S., Pettitt, B. M., Wobus, C. E., & Smith, T. J. (2021a). A Norovirus Uses Bile Salts To Escape Antibody Recognition While Enhancing Receptor Binding. *Journal of Virology*, *95*(13). https://doi.org/10.1128/jvi.00176-21

Williams, A. N., Sherman, M. B., Smith, H. Q., Taube, S., Pettitt, B. M., Wobus, C. E., & Smith, T. J. (2021b). Multiple Signals in the Gut Contract the Mouse Norovirus Capsid To Block Antibody Binding While Enhancing Receptor Affinity. *Journal of Virology*, *95*(22). https://doi.org/10.1128/jvi.01471-21

Wobus, C. E., Karst, S. M., Thackray, L. B., Chang, K. O., Sosnovtsev, S. V., Belliot, G., Krug, A., Mackenzie, J. M., Green, K. Y., & Virgin IV, H. W. (2004). Replication of Norovirus in cell culture reveals a tropism for dendritic cells and macrophages. *PLoS Biology*, *2*(12). https://doi.org/10.1371/journal.pbio.0020432

Wobus, C. E., Peiper, A. M., McSweeney, A. M., Young, V. L., Chaika, M., Lane, M. S., Lingemann, M., Deerain, J. M., Strine, M. S., Alfajaro, M. M., Helm, E. W., Karst, S. M., Mackenzie, J. M., Taube, S., Ward, V. K., & Wilen, C. B. (2023). Murine Norovirus: Additional Protocols for Basic and Antiviral Studies. *Current Protocols*, *3*(7). https://doi.org/10.1002/cpz1.828

Yang, J., Xia, H., Qian, Q., & Zhou, X. (2015). RNA chaperones encoded by RNA viruses. *Virologica Sinica*, *30*(6), 401–409. https://doi.org/10.1007/s12250-015-3676-2

Yen, J.-B., Chen, L.-W., Wei, L.-H., Hung, C.-H., Wang, S.-S., Lin, C.-L., & Chang, P.-J. (2021). Identification and Characterization of Human Norovirus NTPase Regions Required for Lipid Droplet Localization, Cellular Apoptosis, and Interaction with the Viral P22 Protein. *Microbiology Spectrum*, *9*(1). https://doi.org/10.1128/spectrum.00422-21

Yunus, M. A., Chung, L. M. W., Chaudhry, Y., Bailey, D., & Goodfellow, I. (2010). Development of an optimized RNA-based murine norovirus reverse genetics system. *Journal of Virological Methods*, *169*(1), 112–118. https://doi.org/10.1016/j.jviromet.2010.07.006

Acknowledgements

Use of the DeepL translator was used for the translation of the Abstract into German.

Thank you to all of the technicians, researchers and students in the Institute of Virology and Cell Biology that have created an enjoyable working environment over the years I have spent here. Thank you especially to lab technician, Katja Thiele-Bössel, who has ensured a smooth-running lab environment and taken care of cell culture, buffers and equipment.

Special mention must go to my colleague and friend, Maryna Chaika, who has completed her own thesis alongside. We have at times worked on the same project and some figures in this dissertation would not have been possible without her.

Finally, thank you to Prof. Dr. Stefan Taube for giving me the opportunity to not only complete both a Master thesis and PhD thesis under his supervision, but also have me as an active member of his lab and working group since 2019 when I joined as an internship student.

Curriculum Vitae

Education

Higher Education

Universität zu Lübeck, 2021-2026

Doctoral Degree of the University of Lübeck, 1.6 (*cum laude*)

Thesis Title: Reporter-based reverse genetics of murine norovirus reveals insertion-tolerant sites and a position in the capsid linked to antibody escape

Universität zu Lübeck, 2018-2021

Infection Biology, MSc 1.8

Thesis Title: Glycochenodeoxycholic acid triggers murine norovirus escape from neutralising antibody recognition

University of Salford, 2015-2018

Human Biology and Infectious Diseases, BSc (with Hons) First Class

Dissertation Title: Effects of Antibiotic Adaptation on Pseudomonas aeruginosa *Metabolism*

Secondary Education

Maiden Erlegh School, 2007-2014

Publications

- Maass, T., Westermann, L. T., Sharotri, L., Blankenhorn, L., Lane, M. S., Chaika, M., Taube, S., Peters, T., & Mallagaray, A. (2024). NMR Reveals the Synergistic Roles of Bivalent Metal Ions in Norovirus Infections. *BioRxiv*. https://doi.org/10.1101/2024.07.10.602906
- Wobus, C. E., Peiper, A. M., McSweeney, A. M., Young, V. L., Chaika, M., Lane, M. S., Lingemann, M., Deerain, J. M., Strine, M. S., Alfajaro, M. M., Helm, E. W., Karst, S. M., Mackenzie, J. M., Taube, S., Ward, V. K., & Wilen, C. B. (2023). Murine Norovirus: Additional Protocols for Basic and Antiviral Studies. *Current Protocols*, *3*(7). https://doi.org/10.1002/cpz1.828
- Klein, C., Borsche, M., Balck, A., Föh, B., Rahmöller, J., Peters, E., Knickmann, J., Lane, M., Vollstedt, E.-J., Elsner, S. A., Käding, N., Hauswaldt, S., Lange, T., Hundt, J. E., Lehrian, S., Giese, J., Mischnik, A., Niemann, S., Maurer, F., … Katalinic, A. (2022). One-year surveillance of SARS-CoV-2 transmission of the ELISA cohort: A model for population-based monitoring of infection risk. *Science Advances*, *8*(15), 5016. https://doi.org/10.1126/sciadv.abm5016
- Creutznacher, R., Maass, T., Dülfer, J., Feldmann, C., Hartmann, V., Lane, M. S., Knickmann, J., Westermann, L. T., Thiede, L., Smith, T. J., Uetrecht, C., Mallagaray, A., Waudby, C. A., Taube, S., & Peters, T. (2022). Distinct dissociation rates of murine and human norovirus P-domain dimers suggest a role of dimer stability in virus-host interactions. *Communications Biology*, *5*(1). https://doi.org/10.1038/s42003-022-03497-4

Conferences

GfV Ulm 2023: Murine Norovirus Requires Bivalent Cations for Bile Acid Mediated Escape from Antibody Recognition (Poster)

Calicivirus Conference Rotterdam 2023:

Murine Norovirus Reverse Genetics System with a Fluorescent Cellular Reporter Allows for Efficient Rescue of Recombinant Virus (Poster)

GfV Vienna 2024: Impact of Ions on Norovirus Infection and Escape from Antibody Neutralization (Poster)